THESIS ON NATURAL AND EXACT SCIENCES B229

Structures and Catalytic Properties of Titanium and Iridium Based Complexes

IRINA OSADCHUK

TTÜ PRESS

TALLINN UNIVERSITY OF TECHNOLOGY
School of Science
Department of Chemistry and Biotechnology

Dissertation was accepted for defense of the degree of Doctor of Philosophy (Chemistry) on March 23, 2017

Supervisors: Assoc. Prof. Toomas Tamm, Department of Chemistry and Biotechnology, School of Science, Tallinn University of Technology, Estonia

Assoc. Prof. Mårten Ahlquist, Theoretical Chem. & Biology, School of Biotechnology, Royal Institute of Technology, Sweden

Reviewed by: Dr. Andrus Metsala, Department of Chemistry and Biotechnology, School of Science, Tallinn University of Technology, Estonia

Opponents: Prof. Peeter Burk, Institute of Chemistry, Faculty of Science and Technology, University of Tartu, Estonia

Prof. Matti Haukka, Department of Chemistry, Faculty of Mathematics and Science, University of Jyväskylä, Finland

Defense of the thesis: May 25, 2017

Declaration:

Hereby I declare that this doctoral thesis, my original investigation and achievement, submitted for the doctoral degree at Tallinn University of Technology has not been submitted for any academic degree.

Irina Osadchuk

Euroopa Liit
Euroopa
Regionaalarengu Fond

Eesti
tuleviku heaks

ISSN 1406-4723
ISBN 978-9949-83-092-3 (publication)
ISBN 978-9949-83-093-0 (PDF)

LOODUS- JA TÄPPISTEADUSED B229

Titaani ja iriidiumi komplekside struktuur ja katalüütilised omadused

IRINA OSADCHUK

TTÜ KIRJASTUS

Родителям...

CONTENTS

List of publications

I I. Osadchuk, T. Pehk, A. Paju, M. Lopp, M. Öeren, T. Tamm „Isomers and conformers of complexes of $Ti(O\mathit{i}Pr)_4$ with cyclopentane-1,2-dione: NMR study and DFT calculations“ *International Journal of Quantum Chemistry*, 2014, **114**, 1012-1018.

II I. Osadchuk, T. Tamm, M. S. G. Ahlquist „Theoretical investigation of a parallel catalytic cycle in CO_2 hydrogenation by $(PNP)IrH_3$“ *Organometallics*, 2015, **34**, 4932-4940.

III I. Osadchuk, T. Tamm, M. S. G. Ahlquist „Reduced state of iridium PCP pincer complexes in electrochemical CO_2 hydrogenation“ *ACS Catalysis*, 2016, **6**, 3834–3839.

IV D. G. Kananovich, Y. Konik, J. Adamson, M. Kudrjashova, I. Reile, I. Osadchuk, T. Tamm, M. Lopp, V. Snieckus, O. G. Kulinkovich „Alkyltitanium ate complexes generated from Grignard reagents and titanium(IV) TADDOLates: NMR and computational study“ (unpublished manuscript)

Author’s contribution to the publications

The author participated in the planning of and executed calculations for papers **I – IV**. As the first author in papers **I – III**, the author was responsible for writing the manuscript drafts and participated in writing paragraphs containing computational investigations in manuscript **IV**.

Abbreviations

COSMO	Conductor-like screening model
DFT	Density functional theory
DET	Diethyl tartrate
ECP	Effective core potentials
Et	Ethyl
HF	Hartree-Fock method
*i*Pr	Isopropyl
IRC	Intrinsic reaction coordinates
KS	Kohn-Sham method
Me	Methyl
NBO	Natural bond orbital
NHE	Normal hydrogen electrode
NMR	Nuclear Magnetic Resonance
NOESY	Nuclear Overhauser effect spectroscopy
PB	Poisson-Boltzmann equation
PBF	Poisson-Boltzmann model
PES	Potential energy surface
PCP	1,3-bis((ditert-butylphenylphosphino)oxy)benzene
PNP	2,6-bis(diisopropylphosphinomethyl)pyridine
Ph	Phenyl
RI	Resolution of identity approach
SCRF	Self-consistent reaction field
Sub	3-methylcyclopentane-1,2-dione
TADDOL	(4R,5R)-2,2-dimethyl-α,α,α′,α′-tetraphenyldioxolane-4,5-dimethanol
^{t}Bu	Tertiary butyl
TOF	Turnover frequency
TON	Turnover number
TS	Transition state
QTAIM	Quantum theory of atoms in molecules

INTRODUCTION

The ongoing development of chemical industries creates a continuous need for new and improved catalysts. Nowadays more than 60% of chemical syntheses in industry are involving catalysts in at least one of their steps.[1] Catalysts increase the rate of a chemical reaction, provide selectivity and allow to make reaction conditions more mild. Catalysts based on transition metals have got the widest application.[2]

In science, catalysts also attract unflagging interest including those which are based on transition metals. Such type of catalysts is particularly appealing because the catalyst can be built or rebuilt: the transition metal can be changed, ligands can be varied or rearranged, and all those factors together influence the properties of the catalyst. Search and optimization of catalysts can be performed by changing some parameters and analysis of the resulting effects without knowledge of reaction mechanism, but development is much more efficient when the reaction mechanism is known step by step. How does the catalyst interact with the substrate? How does oxidation or reduction occur? How does catalyst regeneration happen? What is the rate-limiting step in the reaction and factors that can cause catalyst degradation? Above-mentioned data can be gained by analysis of experimental results and observations. An alternative option is theoretical investigation using a computational approach where the catalytic system is modelled and its properties are described based on quantum-mechanical calculations.

This thesis is composed of computational work on the investigation of the reactions catalysed by transition metal complexes. Within the framework of this study two transition metals – titanium and iridium – were considered: titanium as a representative from the beginning of the periodic table and iridium as a member of the noble metal group and a representative from the end of the periodic table. Typical reactions were considered for both metals: the Sharpless epoxidation and the Kulinkovich cyclisation reactions for titanium, and carbon dioxide reduction by pincer complexes for iridium. Besides the reaction mechanisms, geometries of the catalytic species and intermediates were considered in order to understand metal-ligand and ligand-ligand co-influence.

1. LITERATURE OVERVIEW

1.1. Theoretical background

1.1.1. Schrödinger equation

In quantum chemistry, the atomic and molecular systems in their stationary state are characterized using the time-independent Schrödinger equation:

$$\hat{H}\Psi = E\Psi \tag{1.1}$$

The equation describes the quantum nature of matter where Ψ is a wave function which contains all information known about the system. E is the numerical value of the total energy of the system and $\hat{H}$ is the Hamiltonian operator corresponding to the total energy of the system. Non-relativistic, non-spin-orbit Hamiltonian for a system takes into account five contributions: the kinetic energies of the electrons and nuclei, the attraction of electrons to the nuclei, the interelectronic and internuclear repulsions[3]

$$\hat{H} = -\sum_{i}^{N}\frac{\hbar^2}{2m_e}\nabla_i^2 - \sum_{\alpha}^{M}\frac{\hbar^2}{2m_\alpha}\nabla_\alpha^2 - \sum_{i}^{N}\sum_{\alpha}^{M}\frac{e^2 Z_\alpha}{r_{i\alpha}} + \sum_{i<j}^{N}\frac{e^2}{r_{ij}} + \sum_{\alpha<\beta}^{M}\frac{e^2 Z_\alpha Z_\beta}{r_{\alpha\beta}} \tag{1.2}$$

where i and j run over electrons and α and β run over nuclei, $\hbar$ is the reduced Planck constant ($\hbar = h/2\pi$), m_e and m_α are electron and nuclear masses, e is electron charge, Z is the atomic number, r_{ab} is the distance between particles and ∇^2 is the Laplacian operator

$$\nabla_i^2 = \frac{\partial^2}{\partial x_i^2} + \frac{\partial^2}{\partial y_i^2} + \frac{\partial^2}{\partial z_i^2} \tag{1.3}$$

If the system of atomic units (where some physical quantities such as m_e, $|e|$, $\hbar$ are set to unity) is used, the Hamiltonian is written as[4]

$$\hat{H} = -\sum_{i}^{N}\frac{1}{2}\nabla_i^2 - \sum_{\alpha}^{M}\frac{1}{2}\nabla_\alpha^2 - \sum_{i}^{N}\sum_{\alpha}^{M}\frac{Z_\alpha}{r_{i\alpha}} + \sum_{i<j}^{N}\frac{1}{r_{ij}} + \sum_{\alpha<\beta}^{M}\frac{Z_\alpha Z_\beta}{r_{\alpha\beta}} \tag{1.4}$$

Since predicting the individual motions of a group of objects interacting with each other (many-body problem) is not trivial and for the majority of cases is impossible, another common simplification called the independent particles model is used. In this approximation, the total wave function is expressed as the product of one-particle functions[3]

$$\Psi = \psi_1\psi_2 \dots \psi_n \tag{1.5}$$

Unfortunately, even in this reduced form the Schrödinger equation is unsolvable for systems of chemical interest because of the correlated motion of particles. Thus a number of approximations are introduced in order to simplify the description.

1.1.2. Born-Oppenheimer approximation

Nuclear mass is much larger than that of the electron and nuclei are moving relatively slowly. The Born-Oppenheimer approximation enables the separation of nuclear and electronic motions. Nuclei are assumed to be stationary during electronic energy calculation and their kinetic energy is set to zero. The energy of nucleus-nucleus attraction is calculated separately and added afterwards.[3,4]

$$\hat{H}_{el} = -\sum_{i}^{N} \frac{1}{2}\nabla_i^2 - \sum_{i}^{N}\sum_{\alpha}^{M} \frac{Z_\alpha}{r_{i\alpha}} + \sum_{i<j}^{N} \frac{1}{r_{ij}} \tag{1.6}$$

$$E_{nucl} = \sum_{\alpha<\beta}^{M} \frac{Z_\alpha Z_\beta}{r_{\alpha\beta}} \tag{1.7}$$

So the Schrödinger equation takes the following form[3]

$$\hat{H}\Psi = \left(\sum_{i=1}^{N} \varepsilon_i\right)\Psi + E_{nucl} \tag{1.8}$$

where ε_i is the energy of the *i*-th electron and $\hat{h}_i$ is the one-electron Hamiltonian

$$\hat{h}_i = \frac{1}{2}\nabla_i^2 - \sum_{\alpha=1}^{M} \frac{Z_\alpha}{r_{i\alpha}} + \sum_{i<j}^{N} \frac{1}{r_{ij}} \tag{1.9}$$

The Born-Oppenheimer approximation simplifies the treatment of a molecular system, but still remains unsolvable for systems of chemical interest because of the many-electron problem.

1.1.3. Hartree-Fock method

The solutions for the many-electron problem are available only for a few simple systems and additional approximations are needed for systems of chemical interest. There are several philosophies on how many-electron systems can be considered. The Hartree-Fock (HF) method treats electrons one by one and each electron „sees" other electrons as an average electric field. The one-electron Hamiltonian in the Hartree-Fock model is[3,4]

$$\hat{h}_i = \frac{1}{2}\nabla_i^2 - \sum_{\alpha=1}^{M} \frac{Z_\alpha}{r_{i\alpha}} + V_i\{j\} \tag{1.10}$$

where $V_i\{j\}$ represents the interaction between the *i*-th electron and the average field created by other electrons of the system.

Usage of average field instead of exact electron-electron repulsion results in inaccurate wave functions and significant energy errors[3]. A number of methods have been developed in order to improve the accuracy of the HF method, such as configuration interaction[5,6], Møller–Plesset perturbation theory[7,8], coupled cluster[9] and many others.

1.1.4. Density functional theory

In density functional theory (DFT), for approaching the many-electron problem another philosophy, based on theorems by Hohenberg and Kohn, is used. DFT does not consider electrons separately as the HF method does. It postulates that the properties of the system can be described through the electron probability density.[3,4]

The Hohenberg-Kohn theorems state that the external potential is a unique functional of the electron density and that the energy of the system can be defined in terms of density, and the ground state will be the minimum value of this functional.[10]

Kohn and Sham suggested to treat a quantum system as a system of non-interacting electrons. To account for the difference between the fictitious and a real quantum system, an additional term E_{xc} was added, which stands for exchange-correlation energy.[11] E_{xc} includes not only electron-electron repulsion, but also the difference between the fictitious non-interacting systems and the real system (the difference in both the kinetic energy and the correlation energy).[3]

The Kohn-Sham (KS) one-electron operator has the form[3,4]

$$\hat{h}_i^{KS} = \frac{1}{2}\nabla_i^2 - \sum_{\alpha=1}^{M} \frac{Z_\alpha}{r_{i\alpha}} + \frac{1}{2}\sum_{i=1}^{N} \frac{1}{r_{ij}} + E_{xc} \tag{1.11}$$

This approximation significantly simplifies the treatment of quantum systems and has become one of the most widely used techniques in computational chemistry.[3,4]

1.1.4.1. Exchange-correlation functionals

The accuracy of DFT critically depends on how the exchange-correlation term is treated. Exchange and correlation energies are usually calculated separately and subsequently incorporated into the E_{xc} term. Thus, commonly the name of the functional contains two parts: the names of exchange and correlation terms.[3,4]

There are numerous approaches on how to calculate exchange and correlation. The oldest and least accurate is the Local Density Approximation (LDA). It is based on the solution for the uniform electron gas and both exchange and correlation depend only on electron density at a certain point.[3,4]

In the General Gradient Approximation (GGA), the E_{xc} depends on electron density and on the derivative of the density, which makes functionals of this type more accurate than LDA.[3,4] The PBE[12] and BP86[13,14] functionals are examples of this group.[15]

Meta-GGA functionals, in addition to the electron density and its first derivative, consider also the second derivative of the density. The accuracy of MGGA is comparable with the best GGA functionals.[3] The TPSS[16] functional is one representative of the MGGA functionals group.[15]

Nowadays hybrid functionals have gained the most popularity. In hybrid functional DFT and HF are combined together and the inclusion of the HF exchange term corrects some of the limitations of the DFT. For example, GGA

functionals underestimate barrier heights of chemical reactions in contrast to the HF, which overestimates them. Combination of those two methods gives better agreement with experiments.[3] B3LYP[13,17,18] and M06[19] are the best known hybrid functionals.[15]

Following this logic, in the last decade researchers have been actively developing double hybrid functionals, which contain additionally to a Hartree-Fock exchange part a Møller–Plesset part as well. At present the usage of such functionals is limited to small molecules.[20,21]

1.1.4.2. Dispersion correction

A well-known problem with DFT is the insufficient description of long-range interactions (*e.g.* π-interactions, van der Waals forces, hydrogen bonding).[15] In order to compensate for this limitation, an empirical correction can be added[22]

$$E_{total} = E_{KS-DFT} + E_{disp} = E_{KS-DFT} + E^{(2)} + E^{(3)} \tag{1.12}$$

with the most important two-body term

$$E^{(2)} = \sum_{ij} \sum_{n=6,8} s_n \frac{C_n^{ij}}{R_{ij}^n} f^{damp}(R_{ij}) \tag{1.13}$$

where s_n is the scaling factor, C_n^{ij} is the dispersion coefficient depending on the atom type, R_{ij} is the distance between atoms i and j, and f^{damp} is a damping function.

The term $\frac{C_n^{ij}}{R_{ij}^n}$ describes the asymptotic behaviour of the potential energy at long range and the damping function (f^{damp}) determines the range of the dispersion correction in order to avoid double counting at short and mid-ranges.[22–24] Pairwise corrections of Grimme (DFT-D[22] – DFT-D3[25]) are the most popular empirical dispersion corrections of this type of dispersion corrections.[15]

1.1.5. Basis sets

We have discussed which operator should be used to calculate the energy of the quantum system, but we have not yet characterized the wave function (Ψ) describing this quantum system. Most of modern calculations make use of the Linear combination of atomic orbitals – molecular orbitals (LCAO-MO) approximation, where for Ψ of a system a trial function (Ψ_{trial}) based on the atomic orbitals is created. For the mathematical description of atomic basis functions two main classes of functions are in common use. The Slater-type functions (STF) with the general form

$$\varphi = N r^{n-1} e^{-\zeta r} \tag{1.14}$$

(where N is a normalization constant, r is the distance from the nucleus, n is the quantum number and the coefficient ζ controls the width of the orbital), and Gauss-

ian-type functions (primitive Gaussian, GTF) with the general form

$$\varphi = Nr^l e^{-\alpha r^2} \tag{1.15}$$

(where N is a normalization constant, r is the distance from the nucleus, l determines the angular momentum and the coefficient α controls the width of the orbital). STFs describe atomic orbitals more accurately, but the corresponding integrals are harder to compute, in contrast to GTFs. Therefore GTFs have become much more popular.[1,2]

In order to make the description of orbitals more accurate, a linear combination of several primitive Gaussians is constructed. This linear combination is called a contracted Gaussian. In a minimal basis set, only one contracted Gaussian is used for describing each type of orbitals. More frequently, split valence basis sets are applied. In these basis sets one contracted Gaussian per orbital is used for the description of core orbitals, and several Gaussians per orbital are used for the description of valence orbitals. Often one of them is contracted and others are not. This kind of treatment gives more flexibility to the valence orbitals and better describes the formation of molecular orbitals. In order to further increase flexibility, polarization functions (corresponding to quantum numbers of a higher angular momentum) and diffuse functions (slowly decaying Gaussians with a small α) are added.[3,26]

1.1.6. Effective core potentials

Computation time increases with the number of orbitals and electrons in the system. Considering that the core electrons do not participate in the molecular orbital formation, an additional approach named effective core potentials (ECP) is used for heavier atoms. In ECP the chemically inert core electrons are replaced with an effective potential and for valence electrons, nodeless pseudo-orbitals are generated so that their behaviour resembles all-electron valence orbitals. In this case the Schrödinger equation has the form[27]

$$\sum_{i=1}^{N} \{ \hat{h}_i + \hat{U}_l \} \chi_i = \left(\sum_{i=1}^{N} \varepsilon_i \right) \chi_i \tag{1.16}$$

where $\hat{h}_i$ is the valence one-electron Hamiltonian, $\hat{U}_l$ is the effective potential, χ_i is the valence pseudo-orbital, and ε_i is the energy of the i-th electron.

In general, the effective core potentials also incorporate relativistic effects that are particularly important for elements near the end of the periodic table.[27]

1.1.7. Analysis of electron density

1.1.7.1. The quantum theory of atoms in molecules

The quantum theory of atoms in molecules (QTAIM) is a model for dividing a molecular system into subsystems or atoms based on the electron density and its Laplacian. During a chemical reaction the uniform sphere of charge concentration

present in the valence shell of a free atom is distorted and local maxima and minima appear. The Laplacian determines where the charge is locally concentrated or depleted. Electron density is maximal at the position of nuclei and drops as one moves away from those positions (**Figure 1a**). Decay of electron density is uneven; between two bonded atoms lays a single line of locally maximal electron density that is called a bond path. The bond path is a universal indicator of chemical bonding of all kinds (weak, strong, closed-shell or open-shell interactions). The point on the bond path with the lowest value of the electron density is called a bond critical point. The distinctive property of a critical point is that the Laplacian at this point is the sum of three curvatures of density: the one through the bond path is positive and the other two perpendicular to the bond path are negative. At the bond critical point the bond path crosses over the interatomic surface separating the two atomic basins from each other. An interatomic surface is defined as a surface which does not cross any gradient vector field lines (**Figure 1b**).[28]

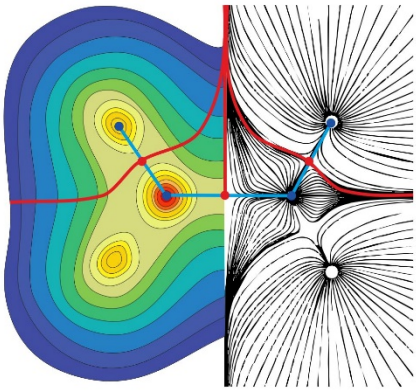

a) **b)**

Figure 1. a) The electron density plot of $H_2C{=}CH_2$; **b)** the Laplacian of electron density of $H_2C{=}CH_2$.[29]

Based on the electron topology, the QTAIM model enables to determine the bond order, the existence of intramolecular interactions or aromaticity, to predict atomic or group contributions to molecules' properties (heat of formation, polarizability), etc.[30]

1.1.8. Modelling of solvation

When the solvent structural information is not a subject of interest, the solute-solvent interaction is frequently modelled by implicit solvation models, where the solvent is represented by an infinite isotropic medium or a continuum. The continuum may be thought of as a configuration-averaged or time-averaged solvent environment.[31,32]

In implicit solvation models, the free energy of solvation consists of three terms: electrostatic energy (G_{el}), energy of interaction with solvent molecules (G_{SASA}), and

energy of cavitation (G_{cav}). Sometimes the two last terms are combined into one, the nonpolar solvation energy (G_{np}):[33]

$$G_{solv} = G_{el} + G_{SASA} + G_{cav} = G_{el} + G_{np} \tag{1.17}$$

1.1.8.1. Electrostatic term

The electrostatic term describes the mutual polarization of the solute and the solvent under the influence of the potential of each other. The solute's charge distribution induces an electrostatic potential field, which interacts with the solvent molecules, changing their orientation and polarizing them. The polarized solvent further polarizes the solute. In order to calculate mutual polarization of the solute and the solvent the charge distribution of the solute in gas-phase is calculated and inserted in the Poisson-Boltzmann equation (PB)[34], which is solved iteratively.[3]

$$\nabla(\epsilon\nabla\phi) = -\frac{4\pi\rho}{k_B T} + \epsilon\kappa^2\phi \tag{1.18}$$

Here ϵ is the dielectric constant, ϕ is the electric potential induced by the solute in the solvent, ρ is the electron density, k_B is the Boltzmann constant, T is the absolute temperature and κ is the distance at which an ion polarizes the solvent (Debye–Hückel length).

PB is best used to calculate the electrostatic potentials of solutes immersed in spherical or ellipsoidal cavities. Most commonly the Self-Consistent Reaction Field (SCRF) approximation is applied in order to solve the PB equation.[35] Cavities with more complex shape are needed for calculation of real solutes. Such calculations are more time consuming and complicated from a mathematical point of view.

There are two ways to treat the continuum: as a dielectric or as a conductor. In one of the most successful approaches for solvent description, the so-called polarizable continuum model (PCM), the continuum is considered as a dielectric.[35,36] Closely related to the PCM is the Poisson-Boltzmann model (PBF)[33,37] implemented in the Jaguar software[38]. Another widely used method, Conductor-like Screening Model (COSMO)[39] implemented, e.g., in the Turbomole software[40–42], considers the continuum as a conductor. However, in both cases it is necessary to solve the PB equation.

1.1.8.2. Nonelectrostatic term

Electrostatic energy describes changes in the solute induced by the solvent, but is not informative towards the interaction between solute and solvent molecules, although these interactions, such as dispersion, hydrogen bonding, hydrophobic effects (basicity-acidity), are far from negligible. In continuum solvation models solute-solvent interactions are usually described as a function of the solvent-accessible surface area (SASA). Since the number of solvent molecules interacting with the solute is proportional to the solvent-accessible surface area, it is assumed that the free energy of interaction between the solute and the solvent is also

proportional to it. This term of energy (ΔG_{SASA}) is parameterized against experiments.[43]

$$\Delta G_{SASA} = \sum_i b_i A \tag{1.19}$$

where b_i is the parameter of atom i, and A is the solvent accessible area.

One remaining term of solvation energy has not been discussed yet. It is the cavitation energy, the energy needed to create the cavity (an empty space in the solvent occupied by the solute). This energy term is also parameterized using the experimental data.[37]

1.1.9. Reaction path and transition state theory

When molecules collide, their kinetic energy can be converted into stretching and breaking of bonds, leading to chemical reactions and the transformation of reactants into products.[44] However not every reactant's geometry distortion ends with the formation of products. A reaction path describes the rearrangement of reactants (R) into products (P), and generally has one or several transition states (TS) (**Figure 2**). A TS is a configuration at the top of the energy barrier separating products from reactants. Reactions usually occur in more than one elementary step and accordingly have more than one TS. In such a case the TS with significantly higher activation energy (energy difference between the previous intermediate with the lowest energy and the TS) corresponds to the rate determining step (**Figure 2**, TS3).[45]

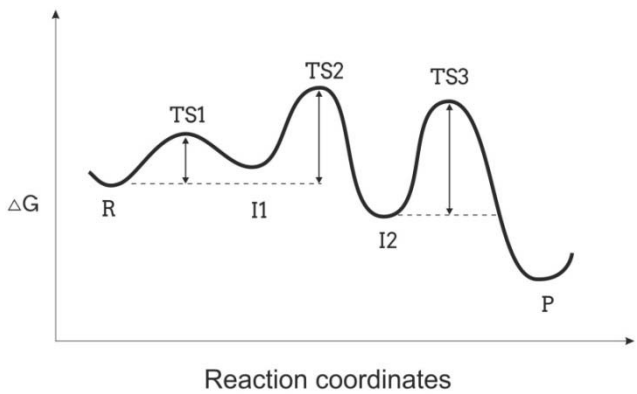

Figure 2. Gibbs free energy dependence on reaction progress.[46,47]

For any reaction to proceed, the reactants must have enough energy to break existing bonds and to cross over the highest energy barrier. A low energy barrier corresponds to a fast reaction; a high energy barrier corresponds to a slow reaction. If the reaction occurs in one elementary step, its reaction rate can be calculated as [48]

$$k = \frac{k_B T}{h} e^{(-\frac{\Delta G^{\ddagger}}{RT})} \tag{1.20}$$

where k is the rate constant, k_B is the Boltzmann constant, T is the absolute temperature, h is the Planck constant, $\Delta G^{\ddagger}$ is the Gibbs free energy difference between the TS and the prior ground state and R is the gas constant.

If reactants are converted into products stepwise, the system will also contain intermediates (I) (**Figure 2**), the population of which depends on their energy and can be calculated by the Boltzmann distribution equation.[45,48] In contrast to TSs, intermediates often have a longer life time and can be detected by spectroscopy.[49]

$$Q_i = \frac{e^{(-\frac{\Delta G_i}{RT})}}{\sum e^{(-\frac{\Delta G_i}{RT})}} \tag{1.21}$$

where Q_i is the probability of the intermediate and ΔG_i is the difference in Gibbs free energy between the intermediates and the lowest ground state.

The aim of study of a reaction mechanism is to find the lowest energy reaction path and attention should be paid here to both the TSs and intermediates. Search for the optimal reaction path is comparable with a search for an optimal mountain passing, but instead of mountains, a chemical reaction overcomes barriers on the potential energy surface (PES), which represents the potential energy altering caused by the change in geometry.[45]

On the PES, all reactants, products and intermediates are local minima which are comparable to valleys in mountains. Those minima can be mathematically characterized as[45,50–52]

$$\frac{\partial U}{\partial q} = 0; \tag{1.22}$$

$$\frac{\partial^2 U}{\partial q^2} > 0 \qquad \text{for all intrinsic coordinates} \tag{1.23}$$

where U is the potential energy and intrinsic coordinates such as bond lengths, bend and torsion angles are denoted by q. Any change in the position of atoms would lead to a deviation from the equilibrium causing an increase in potential energy.

Since any distortion of equilibrium causes a potential energy growth, conversion of reactants into products should have at least one point on the PES higher in energy than reactants and products and lying along the reaction path.[45] The geometry with the highest energy on the reaction path is the TS. It is a first order saddle point on the PES, a maximum along the reaction coordinate (intrinsic coordinates changing during reactants transformation into products) and a minimum along all other coordinates.[48,50,51]

$$\frac{\partial^2 U}{\partial q^2} < 0 \qquad \text{for one intrinsic coordinate} \tag{1.24}$$

$$\frac{\partial^2 U}{\partial q^2} > 0 \quad \text{for all other intrinsic coordinates} \quad (1.25)$$

The transformation of reactants into products occurs on the principle of least "action".[51] Thus, during the transformation only a few atoms change their relative positions. This reorganization is a guiding thread in the PES "mountains" leading from reactants to products through TS and can be plotted in energy profile diagram as a function of distance along the reaction coordinate (**Figure 3**).[45]

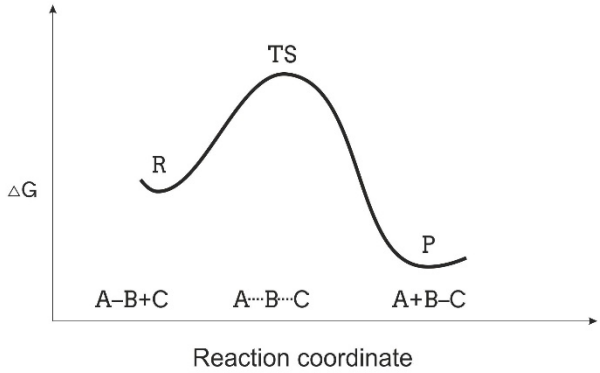

Figure 3. Gibbs free energy dependence on the reaction coordinate.[47]

Despite the simple description, finding the TS is not a trivial task. A good assistant in TS search is the intrinsic reaction coordinates (IRC) approach[50,51]. When a TS geometry is known, it is used as a starting point and the nearest equilibrium geometries are searched by IRC approach in order to confirm that the given TS is an actual TS between those two equilibrium geometries.

1.2. Catalysis

As it was said in the **Introduction** the active development of the chemical industry is closely related to the study and design of catalysts. A catalyst is a substance that accelerates the reaction by guiding it through alternative pathways with different transition states and lower activation barriers (**Figure 4**), thus, enables reactions blocked or slowed by a kinetic barrier. The catalyst acts on both the forward and the reverse reaction, therefore it does not change the extent of a reaction nor the chemical equilibrium. Another characteristic feature of a catalyst is that it is not consumed during the reaction.[44,49]

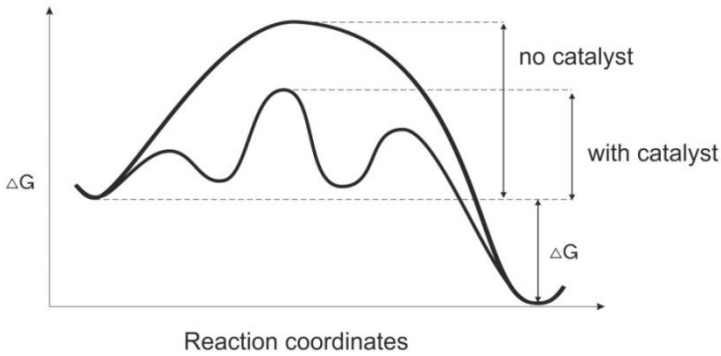

Figure 4. Gibbs free energy dependence on the presence or absence of catalyst.

Catalysts are widely used in nature and industry. Photosynthesis, oxygen transport and nitrogen binding in organisms, production of antibiotics, polyethylene synthesis and fuel production in industry – they all are catalytic processes. A survey of U.S. industries revealed that "more than 60% of the 63 major products and 90% of the 34 process innovations from 1930 to 1980 have involved catalysis".[2] In science catalysts also attract interest (**Figure 5**).

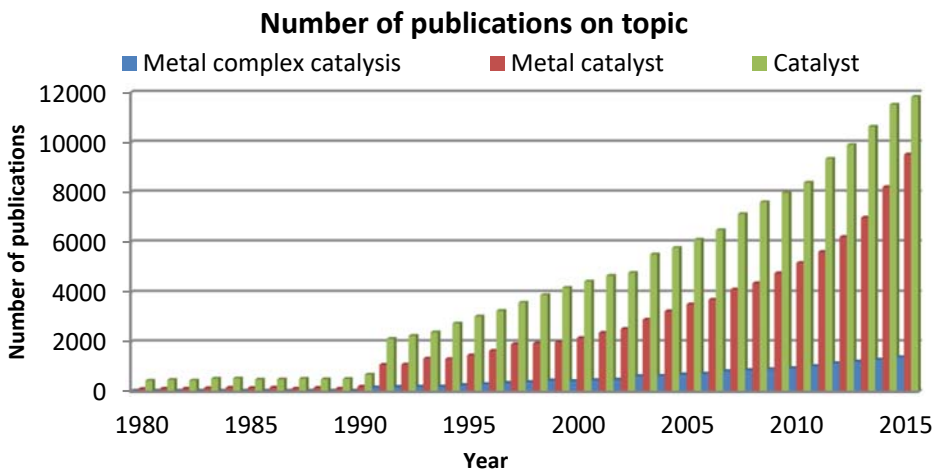

Figure 5. Number of articles published per year on the topic "catalyst".[53]

Design of catalysts is a challenging task since the ideal catalyst should simultaneously satisfy many requirements: be cheap and easy to prepare, to have a high catalytic activity (TOF) and to operate under mild conditions, to be easily separable from products and to have a big turnover number (TON) before poisoning. Moreover, every part of a catalytic system (solvent, reactants, the catalyst itself) influences the yield, selectivity and the rate of a reaction. In the case of catalysts based on a metal, characteristics of the metal, the number and nature of the ligands, as well as their position, all play a critical role in the catalytic properties of the complex.[54] A unique feature of organometallic complexes is that they can be manipulated molecularly by varying the ligands. Thus an understanding of the mechanisms in catalytic reactions and knowledge of metal-ligand, ligand-ligand co-influences will be of great importance in designing catalysts and optimizing reaction conditions.

1.2.1. Titanium-based catalysts

In the context of investigation of reactions catalysed by transition metal complexes titanium was chosen as a representative from the beginning of the periodic table and as one of the most abundant metals. Titanium is a first-row transition metal and it is the seventh most abundant metal on Earth. Titanium complexes are widely used as catalysts in organic, inorganic and polymer chemistry. The important virtues of titanium compounds are the low cost, high degrees of chemo- and stereoselectivity and low toxicity.[55]

Ti-based complexes are best known for their ability to catalyse C–C bond formation in such reactions as polymerisation, coupling reactions (where two hydrocarbon fragments are joined with the aid of a catalyst) and cyclization reactions.[55,56] Additionally, chiral titanium complexes catalyse the formation of bonds with high enantioselectivity. The Kulinkovich reaction[57] is an example of an enantioselective C–C bond formation and a cyclization reaction.

Ti-based catalysts can also be used for C–O[58], C–N[59–62] and C–H[63–65] bond formations in such reactions as epoxidation, hydroamination and isomerisation. Epoxidation of alkenes is a powerful tool for introducing oxygen into hydrocarbons. The Sharpless enantioselective epoxidation[66] was an important development that allowed the synthesis of chiral epoxides with good yield and high selectivity (> 90%).

1.2.1.1. Sharpless epoxidation

In 1980, Katsuki and Sharpless[66] reported the Ti-tartrate complex to be an efficient catalyst for enantioselective epoxidation of allylic alcohols, where peroxide was the oxidising agent. The kinetics and the reaction mechanism of the Sharpless epoxidation have been widely studied. Originally, in 1980, Sharpless proposed a monomeric titanium complex as a catalyst for epoxidation[67], but further investigations showed that the catalytic complex should be dimeric, so Sharpless and co-workers suggested a ten-membered cyclic Ti-tartrate complex as the catalytic species, analogous with the already known solid-state vanadium (IV)

tartrate complex[68] (**Scheme 1**). A year later, Ian *et al.*[69] reported another titanium complex with a dimeric structure based on X-ray data. The possibility of the dimeric complex dissociating into cationic and anionic complexes, where only the cationic species catalyses oxidation, has been studied by Corey[70]. However, the monomeric Ti-tartrate catalyst did not fit in with the kinetics of the reaction and all further investigations[69,71] have agreed that Sharpless epoxidation is catalysed by a dimeric six-coordinated Ti-tartrate complex (**Scheme 1b**).

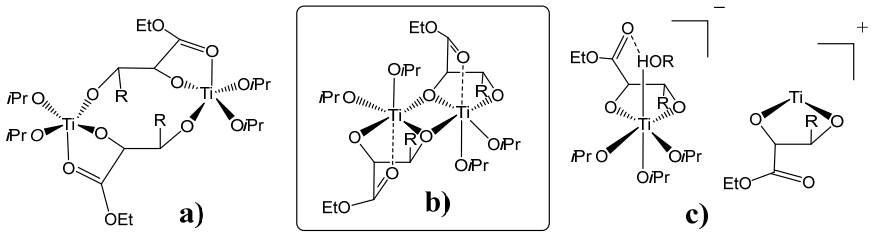

Scheme 1. Proposed structures of the Ti-tartrate catalyst in a Sharpless epoxidation reaction **a)** a ten-membered cyclic titanium complex[68]; **b)** a dimeric titanium complex based on X-ray data[67]; **c)** a cationic titanium catalyst[70]. R=C(O)OEt.

The roles of peroxide, tartrate as well as substituents in allylic alcohol have also been carefully considered.[72,73] Those studies included several computational investigations.[74–76] Jørgensen *et al.*[74] showed that peroxide binds to titanium in such a way that the hydrogen of peroxide situates in axial position and is directed away from the Ti–O bridging bond, as depicted in **Scheme 2a**. The isomer, where the hydrogen of peroxide is directed away from the Ti–O bridging bond, is by 9.9 kcal mol^{-1} more stable than the sterically less crowded isomer with the peroxide hydrogen in equatorial position.[74] Moreover, in the isomer depicted in **Scheme 2a**, the bond between titanium and the equatorial oxygen of peroxide is already weakened, facilitating oxidation. Investigations by Wu and Lai[75] confirmed that axial position of the hydrogen of peroxide is more favourable, explaining this by absence of repulsion between lone pairs of the peroxide oxygen and the nearest diolate oxygen.

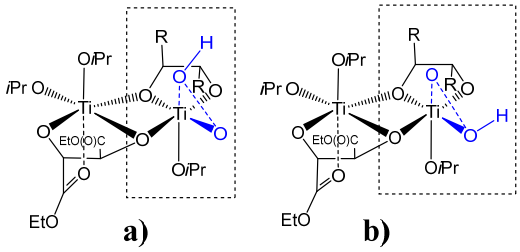

Scheme 2. Feasible positions of the peroxide in a dimeric Ti-tartrate complex.[74] R=C(O)H.

Different possibilities for allylic alcohol association to the titanium complex were also discussed.[73,75–77] The enantiomer with the lowest energy is depicted in **Scheme 3a**. This position of the alcohol is caused by the decrease of steric interactions between bulky peroxide and formyl groups of tartrate.[75,76] Experimental

studies also agreed with the conclusion that the size of peroxide and formyl groups determine the selectivity of the reaction.[73,77]

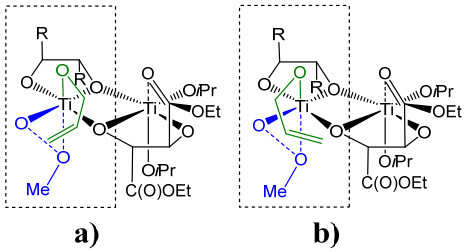

Scheme 3. Feasible positions of the allylic alcohol.[75,76] R= C(O)H.

Oxygen transfer to the alcohol has also been discussed. Bach *et al.*[78] found that the spiro orientation of the double bond relative to the titanium-peroxide plane is by 1.0 kcal mol^{-1} more stable than a planar one (**Scheme 4**). Jørgensen *et al.*[74] reported a difference of 14.3 kcal mol^{-1} between spiro and planar configurations. He explained this difference in energy with the additional stabilization of the spiro isomer due to the interaction between the oxygen lone pair and the π* orbital of alkene. Wu and Lai[75] confirmed that the spiro configuration is lower in energy (by 3.0 kcal mol^{-1}) and this is in accord with the observation that the R′ substituent has little influence on the enantioselectivity, but varying the R″ substituent can cause some reduction in enantioselectivity[72]. Cui *et al.*[79] came to the same conclusions by studying the influence of substituents on diastereoselectivity.

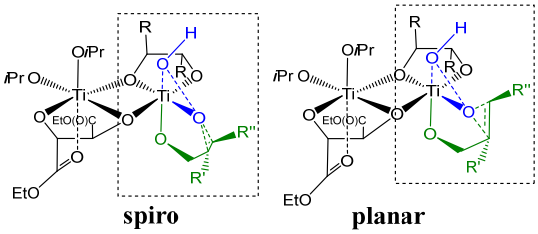

Scheme 4. Feasible orientations of the allylic alcohol in a dimeric Ti-tartrate complex.[74,75] R= C(O)H.

In 1995, Wu and Lai[75,76] proposed a reaction mechanism for the Sharpless enantioselective epoxidation based on the performed calculations (**Scheme 5**). Titanium tetraisopropoxide reacts with diethyl tartrate and a catalytic dimeric complex is formed. This is followed by a consistent association of peroxide and allylic alcohol (**Steps I and II**). Next, the equatorial oxygen is transferred to allylic moiety in order to form the epoxide (**Step III**), and finally the catalyst is regenerated by ligand exchange (**Step IV**).

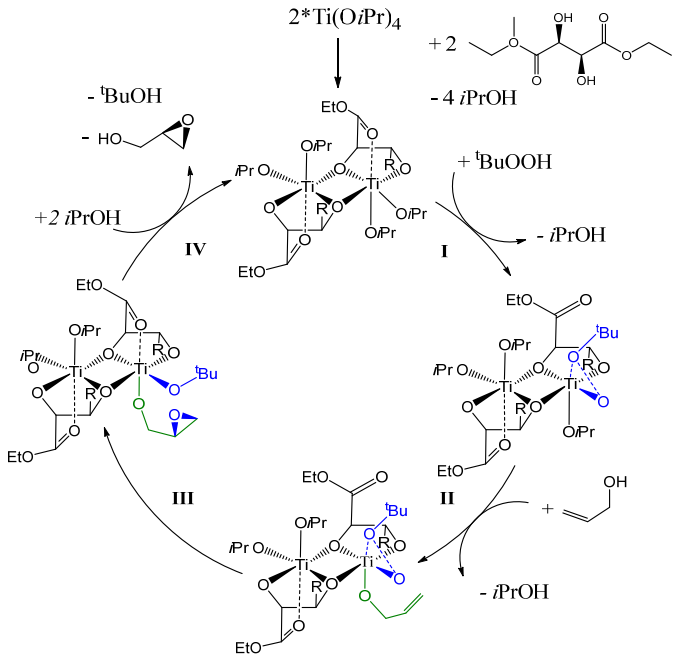

Scheme 5. Mechanism of the Sharpless epoxidation.[75,76] (R=C(O)OEt).

1.2.1.2. Kulinkovich reaction

The Kulinkovich reaction[57] is an example of C–C bond formation and a cyclisation reaction catalysed by titanium complexes. In the presence of a titanium(IV) alkoxide, esters (amides, and other carboxylic acid derivatives) react with two equivalents of a Grignard reagent (or its higher homologues) forming cyclopropane derivatives.[80–84] The first reaction mechanism was postulated by Kulinkovich *et al.*[85] in 1990 (**Scheme 6**). It was stated that the key step of this reaction is the formation of titanacyclopropane. This occurs when two equivalents of an organomagnesium bromide react with Ti(O*i*Pr)$_4$ (**Steps I and II, Scheme 6**).[86] The formation of diisopropoxytitanacyclopropane is followed by ester insertion (**Step III, Scheme 6**). Subsequently the oxatitanacyclopropane is transformed into titanium cyclopropoxide (**Step V**) accompanied by the migration of the alkoxide group of cyclopropane at titanium (**Step IV**). Analysis of by-products and deuterium insertion into products confirmed the proposed reaction mechanism.[80]

In 2001, the reaction mechanism was studied computationally by Wu and Yu[87]. Titanium (IV) methoxide was used as a model compound since a methyl substituent is less demanding of computational resources. However not all steric effects can be simulated with just a methyl group. The authors[87] carefully investigated the insertion of an ester into the titanium complex and the formation of the five-membered ring (**Step III, Scheme 6**). It was found that the formation of *cis* cyclopropanols had lower energy barriers, including the rate limiting step of ring closure (**Step V, Scheme 6**). ΔE for the *cis* isomer was 18.0 kcal mol^{-1}, and 20.5 kcal mol^{-1} for *trans*. The authors[87] explained the difference in energy by the

agostic stabilization (formation of Ti–H bond) in the *cis* complex (**Figure 6**). This stabilization could account for the preferable formation of *cis*-cyclopropanols observed in experiment. However, it does not explicate why three equivalents of organomagnesium bromide are needed for the reaction.

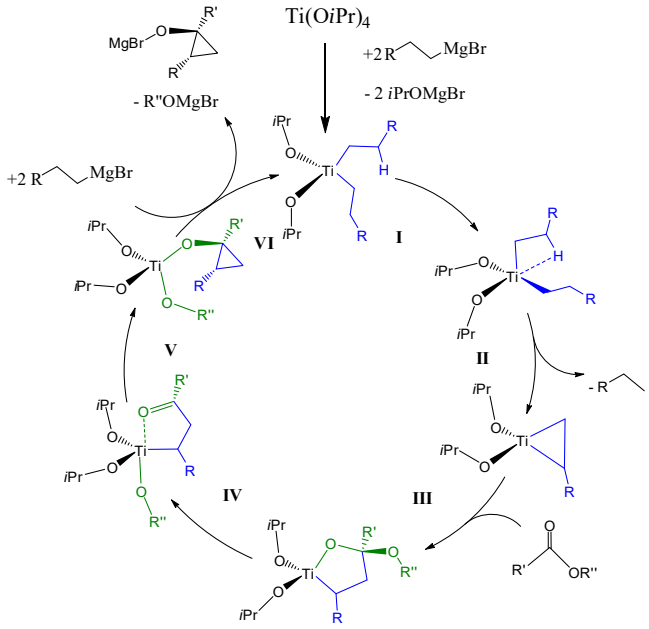

Scheme 6. Originally proposed reaction mechanism for the Kulinkovich reaction.[85]

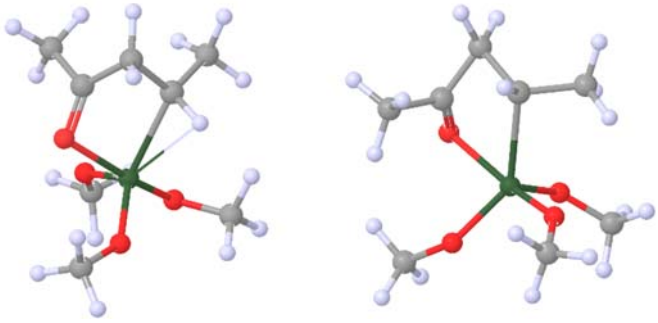

Figure 6. Transition states for the formation of *cis* (left) and *trans* (right) isomers in the ring closing step.[87]

In 2007, an up-date of the original reaction mechanism was proposed by Kulinkovich *et al.*[88]. This mechanism explains why three equivalents of organomagnesium bromide are necessary. The main feature of the mechanism is the formation of the highly coordinated titanium ate-complex intermediates instead of tetracoordinated species (**Scheme 7**). In the update mechanism the formation of titanacyclopropane is accompanied by the association of an ester (**Step I**). Next, complex is attacked by the third equivalent of organomagnesium compound (**Step II**) which enhances nucleophilicity of carbons in titanacyclopropane. The subsequent cyclopropane ring closure (**Step IV**) affords cyclopropoxide ate-

complex which in the absence of carboxylic ester substrate rapidly degrades to form catalytically inactive Ti^{III} complex.

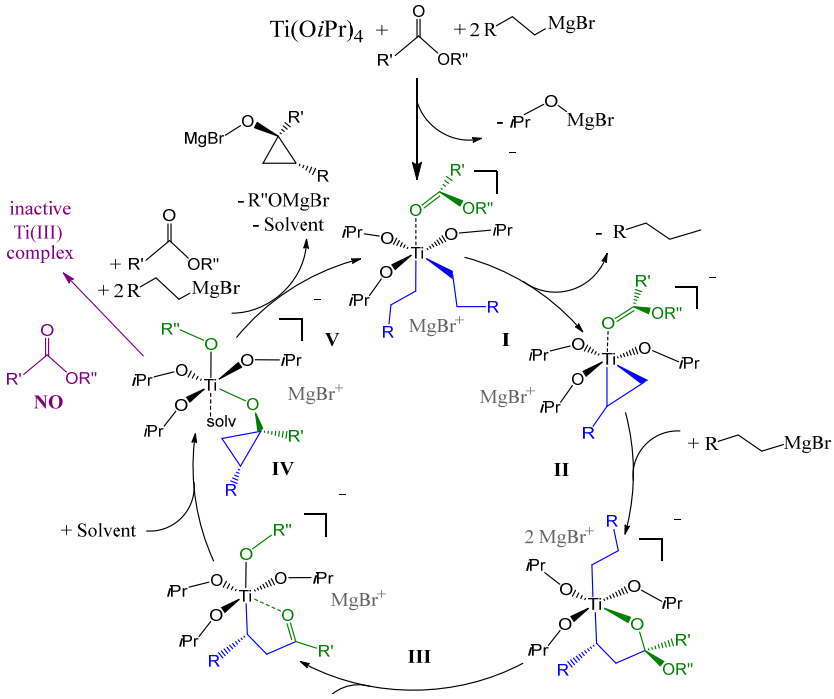

Scheme 7. Ate-complex reaction mechanism for the Kulinkovich reaction.[88]

The origin of high *cis*-diastereoselectivity was explained by Kulinkovich *et al.*[89] *via* a repulsive interaction between the ligands of highly coordinated titanium and the R″ substituent in the transition state of cyclopropane ring closure (**Scheme 8**).

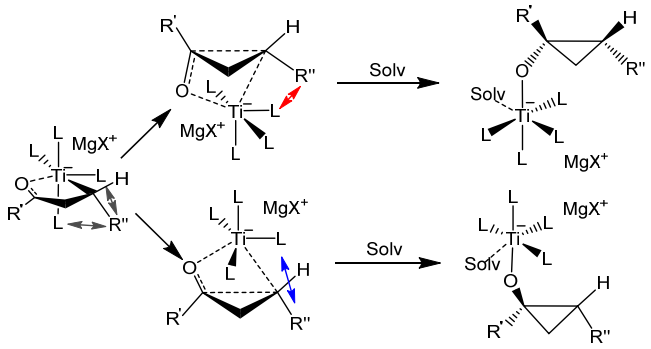

Scheme 8. Steric hindrance in different transition states of the titanium complexes.[89]

The Kulinkovich reaction usually produces 1,2-disubstitited cyclopropanols with high yield (of up to 91%) and cis-diastereoselectivity (up to 96%).[89] In order to induce enantioselectivity, instead of achiral Ti(O*i*Pr)$_4$, the chiral titanium TADDOLate complex has been used. First it was done by Corey *et al.*[90] in 1994. Corey reported the formation of cyclopropanol derivatives with a yield of 65–72%

and an enantioselectivity of 70–78% *ee*. After unsuccessful attempts[91] Kulinkovich and co-wokers[92] reported formation of chiral cyclopropanol derivatives with a yield of 50–70% and enantiomeric excess up to 65% *ee*. Moreover, Kulinkovich et al.[93] found that the titanium TADDOLate complex is more resistant towards reduction with an excess of Grignard reagents than Ti^{IV} isopropoxide complex. The enantioselectivity was further enhanced (up to 84% ee) using hexafluoroisopropyl esters as the substrates.[93]

In 2014, Kulinkovich *et al.*[93] for the first time experimentally confirmed that intermediates are indeed pentacoordinated titanium ate-complexes. The origin of enantioselectivity in the reaction has been explained by the steric repulsion from the bulky TADDOL ligand.[93] It was assumed that the TADDOL ligand is situated in the equatorial-equatorial position in the penta-coordinated titanium complex and prevents the formation of all titanacyclopropane isomers except one (**Scheme 9**).

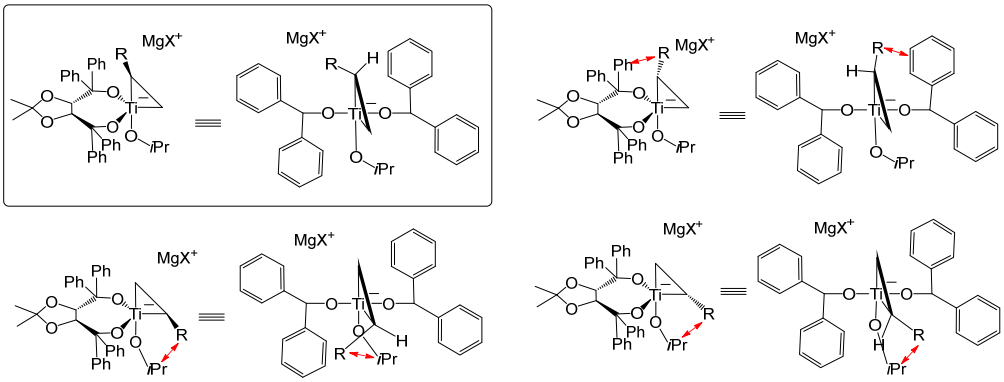

Scheme 9. Four isomers of the titanacyclopropane complex.[93]

1.2.2. Iridium-based catalysts

Iridium was chosen as a second object of the present study as a representative from the end of the periodic table and as a member of the noble metals family. Iridium is a third-row transition metal, a member of the platinum-group of precious metals and a relatively rare element. Iridium is mostly used for electrical and electrochemical applications and about 20% of it is used in the chemical industry.[94] One of the largest-scale Ir-catalysed processes is the carbonylation of methanol by the $[Ir(CO)_2I_2]^-$ complex in acetic acid production.[95]

Ir-based complexes are known for their ability to catalyse hydrogen transfer reactions.[96–98] They are efficient in both hydrogenation and dehydrogenation reactions, and are used in such reactions as the alkylation of ketones[99,100] and amines[99,101], dehydrogenation of alkanes[101], as well as reduction of imines[102], ketones[101,103] and olefins[104].

Recently a lot of attention is being paid to the hydrogenation of CO_2.[105] On one hand this is related to the desire to reduce the concentration of CO_2 in the atmosphere,[106,107] but on the other hand, CO_2 is a very attractive carbon source because of its low cost, high abundance and low toxicity.[105,107] Unfortunately, CO_2

needs a high activation energy and nowadays its use is limited to syntheses of a few products such as urea and its derivatives, salicylic acids and carbonates.[107,108] Still incessant attempts are being made to hydrogenate CO_2 and convert it into CO, methanol, formic acid and many other useful organic compounds.[107,109]

Among the various CO_2 reductions, hydrogenation of CO_2 to formic acid is a particularly attractive process due to its small endergonicity[110] and potentially wide range of applications. Formic acid can be used as a raw material for many syntheses or production of renewable fuels.[105,107–109,111]

1.2.2.1. CO_2 hydrogenation by the (PNP)Ir pincer complex

In 2009, Tanaka *et al.*[112] found a new, very efficient catalyst for CO_2 reduction to acetic acid, an Ir^{III} pincer complex (PNP)IrH_3. In aqueous KOH, under the pressure of 5 atm and at the temperature of 200 °C, (PNP)IrH_3 showed TOF of 150 000 h^{-1} and TON of 300 000. Experimental investigation of the CO_2 hydrogenation by the (PNP)IrH_3 complex was done mainly with NMR spectroscopy. Based on the identified species Tanaka *et al.*[112] proposed a reaction mechanism consisting of three main steps (**Scheme 10**):

I CO_2 reduction to formate;

II formate release and dearomatization of the PNP ligand ring;

III catalyst regeneration by hydrogen splitting.

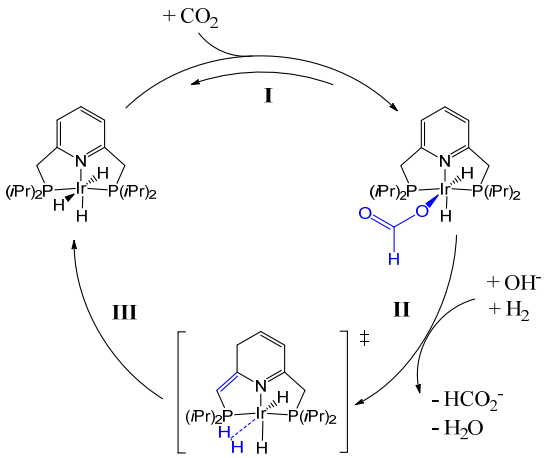

Scheme 10. Originally proposed catalytic cycle.[112]

Computational investigation of this reaction was also performed and all researchers agreed that the catalytic cycle starts from a CO_2 attack on one of the axial hydride ligands of the (PNP)IrH_3 complex (**Scheme 11**).[113–116]

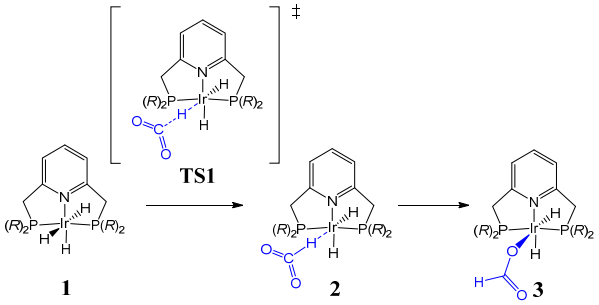

Scheme 11. CO_2 hydrogenation by the (PNP)IrH_3 complex (R = H in Ahlquist investigation and R = *i*Pr in all others).[113–116]

For catalyst regeneration several pathways were suggested by different explorer groups.[113–116] Ahlquist proposed that after the cleavage of formate, H_2 coordinates to the vacant site on Ir^{III} and this complex is deprotonated by a hydroxide anion from solution (**Scheme 12**). The activation free energy for catalyst regeneration is 26.1 kcal mol^{-1}.[113]

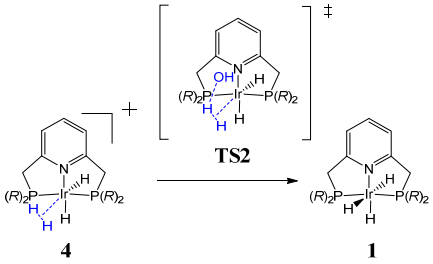

Scheme 12. Regeneration of catalyst through deprotonation by a hydroxide anion from solution (R = H in Ahlquist investigation and R = *i*Pr in all others).[113–116]

Tanaka *et al.*[112] proposed that catalyst regeneration occurs through the deprotonation of the methylene group of the PNP ligand and ring dearomatization (**TS3, Scheme 13**). A hydroxide anion from the solution replaces the formate ligand (**5**), abstracts one proton from the methylene group (**6**) and the formed H_2O cleaves (**7**). Next, H_2 binds to the vacant coordination site and is split. (**TS4**).[116]

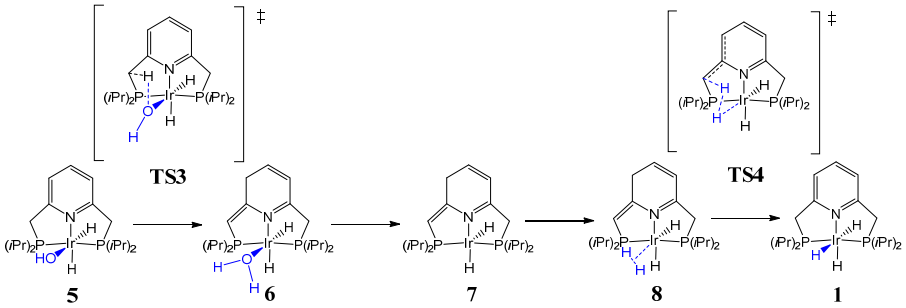

Scheme 13. Regeneration of catalyst through ring dearomatization proposed by Tanaka *et al.*[112]

The pathway in which the associated hydrogen is split by the hydroxide anion from solution (**Scheme 12**) was also considered by Tanaka and co-workers.[116] It was found that regardless of the pathway, the energy needed for catalyst regeneration is approximately the same (14.4 kcal mol^{-1} and 12.7 kcal mol^{-1} respectively). This is in disagreement with the research by Yang[114], who showed that the pathway through ring dearomatization is by 20.0 kcal mol^{-1} higher in enthalpy than the pathway where hydrogen is split by the hydroxide anion. Li and Yoshizawa[115] also studied this catalytic system and reported that catalyst regeneration goes through ring dearomatization.

Ahlquist[113] proposed one more pathway for the catalyst regeneration (**Scheme 14**), but 35.4 kcal mol^{-1} was needed for Ir^{III} reduction to Ir^{I} (**TS5**), that is much higher than in the cases considered above.

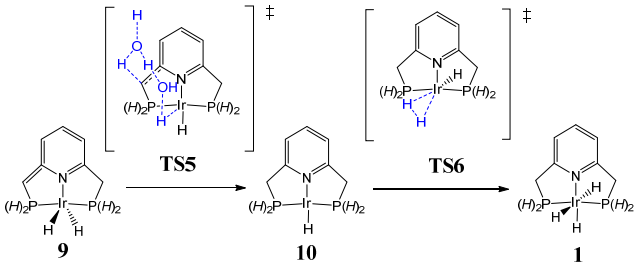

Scheme 14. Regeneration of catalyst through Ir^{III} reduction to Ir^{I}.[113]

Unfortunately, direct comparison of those studies is difficult because different calculation techniques and kinds of energy (*ΔE, ΔH* or *ΔG*) were used. However, all studies agree that regeneration of the (PNP)IrH_3 catalyst is the rate determining step of the reaction.[113–116]

1.2.2.2. CO_2 hydrogenation by the (PNP)Ir pincer complex

In 2012, Kang *et al.*[117] reported (PCP)IrH_2 complex as an efficient catalyst for CO_2 reduction to formate. In an acetonitrile-water solution at a potential of −1.4 V at a glassy carbon electrode, (PCP)IrH_2 had selectivity up to 85%. A year later a water-soluble analogue of the iridium pincer complex was proposed,[118] and in 2014 the (PCP)IrH_2 catalyst immobilized on carbon nanotube electrodes was reported.[119] In water solution (1% vol acetonitrile) at potentials between −1.1 V and −1.4 V *vs.* normal hydrogen electrode (NHE) it gave TON of 203 000 and selectivity of up to 96%.

Based on NMR data and cyclic voltammograms, a reaction mechanism was proposed.[117] (PCP)IrH_2 complex activation is followed by a catalytic cycle that consists of three main steps (**Scheme 15**):

I CO_2 reduction to formate;

II formate release and association of a second acetonitrile molecule;

III catalyst regeneration by water splitting.

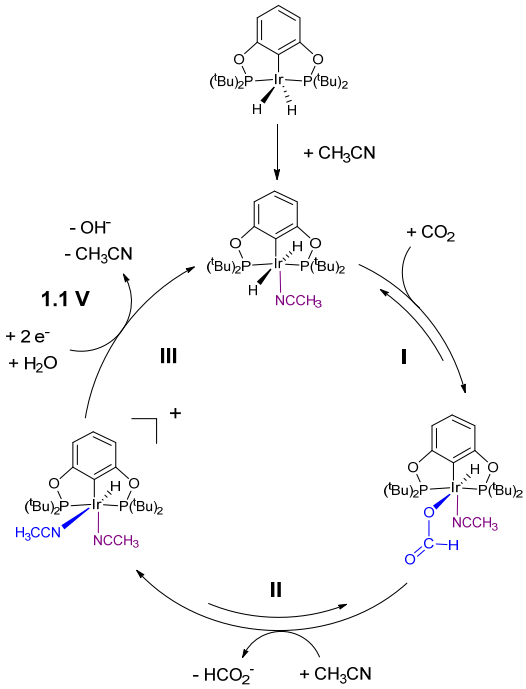

Scheme 15. Originally proposed catalytic cycle .[117]

This reaction mechanism was computationally investigated by Cao *et al.*[120] in 2013. The barrier for CO_2 insertion into (PCP)IrH_2($NCCH_3$) complex was found to be 14.4 kcal mol^{-1} in water and 17.4 kcal mol^{-1} in acetonitrile (**Step I, Scheme 15, Scheme 16**). CO_2 reduction is followed by formation of (PCP)IrH_2(OCHO) complex and formate exchange to acetonitrile (**Scheme 16**). Formation of complex **14** is endergonic by 3.4 kcal mol^{-1} (6.5 kcal mol^{-1} in acetonitrile) and formation of complex **15** is exergonic by 12.7 kcal mol^{-1} (−6.6 kcal mol^{-1} in acetonitrile).

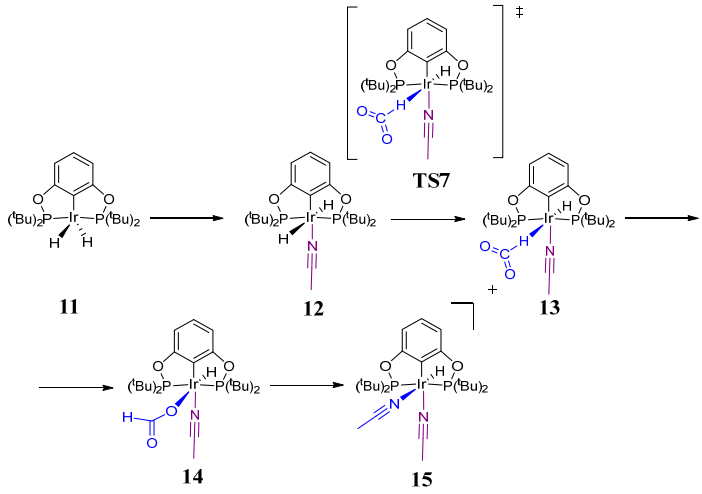

Scheme 16. CO_2 hydrogenation by the (PCP)IrH_2($NCCH_3$) complex.

After the reaction has occurred, it is necessary to regenerate the catalyst (**Step III, Scheme 15**). Kang *et al.*[117] reported that catalyst regeneration proceeds between −1.1 V and −1.4 V *vs*. NHE[118] and is a two-electron, one-proton reduction, where water is the proton source. Cao *et al.*[120] found that catalyst regeneration occurs through the intermediate $[(PCP)IrH(NCCH_3)]^-$ (**Scheme 17**) formed by accepting of two electrons at −1.5 V and simultaneous dissociation of one acetonitrile ligand. Formation of $[(PCP)IrH(NCCH_3)]^-$ is followed by water splitting by another CO_2 molecule with free-energy barrier of 26.0 kcal mol^{-1} (28.5 kcal mol^{-1} in acetonitrile). According to computational data, water as a solvent facilitates the reaction, which is in agreement with experiments.[118]

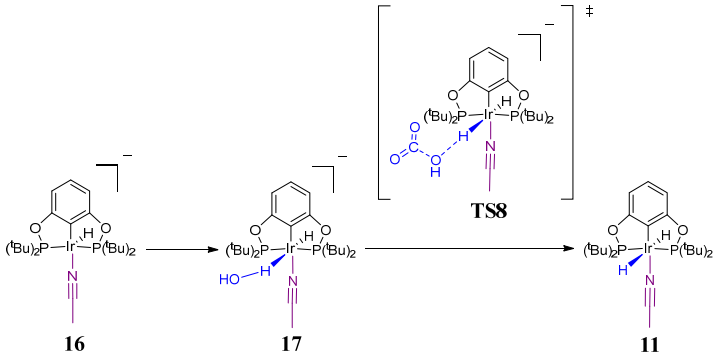

Scheme 17. Regeneration of catalytic complex.[120]

However, it should be mentioned that Kang *et al.*[118] reported that CO_2 insertion into Ir−H bond is the rate-limiting step in contrast to the finding of Cao *et al.*[120].

2. AIMS OF THE PRESENT WORK

Computational modelling using quantum chemistry enables us to examine reaction mechanisms in great detail and gives us a possibility for faster and in-depth study of mutual influence of different parts in the catalytic complex. The aim of the present study is the investigation of titanium and iridium complexes and some typical reactions, where they are involved: the complexation of cyclopentane-1,2-dione with $Ti(O\mathit{i}Pr)_4$, the formation of titanium TADDOLate complexes in the Kulinkovich reaction, and CO_2 reduction catalysed by (PNP)Ir and (PCP)Ir pincer complexes.

Emphasis was placed on:

- Study of reaction mechanisms proposed on the basis of NMR data.
- Search for alternative reaction pathways.
- Examination of titanium and iridium metal cation characteristics such as coordination number and oxidation state.
- Analysis of geometries (including *cis-, trans-* and chelate effects, and steric repulsion).
- Consideration of factors such as charge transfer and donor-acceptor interactions.
- Observation of transition state features caused by varying of ligands, geometry or oxidation state.

3. METHODS

3.1 Exchange-correlation functionals

The geometry optimization process is usually not sensitive to the choice of a functional[121,122] nor basis set[121]. The opposite is true for energy that is very sensitive to the choice of a functional[25,123] and basis set[20].

For geometry optimization of rigid molecules (Ir complexes) with small number of conformers, the time-tested B3LYP[18] functional was used, followed by single point calculations with the M06[19] functional to obtain more accurate energies. The M06 has been specially parameterized for treatment of metals and TS calculations and also accounts for short- and medium-range dispersion effects.[19]

In the case of time-demanding conformational searches in flexible systems (Ti complexes), the BP86[13,14] functional was used. It has also been recommended for treatment of metals[123,124], and can be used with the Resolution of identity (RI) approximation[125–127], speeding up the calculations. In order to account for dispersion effects in aryl groups, the dispersion-corrected version of this functional (BP86-D3[25]) was used.

3.2 Resolution of identity approach

The calculation of the Coulomb integrals is a time-demanding bottleneck in DFT calculations. In the RI approximation[125], electron density is expanded in an auxiliary basis set. The number of functions used for system treatment decreases, which usually leads to a more than tenfold speedup for non–hybrid DFT compared to the conventional method.[128,129]

3.3 Basis sets

As indicated above, geometry is not very sensitive to the choice of basis set. In order to speed up geometry optimization, small basis sets such as SV(P)[130] (quality similar to 6-31G*[131])[40–42] or LACVP**[27] (quality similar to 6-31G**[131])[38] were used.

For accurate energy calculations, larger basis sets such as def2-TZVP[127] (quality is slightly better than 6-311G**[132])[40–42] or LACV3P**++[133] (quality similar to 6-311G**++[134])[38], augmented with two *f* functions on Ir as suggested by Martin[135], were used.

For heavy atoms beyond Kr the LAC basis sets and effective core potentials (ECP) were employed.[133] LAC basis sets are designed to work together with ECPs which account for relativistic effects. The latter are particularly significant for heavy atoms. For non-metals, the LAC basis contains the highest *s* and *p* shells, and for transition metals, the highest *s*, *p* and *d* shells.[27]

3.4 Natural bond orbital analysis

The natural bond orbital (NBO)[136] method uses the one-electron density matrix to localize electrons into atomic orbitals. As a result, the molecular wave function can be reduced to a formal Lewis structure and atomic charges as well as orbitals involved in the bonding can be defined.[48]

3.5 Modelling of solvation

For description of solvent effects, continuum polarization models were used: BPF[33] as implemented in Jaguar[38] and COSMO[137] as implemented in Turbomole[40–42].

In the case of rigid molecules (Ir complexes), single point calculations with B3LYP/LACVP** level of theory were made in order to include solvent effects and free energy of solvation was summed with energy of the optimized gas-phase structure. Such a treatment is a good approximation for relatively rigid molecules.[34] In the case of flexible molecules (Ti complexes), optimization was done either in gas phase or in solvent using BP86/def2-TZVP level of theory.

For modelling of water, the dielectric constant (ϵ) of 80.37 and probe radius of 1.4 (default settings) were used. For $CDCl_3$, the permittivity constant (ε) of 4.81[138] and a probe optimized radius were used. In the case of Ti TADDOLates, only gas-phase calculations were done since the influence of apolar solvent on the stability of complexes is insignificant.

Since uncertainties in the aqueous solvation free energies for ionic solutes are greater,[139] for small molecules and ions experimental solvation energies were used.[140]

In order to incorporate the specific solute-solvent effects, explicit solvent molecule(s) were added into continuum solvent calculations.

3.6 Transition state search

The TS search was preformed via relaxed potential energy surface scan over the corresponding reaction coordinate. The TS was determined as the highest-energy point in the energy profile between reactant and product. The geometry was then additionally optimized as TS and harmonic frequency calculations were done (B3LYP/ LACVP**). The TS has a single imaginary frequency in contrast to local minima that have all real frequencies. Finally, TS were confirmed by IRC calculations.

In the cases when solvent could stabilize a transition state, explicit solvent molecule(s) were added in gas phase calculations.

3.7 Software

All calculations were performed using Turbomole 5.10[40,41], 6.5[40,42] and Jaguar 7.5[38] program packages.

The presence of a chemical bond was tested by performing an atoms-in-molecules[28] analysis with the AIMAll[141] software.

4. RESULTS AND DISCUSSION

The aim of present study is the investigation of titanium and iridium complexes and the reactions catalysed by them. For this purpose two typical reactions for each transition metal will be considered:

- complexation of 3-methylcyclopentane-1,2-dione with Ti(O*i*Pr)$_4$;
- formation of titanium TADDOLate complexes;
- CO_2 reduction catalysed by (PNP)Ir complexes;
- electrochemical CO_2 reduction catalysed by (PCP)Ir complexes.

The subsequent sections are all structured similarly. The section starts with the description of structures and reaction mechanisms. Then, analysis of coordination number of metals follows. Next, the co-influence of ligands (such as *trans*-, *cis*- and chelate effects) will be discussed and, finally, transition states in reactions of CO_2 with iridium complexes will be analysed, in order to understand influence of geometry and partial charge on the energy.

4.1. Complexation of cyclopentane-1,2-dione with Ti(O*i*Pr)$_4$

4.1.1. Structures and reaction mechanism

The mechanism of an asymmetric oxidation cascade reaction catalysed by a Ti-based catalyst had been studied experimentally using 3-phenylcyclopentane-1,2-dione **1** as a substrate, where tert-butyl hydroperoxide was used as an oxidant (**Scheme 18**).[142] It had been shown that the first step of the reaction (the formation of **2** through the Sharpless epoxidation[66]) is the rate-limiting step (**Scheme 18**).[142]

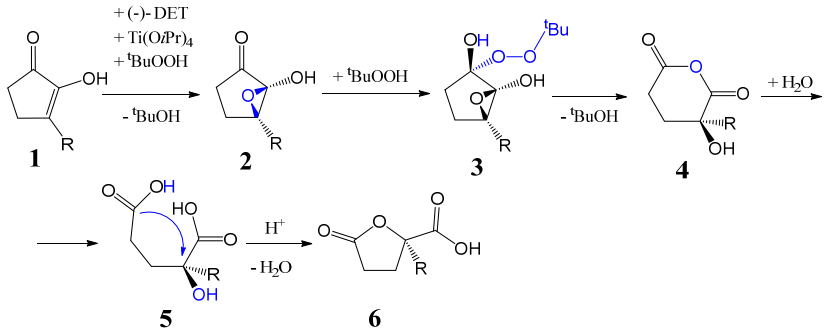

Scheme 18. Proposed catalytic cycle for asymmetric oxidation cascade reaction.

Moreover, NMR studies had shown that when Ti(O*i*Pr)$_4$ was mixed with 3-methylcyclopentane-1,2-dione **1** (hereafter called "substrate" or "Sub") or simultaneously with compound **1** and diisopropyl tartrate, the formation of the hexa-coordinated intermediate Ti(O*i*Pr)$_2$(Sub-κ^{2}O,O)$_2$ (**8**) occurs (**Scheme 19**).[143] No mono-substituted titanium complexes had been observed in the reaction mixture in deuterated chloroform ($CDCl_3$) at –20 °C.[143,144] Our investigation (Paper I) provided computational support for this observation. For the computational study, Ti(O*i*Pr)$_4$ + 3-methylcyclopentane-1,2-dione was used as a model system.

Calculations showed that the formation of bi-substituted complex **8** is energetically the most favourable among the substituted titanium complexes. Complex **8** is by 3.7 kcal mol^{-1} lower in Gibbs free energy than complex **7** and by 3.8 kcal mol^{-1} lower than the reactants (**Scheme 19**).

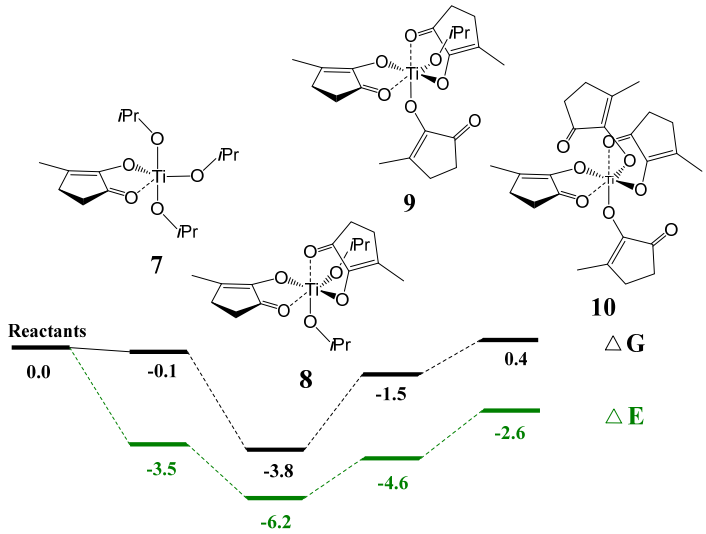

Scheme 19. Relative energies of Ti-substituted complexes (in kcal mol^{-1}).

The energy of formation of the tri-substituted titanium complex **9** is higher than the energy of formation of complex **8** by 2.3 kcal mol^{-1}. This is in agreement with experiment. Complex **9** is observed only in the case of high concentration of **1** when molar ratio of cyclopentanedione to Ti(O*i*Pr)$_4$ is 3:1 or 4:1. At molar ratio 4:1 traces of four-substituted titanium complex **10** were also found. Calculations showed that complex **10** is by 0.4 kcal mol^{-1} higher than the reactants. It should also be mentioned that, regardless of the substitution number, only two cyclopentanedione ligands are bidentate and in complexes **9** and **10** some substrate ligands are mono- and some are bidentate.

The ability of cyclopentanedione to form a stable bi-substituted hexa-coordinated titanium complex (**8**) where cyclopentanedione is coordinated in bidentate fashion, prevents the formation of catalytic species. In order to avoid this, substrate should be added after addition of tartrate when Sharpless catalyst has already been formed.

4.1.2. Coordination number of metal

One of the reasons for the coordination number growth from four in Ti(O*i*Pr)$_4$ to six in complex **8** is donor-acceptor interactions of ligands. Isopropoxy ligands are both σ- and π-donors and each donates four electrons to the electron-poor Ti^{IV}. This π-donation causes relatively large Ti–O–H angles (133°, 142°) in the model system Ti(OH)$_3$(η^2-O$_2$H).[75] In Ti(O*i*Pr)$_4$, the Ti–O–*i*Pr angles were 143° and 147°, in Ti(O*i*Pr)$_3$(Sub-κ^{2}O,O) they were 140°, 143° and 144°, and in Ti(O*i*Pr)$_2$(Sub-κ^{2}O,O)$_2$, 141° and 143°.[143] The carbonyl group of cyclopentanedione is a σ-donor

and also a π-acceptor, thus the coordination of **1** in bidentate fashion decreases electron density at titanium and stabilizes the formed complex. This may explain the formation of a thermoneutral (–0.1 kcal mol^{-1}) penta-coordinated complex **7**. The addition of a second cyclopentanedione ligand further stabilizes the complex by decreasing electron density at titanium.

The transformation of $Ti(OiPr)_4$ into a hexa-coordinated complex **8** is also favoured by the steric factors: the small size of oxygen atoms through which isopropoxy and cyclopentanedione ligands coordinate to titanium, the relatively small size of ligands and the fact that for bidentate coordination to titanium, the compound **1** undergoes only minor geometric transformations (**Figure 7**).[145]

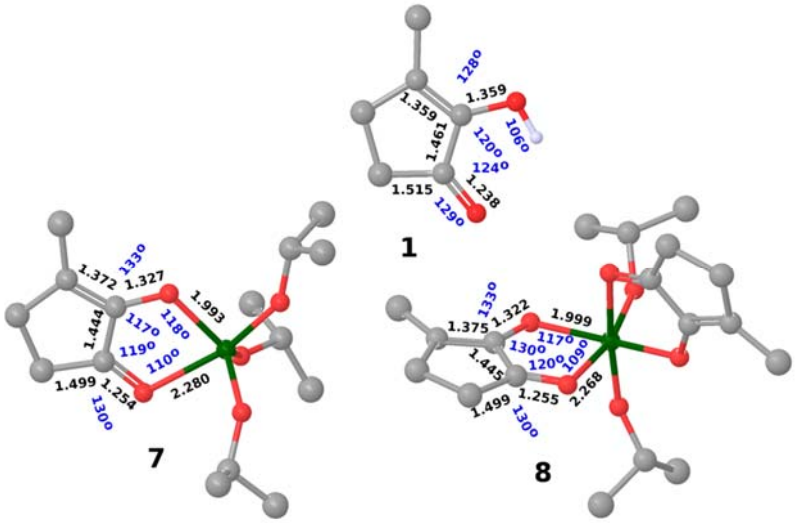

Figure 7. Changes in the geometry of cyclopentanedione in complexes **7** and **8**. Hydrogen atoms, which are irrelevant for the reaction, have been removed for clarity.

Further replacement of isopropoxy ligands with cyclopentanediones results in the hexa-coordinated complexes **9** and **10**, where only two substrate ligands are coordinated in bidentate fashion and neither hepta- nor octa-coordinated complexes were found during the conformational search. The reason for this may be steric factors. Ti atom has small size, but with coordination number growth ligand-ligand distances become smaller and repulsion becomes stronger. High coordination numbers can be observed only in the case of metals with big radii surrounded by small ligands.[145]

The fact that the coordination number in complexes **8**, **9** and **10** remains six, regardless of the number of cyclopentanedione ligands coordinated to titanium, can also be explained by the 18-electron rule. According to this rule, titanium is able to accept two additional electrons, since in hexa-coordinated complexes **8** – **10** it has only 16 electrons in its valence shell, but coordination of third and fourth substrate ligands in bidentate fashion does not formally increase the number of electrons in the valence shell of titanium. Bidentate coordination of third and fourth cyclopentanedione replaces π-donation of oxide oxygen with σ-donation of a

carbonyl group and electron count at titanium valence electron shell remains the same, 16 electrons. Moreover, with the departure of isopropoxy ligands, the number of π-donors decreases and that of π-acceptors increases, which is not favourable.

4.1.3. Influence of ligands

4.1.3.1. Chelate effect

The possibility of incorporation of HO*i*Pr into the penta-coordinated Ti(O*i*Pr)$_3$(Sub-κ^{2}O,O) complexes **7** as a sixth ligand was also considered. The lowest-energy isomer of the TiHO*i*Pr(O*i*Pr)$_3$(Sub-κ^{2}O,O) complex was higher in energy (ΔE) than the reactants by 3.5 kcal mol^{-1}. One of the reasons for this is the absence of chelate effect that enhances stability of complexes **8–10**. Moreover, the five-membered chelate ring association requires only minimal changes in geometry: ligand-metal-ligand angle remains close to 90°, an ideal angle in octahedral complexes, and distortion energy related to altering in geometry of the chelate is insignificant.[145] Changes of the cyclopentanedione geometry in complexes **7** and **8** are depicted in **Figure 7**.

4.1.3.2. Donor-acceptor interactions and trans effects

The Ti(OiPr)$_2$(Sub-κ^{2}O,O)$_2$ complex **8** has an interesting feature: the sterically less crowded isomers are higher in energy than the more crowded ones (**Table 1**). The same tendency is observed for three- and four-substituted isomers **9** and **10.** *Cis-cis-trans* position of ligands (where the first *cis* describes the relative position of the monodentate ligands, the second – the relative position of the carbonyl oxygens, and *trans* indicates the locations of the titanium-oxygen bonds of the bidentate cyclopentanediones) is the energetically most favourable and therefore the most probable (Boltzmann probability > 90%). This can be explained via the *trans* effect between the ligands, where the ligand weakens or strengthens the bond of the metal with a transiently-located ligand depending on the donor-acceptor properties of both ligands. As was said above, the isopropoxy ligand is a σ- and π-donor. It is most beneficial when a π-acceptor (like the carbonyl group in cyclopentanedione) is situated opposite to a π-donor as it is in the *cis-cis-trans* isomer. On the contrary, the energetically most costly variant is to locate a π-donor ligand opposite to another π-donor or a π-acceptor *trans* to another π-acceptor, like it is in the *trans-syn* and *trans-anti* isomers (where *trans* determines the relative position of the monodentate ligands and *syn* or *anti* describe the position of the methyl substituents of the cyclopentanedione).

The *cis-cis-cis* isomer, where only one isopropoxy ligand is opposite to the π-acceptor carbonyl group, is higher in energy by about 1.4 kcal mol^{-1} relative to the *cis-cis-trans* isomer. The *cis-trans-cis* isomer, where none of π-donors are located in *trans* position to π-acceptors, is higher in energy by about 6.2 kcal mol^{-1} compared to the *cis-cis-trans* isomer. *Trans-syn* and *trans-anti* isomers were discussed above. Those isomers are the highest in energy since two π-donors compete for electron density and destabilize bonds with titanium.

4.1.4. Summary

The predominant generation of hexa-coordinate $Ti(OiPr)_2(Sub\text{-}\kappa^2O,O)_2$ complex **8** relative to other substituted titanium complexes and the preferential formation of *cis-cis-trans* isomers of $Ti(OiPr)_x(Sub\text{-}\kappa^2O,O)_y$ complexes were explained in terms of donor-acceptor, *trans* and chelate effects, steric factors and the 18-electron rule.

Table 1. Isomers of complexes **8**, **9** and **10**, their relative energies and Boltzmann probabilities at –20 °C.

Geometry	Isomer	Δ G, kcal mol $^{-1}$			Boltzmann probability, %		
		8 (R, Q = *i*Pr)	**9** (R = *i*Pr; Q = Sub)	**10** (R, Q = Sub)	**8**	**9**	**10**
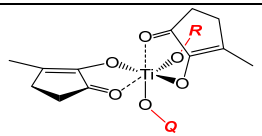	*Cis-cis-trans*	0.00	0.00	0.00	94.0	93.9	92.8
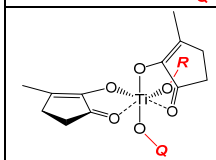	*Cis-cis-cis*	1.4	1.5	1.3	6.0	4.4	7.2
R = Sub; Q = *i*Pr	*Cis-cis-cis'*	–	2.0	–	–	1.8	–
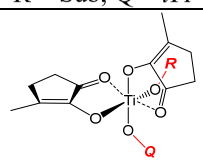	*Cis-trans-cis*	6.1	6.4	6.1	0.0	0.0	0.0
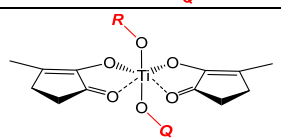	*Trans-syn*	6.8	7.5	7.7	0.0	0.0	0.0
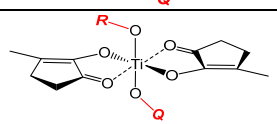	*Trans-anti*	13.0	13.8	12.8	0.0	0.0	0.0

4.2. Enantioselective Kulinkovich reaction

4.2.1. Structures and reaction mechanism

4.2.2. Influence of ligands

4.2.2.1. Interrelation of ligand volume and its position

4.2.2.2. Deformation of the TADDOL ligand

4.2.3. Summary

The conformer search for different isomers of titanium TADDOLate complexes was performed and it confirmed that the axial-equatorial position of TADDOL corresponds to the low-energy isomers in five-coordinated complexes with trigonal bipyramidal geometry. This was explained in terms of steric repulsion and electronegativity. Additionally, the influence of monodentate ligands on the geometry of the TADDOL ligand was considered. Variation of monodentate ligands causes deformation of the Ti–O–C angle and change in the corresponding C–O and O–Ti bond lengths.

4.3. CO_2 hydrogenation by the (PNP)Ir pincer complex

4.3.1. Reaction mechanism

In 2009, Tanaka *et al.*[112] reported the most efficient catalyst for CO_2 reduction to acetic acid known at the time, a (PNP)IrH_3 complex. This discovery has caused strong interest from computational chemists and a number of articles on the reaction mechanism has been published.

The first step in our investigation of CO_2 hydrogenation by the (PNP)IrH_3 complex was modelling of CO_2 attack on one of the axial hydride ligands of the (PNP)IrH_3 complex as it had been proposed in the original article of Tanaka *et al.*[112]. CO_2 insertion into Ir–H bond proceeds via a free energy barrier of 13.6 kcal mol^{-1} (**TS1, Scheme 25**) (Paper II).[155] This is in agreement with previous studies.[113–115] Next, the formate cleaves and H_2 coordinates to the vacant site on Ir^{III}. Regeneration of the catalyst occurs through deprotonation of complex **21** by a hydroxide anion from solution (**TS2**). The activation free energy for the (PNP)IrH_3 complex regeneration was calculated as 25.9 kcal mol^{-1} and it is the rate-limiting step of the reaction. This observation is also in agreement with previous studies.[113–116]

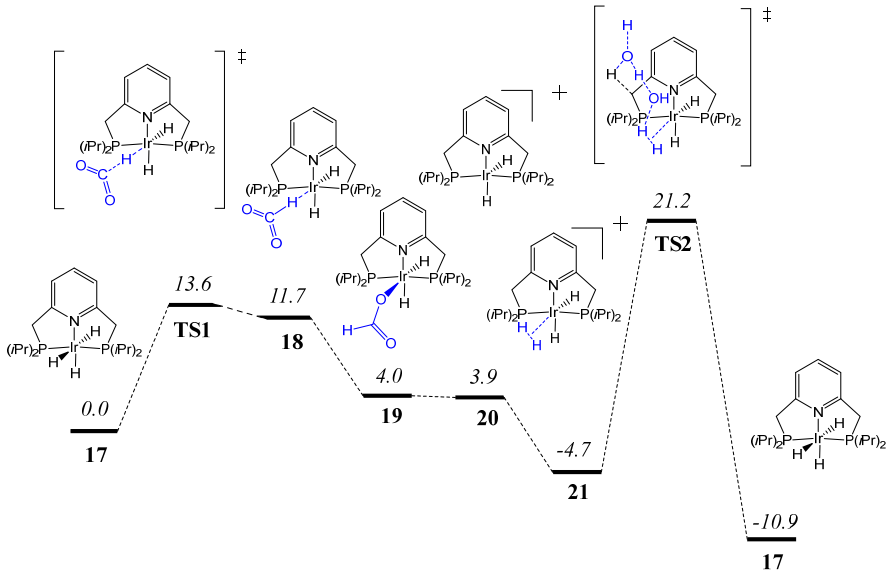

Scheme 25. Gibbs free energy profile (in kcal mol^{-1}) for the catalytic cycle proposed by Tanaka *et al*[116].

Since the catalyst regeneration is the rate limiting step, we proposed that there may be a second CO_2 reduction before the catalyst regeneration takes place. Tanaka *et al.*[112,116] had proposed the reaction mechanism based on NMR spectroscopy, but this method cannot detect high energy, short-lived or low concentration species. Considering that the reaction is taking place in aqueous KOH, we proposed that the hydroxyl ligand in the equatorial position could be a reasonable substitute to the hydride ligand. We suggested a parallel catalytic cycle (**Scheme 26**).[155]

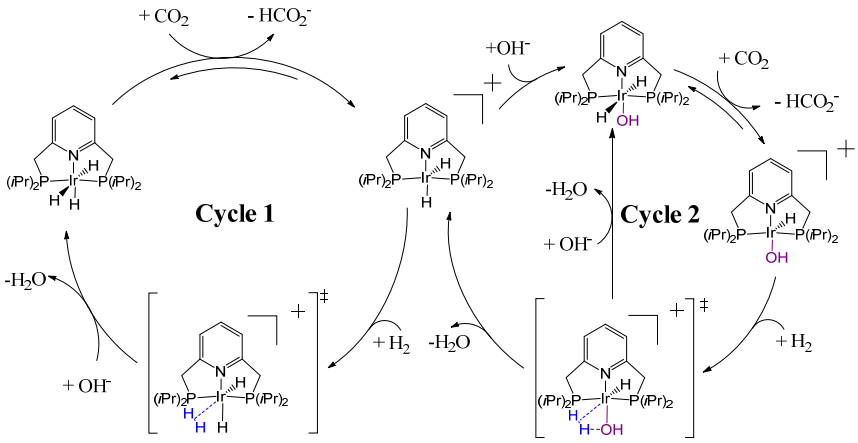

Scheme 26. Two parallel cycles for CO_2 hydrogenation.

The proposed parallel cycle consists of three main parts (**Scheme 27**):

I. CO_2 reduction to formate;

II. formate substitution by a hydrogen molecule;

III. catalyst regeneration by hydrogen splitting.

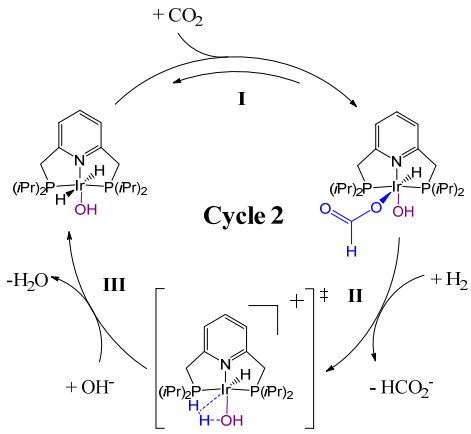

Scheme 27. Mechanism for the second CO_2 hydrogenation before the catalyst regeneration.

However, for the second cycle to proceed, the new catalytic species – the (PNP)IrH_2OH complex (**24**) – should be formed. Several possibilities for (PNP)IrH_2OH complex formation were investigated (**Scheme 28**):

I. through direct insertion of hydroxide into the cation **20**;

II. through formation of intermediate **22** with further hydroxide association;

III. through association of water molecule followed by cleavage of a proton.

The last one is the most favourable pathway. The barrier for water molecule association is 29.0 kcal mol^{-1}. This is rather high, but considering the reaction conditions (aqueous KOH solution at 120 °C) such mechanism cannot be ruled out.

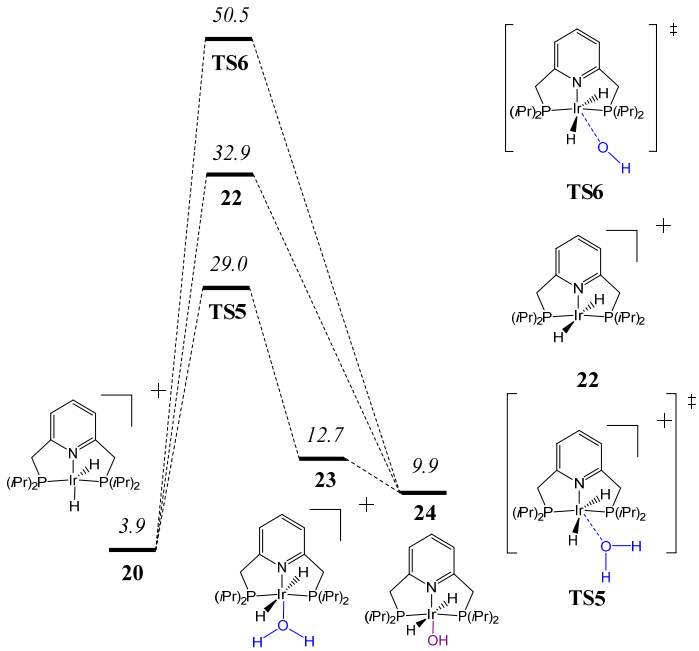

Scheme 28. Gibbs free energy profile (in kcal mol^{-1}) for the (PNP)IrH$_2$OH complex formation.

After formation of complex **24**, it can be attacked by CO_2. This proceeds via a free energy barrier of 21.7 kcal mol^{-1} (**TS7, Scheme 29**), and the regeneration of the (PNP)IrH$_2$OH complex occurs through the deprotonation of associated hydrogen molecule by the hydroxyl ligand (**TS8**) with a barrier of 22.3 kcal mol^{-1}. The barrier for the second CO_2 insertion is significantly higher than for the first one (13.6 kcal mol^{-1}), but the barrier for the (PNP)IrH$_2$OH complex regeneration is by 3.6 kcal mol^{-1} lower than the barrier for the (PNP)IrH$_3$ complex regeneration (25.9 kcal mol^{-1}).

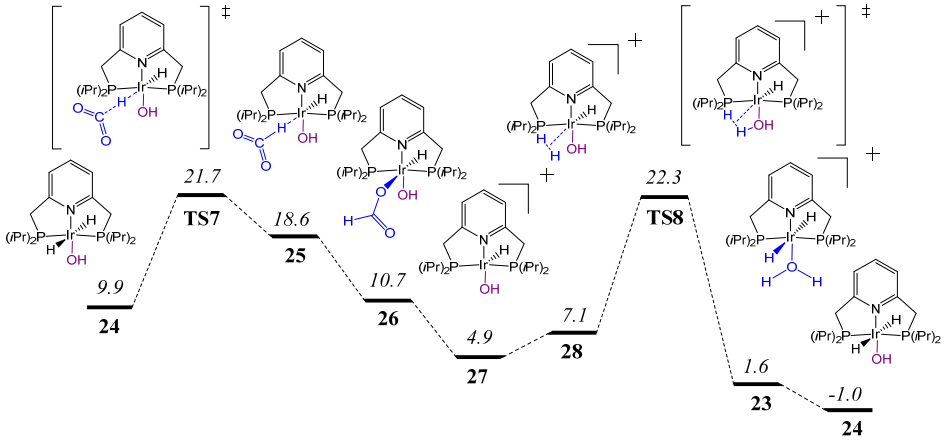

Scheme 29. Gibbs free energy profile (in kcal mol^{-1}) for the second CO_2 hydrogenation by the (PNP)IrH$_2$OH complex.

Based on the data given above, we concluded that formation of complex **24** under the reaction conditions is possible. Moreover, when the (PNP)IrH_2OH complex is formed, it becomes an efficient catalyst in CO_2 reduction since the reaction barriers of the second cycle are comparable with the barriers of the first cycle.

4.3.2. Influence of ligands: *cis*-effect

A metal-based homogenous catalyst is a complex system, where both the metal and the ligands influence each other and properties of the catalyst depend on many such co-influences. The *trans*-effect of ligands was discussed in **Section 4.1.3.2**. Ligands in the *cis* position also impact the catalytic properties of the complex, although their effect is not so obvious and cannot be unambiguously predicted.

We already compared the properties of the (PNP)IrH_3 and the (PNP)IrH_2OH complexes. Ligand in equatorial position has significant influence on the charge of the axial hydrides, thereby increasing or decreasing the barrier for CO_2 insertion (**Scheme 30**, **Table 2**). Ligands with either σ- or π-donating properties raise the partial charge of the hydrides and thus facilitate the electrophilic attack of CO_2. The π-accepting CN^- ligand gives the opposite effect. It reduces the partial charge of the hydrides, increasing the energy barrier for CO_2 insertion. Moreover, σ- and π-donating ligands stabilize the reaction products, further facilitating the reaction, in contrast to the CN^- ligand.

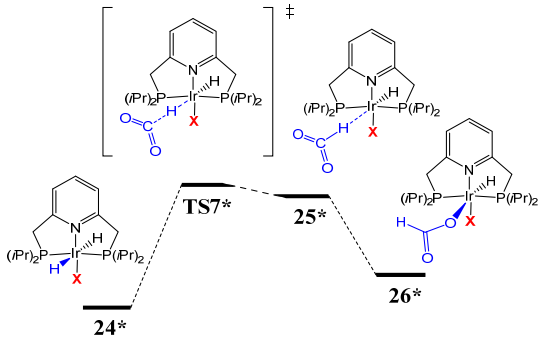

Scheme 30. Pathway for CO_2 reduction.

Table 2. Influence of various equatorial ligands on the energy of CO_2 insertion.

Ligand	Charge	ΔG, kcal mol^{-1}		
		TS7*	**25***	**26***
CN^-	–0.232	16.7	16.7	16.7
I^-	–0.248	15.3	12.4	5.3
Cl^-	–0.250	14.6	12.0	3.8
F^-	–0.260	14.6	12.3	4.2
H^-	–0.251	13.6	11.7	4.0
CH_3^-	–0.253	12.1	7.3	1.7
SH^-	–0.248	13.9	11.5	3.1
OH^-	–0.245	14.2	10.7	3.7

Following further along the reaction path, the influence of various equatorial ligands on the catalyst regeneration was considered. It was found that both σ- and π-donating ligands, in contrast to the π-accepting ligand CN^-, facilitate the formation of complexes with a hydrogen molecule (**Scheme 31**, **Table 3**). The data in Table 3 indicates that complex **28*** with a CN^- ligand in the equatorial position is significantly higher in energy than other complexes **28***. Another trend is also revealed: complexes **28*** with halogen ligands are higher in energy than complexes with H^- or π-donating ligands, because halogen ions are not as good donors as the H^-, CH_3^-, OH^-or SH^- ligands.

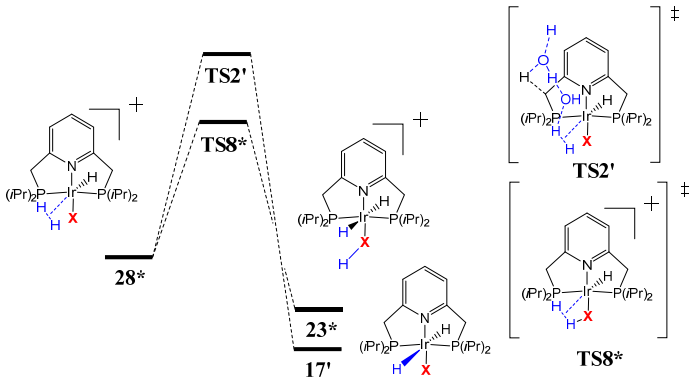

Scheme 31. Pathways for catalyst regeneration.

Table 3. Influence of various equatorial ligands on the energy of catalyst regeneration.

Ligand	ΔG, kcal mol^{-1}		
	28*	**TS8*/ TS2 ′**	**23*/17′**
CN^-	6.3	28.0′	–
I^-	0.5	41.1	33.1
Cl^-	0.6	37.0	32.7
F^-	0.0	28.8	18.8
H^-	–4.7	21.2′	–
CH_3^-	–5.2	8.7	2.9
SH^-	–1.3	18.6	7.7
OH^-	–2.7	12.3	–8.2

Similar trends can be observed in transition states where the hydrogen molecule is split and the proton transfer occurs. Transition states in complexes with CH_3^-, OH^-, SH^- ligands have the lowest energy. Moreover, the OH^- ligand stabilizes the newly formed complexes **23***.

In the case of H^- and CN^- ligands we were unable to find a transition state similar to **TS8***. In those two cases the hydrogen molecule splitting was calculated as **TS2′** with barrier of 25.9 and 28.0 kcal mol^{-1}, respectively. That barrier is higher than the transition states in complexes with CH_3^-, OH^-, SH^- ligands.

Based on the data given above it can be concluded that π-donating ligands in *cis* position to hydrides facilitate CO_2 insertion as well as hydrogen molecule splitting during the catalyst regeneration.

4.3.3. Transition states

4.3.3.1. Hydrogen bonds

Analysis of the transition state geometries revealed that orientation of the equatorial ligand influences the barrier of CO_2 insertion into the (PNP)IrH_2X complexes (X=OH^-, SH^-) (**Table 4**, **Figure 8**). In the case where the hydrogen of ligand X is directed towards the side with CO_2, a hydrogen bond will be formed between one of the oxygens in CO_2 and the hydrogen of ligand X. This bond additionally stabilizes the TS and decreases barriers for CO_2 insertion by 2.6 and 1.7 kcal mol^{-1} for OH^- and SH^-, respectively. Also, insignificant differences in hydride charges were observed.

Table 4. Influence of orientation of equatorial ligands on the energy barrier of CO_2 insertion

Ligand	Position	Charge	**ΔG,** kcal mol^{-1}		
			TS7*	**25***	**26***
SH^-	a	–0.248	13.9	11.5	3.1
	b	–0.253	12.2	9.9	3.7
OH^-	a	–0.245	14.2	10.7	3.7
	b	–0.280	11.6	8.6	0.8

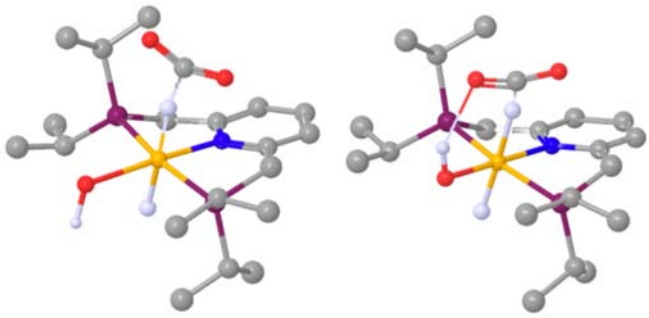

a) **b)**

Figure 8. Possibilities for CO_2 insertion into complexes with OH^- (shown in the figure) and SH^- ligands **a)** without hydrogen bond formation; **b)** with hydrogen bond formation. Hydrogen atoms irrelevant for the reaction are not shown.

4.3.3.2. Distortion energy

We modelled several possibilities for (PNP)IrH_2OH complex regeneration in order to find the lowest-energy pathway. First of all, the pathway analogous with (PNP)IrH_3 complex regeneration through **TS2** was considered. The barrier for the splitting of the hydrogen molecule by a hydroxide anion from the solution is 25.9 kcal mol^{-1} for the (PNP)IrH_3 complex (**TS2**, **Figure 9**), but for the (PNP)IrH_2OH complex the barrier increases to 36.3 kcal mol^{-1} since **TS9** needs more rearrangements. In **TS9** the bond in the hydrogen molecule is elongated to 1.004 Å, compared to 0.843 Å in **TS2** and the distance between the hydroxyl oxygen and the methylene proton increases to 1.486 Å, compared to 1.204 Å in **TS2**. These rather significant geometry distortions cause increase in energy of the TS.

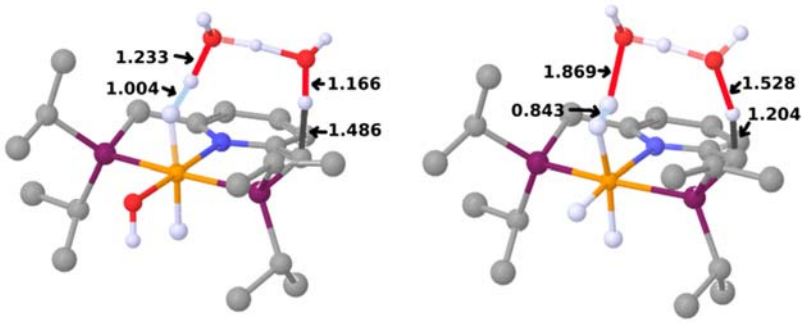

Figure 9. Geometries of the complexes **TS9** and **TS2**. Hydrogen atoms irrelevant for the reaction, are not shown.

Next, another pathway was considered where the equatorial hydroxyl ligand leaves the complex and a hydrogen molecule is split by a formate ligand (**Scheme 32**). The barrier for the catalyst regeneration through this pathway is 32.6 kcal mol^{-1} (**TS10**, **Scheme 32**).

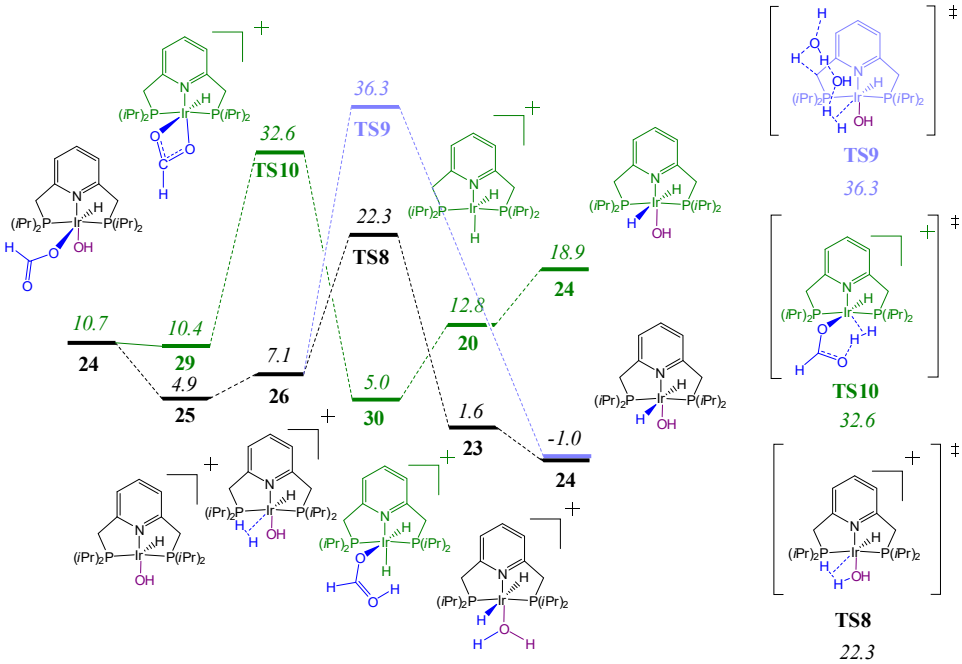

Scheme 32. Gibbs free energy profiles (in kcal mol^{-1}) for the three pathways for regeneration of the catalytic complex **24**.

The third and the lowest energy pathway goes through formate ligand cleavage and hydrogen molecule association. Catalyst regeneration occurs through the proton transfer to the hydroxyl ligand with a barrier of 22.3 kcal mol^{-1} (**TS8**). It is supposed that subsequently the water ligand is deprotonated by a hydroxide anion from the solution and complex **24** is regenerated. Deprotonation of the water ligand

occurs easily since the hydroxide anion has the function of a pendant base[156,157], and proton exchange occurs with low barriers.

The difference of 10.2 kcal mol^{-1} between the transition states **TS8** and **TS10** can be explained by diverse types of transition states (**Scheme 33**). **TS8** is categorized as an electrophilic substitution and **TS10** as a chelate-assisted cleavage with a six-member ring. Although it had been shown before[158] that hydrogen splitting is more favourable through a TS with a six-membered ring, in our case it is the opposite due to the more significant rearrangements needed for **TS10**. The geometry of **TS8** is very similar to that of the precursor complex **25**. The main changes are: the increase of one H–Ir–O angle from 92.1° to 103.1°, the decrease of another H–Ir–O angle from 82.8° to 68.8°, and elongation of the H–H bond by 0.169 Å from 0.798 Å to 0.967 Å. Single-point calculations showed that the distortion of H_2 and complex **25** to the geometry of **TS8** without interaction between the fragments requires 12.0 kcal mol^{-1} and interaction between the fragments compensates 5.9 kcal mol^{-1}. In agreement with the study by Ess *et al.*[158], our calculation confirmed that in **TS10** the H–H bond is cleaved spontaneously by approaching iridium, but the geometry rearrangements needed for **TS10** require significant energy input. The geometry of **TS10** is closer to that of complex **30** (**Scheme 32**) than to the initial complex **29** and requires 17.8 kcal mol^{-1} for geometry distortion, of which only 3.9 kcal mol^{-1} is compensated by interaction of fragments.

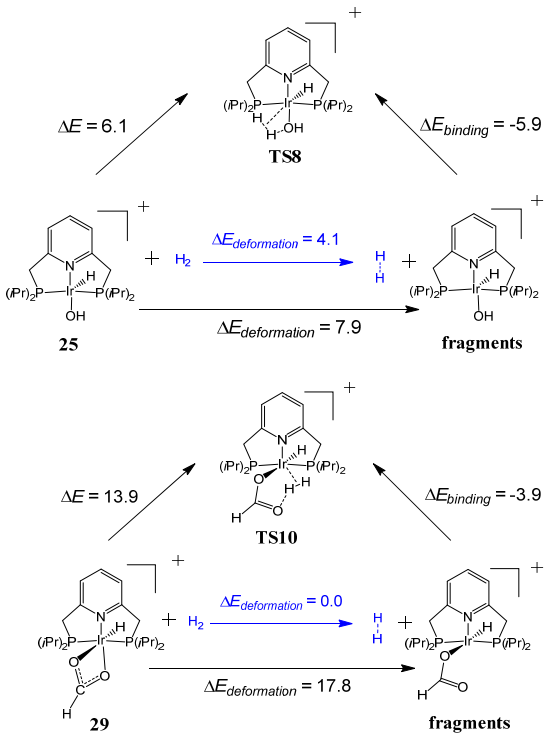

Scheme 33. Activation strain energies for **TS8** and **TS10** (kcal mol^{-1}).

4.3.4. Summary

Reaction mechanism for CO_2 hydrogenation by (PNP)IrH_3 complex, proposed earlier based on the experimental evidence, was modelled and a new parallel cycle was proposed, where the catalytic species is (PNP)IrH_2OH complex formed *in situ*. Several pathways for (PNP)IrH_2OH complex formation and catalytic species regeneration were examined and analysed. Additionally, effect of equatorial ligands on charges of hydrides and consequently their ability to reduce were analysed.

4.4. CO_2 hydrogenation by the (PCP)Ir pincer complex

4.4.1. Reaction mechanism

In 2009, Kang *et al.*[117] reported an efficient catalyst for electrochemical CO_2 reduction to formate. Our investigation of CO_2 hydrogenation by the (PCP)Ir complex was started with modelling of the originally proposed catalytic cycle[117], where formation of the (PCP)IrH_2(NCCH_3) complex is followed by CO_2 attack on one of the axial hydride ligands of this complex. The Gibbs free energy profile for the (PCP)IrH_2 complex activation and steps I−II of the proposed catalytic cycle are depicted in **Scheme 34**. The barrier for CO_2 insertion into complex **32** is 16.6 kcal mol^{-1}. This is in agreement with the previous computational study by Cao *et al.*[120], who had found this barrier to be 14.4 kcal mol^{-1}. CO_2 reduction is followed by the formation of complex **34**, which is endergonic by 2.1 kcal mol^{-1}, or the formation of cation **35**, which is endergonic by 6.0 kcal mol^{-1}. This agrees with experimental observations: the complexes **32**, **34** and **35** had been determined by NMR and cation **35** had been named as a „rest-state complex“.[118] A similar tendency where intermediates **32** and **34** are higher and intermediate **35** is lower in energy than the reactants had been observed by Cao *et al.*[120], although in their case the differences in energy were more significant.

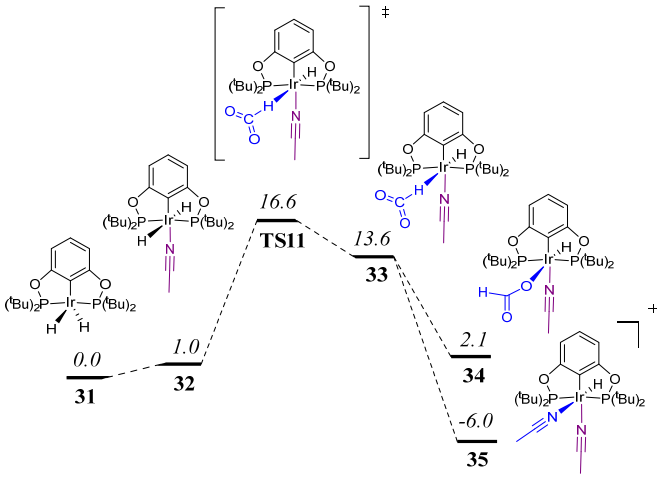

Scheme 34. Gibbs free energy profile (in kcal mol^{-1}) for CO_2 reduction by (PCP)Ir$^{III}H_2$(NCCH_3) complex **32**.

The possibility that complex **31** catalyses CO_2 reduction to formate by itself was also considered by us (**Scheme 35**). The barrier for CO_2 insertion directly into complex **31** is 19.0 kcal mol^{-1}. This value is by 2.4 kcal mol^{-1} higher than the analogous insertion into complex **32**. Thus the (PCP)IrH_2 complex can catalyse CO_2 reduction, but the reaction with complex **32** is more favourable.

After the reaction has occurred, it is necessary to regenerate the catalyst (**Section 1.2.2.2. Scheme 15**, **step III**). It had been reported that the catalyst regeneration proceeds between −1.1 V and −1.4 V *vs* NHE.[118] Catalyst regeneration is a two-

electron, one-proton reduction, where water is the proton source.[117] Cao *et al.*[120] had reported that catalyst regeneration occurs through the intermediate $[(PCP)IrH(NCCH_3)]^-$ formed by accepting two electrons at potential −1.5 V and simultaneous cleavage of one acetonitrile ligand. The formation of $[(PCP)IrH(NCCH_3)]^-$ is followed by water splitting with the free-energy barrier 26.0 kcal mol^{-1}.

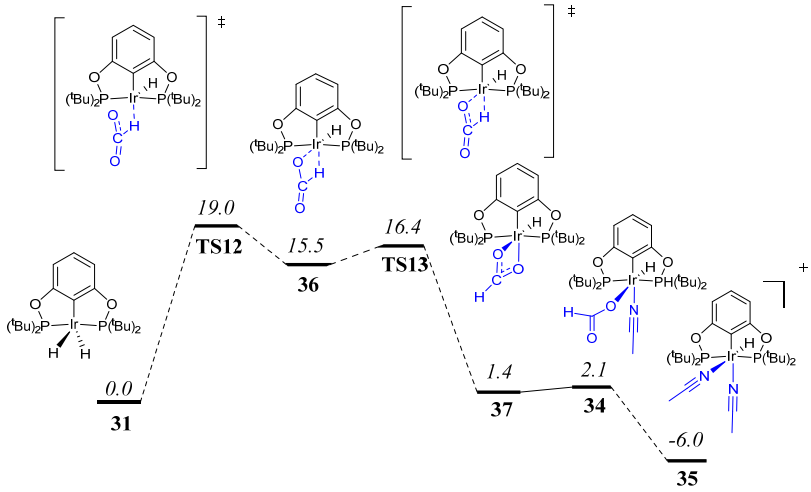

Scheme 35. Gibbs free energy profile (in kcal mol^{-1}) for CO_2 reduction by $(PCP)Ir^{III}H_2$ complex **31**.

According to our calculations, the two-electron potential for Ir^{III}/Ir^{I} reduction is −0.82 V and the reduction is accompanied by simultaneous cleavage of both acetonitrile ligands from the complex **35**. The calculated potential was in disagrement with the experimental observations and it was proposed that the regeneration of the catalyst occurs by non-Nernstian behaviour[159], when the first reduction happens at higher potential than the second one. Calculations showed that the first electron transfer and Ir^{III}/Ir^{II} reduction proceeds at −1.15 V and the second one (Ir^{II}/Ir^{I} reduction) proceeds at −0.5 V. This is in agreement with the experimental result of −1.1 V. Simultaneously with electron transfer, acetonitrile ligands are released and complex **38** is formed (**Scheme 36**). The regeneration of the catalyst occurs through water splitting with a free-energy barrier of 14.0 kcal mol^{-1} and the formation of complex **31** should be rapid at room temperature.

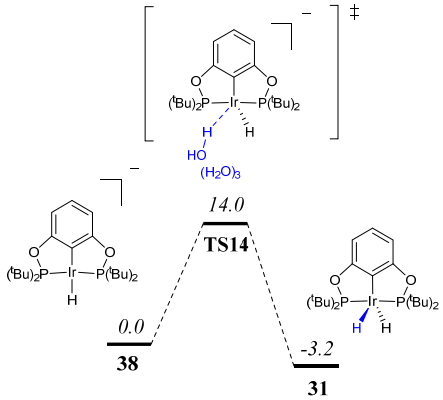

Scheme 36. Gibbs free energy profile (in kcal mol^{-1}) for catalyst regeneration.

Based on the calculations, we proposed a new catalytic cycle for CO_2 reduction by the (PCP)Ir complex. The new catalytic cycle consists of four main steps (**Scheme 37**):

I. complex activation by association of an acetonitrile molecule;

II. CO_2 reduction to formate;

III. formate release and association of a second acetonitrile molecule;

IV. catalyst regeneration by water splitting.

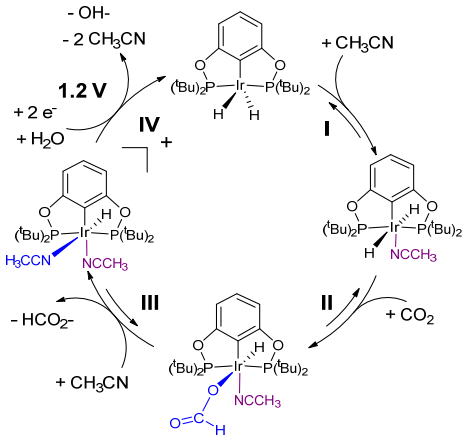

Scheme 37. Proposed catalytic cycle with (PCP)Ir^{III}H$_2$ complex.

Moreover, our computational study of the catalytic system showed that a monohydride anion [(PCP)IrH]$^-$ (**38**) can also catalyse CO_2 reduction. In this case the catalytic cycle also consists of four main parts (**Scheme 38**):

I. CO_2 reduction to formate;

II. formate release and water splitting;

III. association of two acetonitrile molecules;

IV. reduction of the catalytic complex.

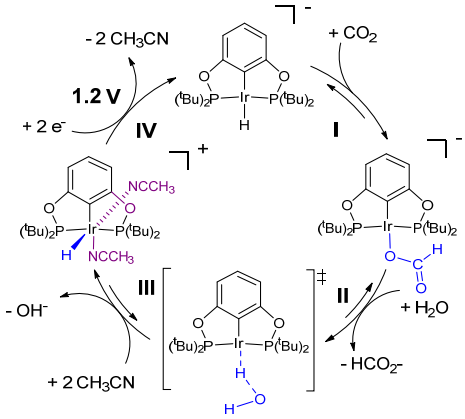

Scheme 38. Proposed catalytic cycle with $[(PNP)Ir^{I}H]^{-}$ complex generated *in situ*.

The barrier for CO_2 insertion into the monohydride complex **38** is 12.3 kcal mol^{-1} (**Scheme 39**). It is by 4.3 kcal mol^{-1} lower than the insertion of CO_2 into complex **32**. In contrast to the previously considered formation of formate complexes **34** and **37** (**Scheme 34** and **35**), the formation of complex **40** is exergonic.

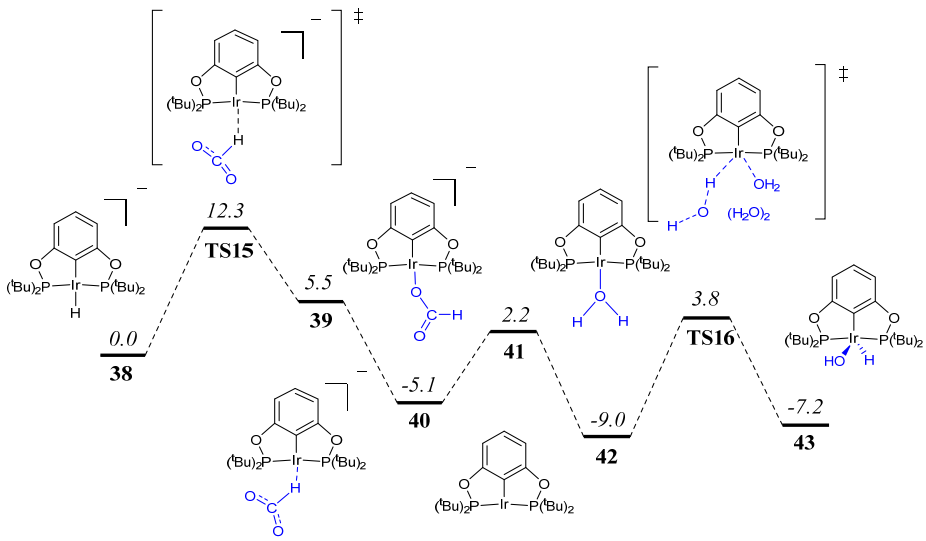

Scheme 39. Gibbs free energy profile (in kcal mol^{-1}) for CO_2 reduction by $[(PNP)Ir^{I}H]^{-}$ complex **38**.

To complete the cycle, the catalyst must be regenerated. Regeneration of the $[(PCP)IrH]^{-}$ complex (**38**) involves proton transfer to a tetracoordinated complex **42** with a barrier of 12.8 kcal mol^{-1}. This barrier is by 1.2 kcal mol^{-1} lower in energy than the barrier for $(PCP)IrH_2$ complex regeneration. Ir^{III}/Ir^{I} reduction has Nernstian behaviour and proceeds at −1.17 V (calculated) that is in agreement with the experimental result of −1.1 V.

It was concluded that both of the reaction paths given above are possible, especially considering the fact that the calculated potentials for catalyst regeneration are similar. However, reduction of CO_2 by monohydride complex **38** is expected to be more favourable since this pathway has lower activation energy.

4.4.2. Coordination number of metal

In **Section 4.1.2.** the alternation of coordination number during the reaction was considered. One more example of this phenomenon can be found in the reaction of CO_2 hydrogenation by the (PCP)Ir pincer complex. From **Figures 34** and **35** it can be seen that along the reaction the penta-coordinated (PCP)IrH_2 pincer complex is transformed into the hexa-coordinated octahedral complex and this geometry will remain during all subsequent transformations. This can be explained by the 18-electron rule. Iridium in the oxidation state III has six electrons in the valence shell. The pincer ligand donates another six electrons to iridium through three σ bonds, each hydride ligand donates two electrons and the associated acetonitrile also donates two electrons. Thus, iridium has a total of 18-electrons in the valence shell. Along the reaction the donating ligands change, but the octahedral geometry of the iridium complex and the number of electrons in the iridium valence shell remains the same.

During the Ir^{III}/Ir^{I} reduction, where the $[(PCP)IrH(NCCH_3)_2]^+$ cation **35** gets two electrons, a spontaneous acetonitrile release occurs and the hexa-coordinated octahedral complex is transformed into a tetra-coordinated square planar complex **38**. The coordination number of Ir^{I} remains four during all subsequent transformations as long as the oxidation state of Ir does not increase. Even the formate ligand that can coordinate in bidentate fashion, remains monodentate in Ir^{I} complex (**40**). Such a situation is typical for metals with d^8 electron configurations and can be explained by the crystal field theory.[145] According to this theory, when four ligands are placed around the metal in a square planar fashion, they produce a static electric field that breaks the degeneracies of *d*-electron orbitals. Thus the energy of the fifth *d*-orbital increases and because of this it remains unoccupied.

4.4.3. Transition state

In our calculations, we considered the intramolecular and intermolecular pathways for the (PCP)IrH_2 pincer complex regeneration. In the first case, the water molecule is simultaneously associated and split by the $[(PCP)IrH]^-$ anion (**38**). The barrier for such an oxidative addition of water is 50.4 kcal mol^{-1} (**Scheme 40**). It is supposed that the high barrier is related to the significant rearrangement of the complex. To adopt the geometry of **TS17** the hydride from the equatorial position is moved into axial position (**Figure 10**) and the stable square planar complex **38** is rearranged into a complex with almost octahedral geometry. **TS17** can be assigned to a late transition state since its geometry is closer to the geometry of the product than to the geometry of reactants. The newly formed Ir–O and Ir–H bonds are elongated only by 0.18 and 0.10 Å, respectively compared to the product complex **44**. Distortion of angles is more significant. In **TS17** C–Ir–H angle is 100.3° and the

H–Ir–OH angle is 33.4°, compared to complex **44**, where they are 87.6° and 84.1°, respectively.

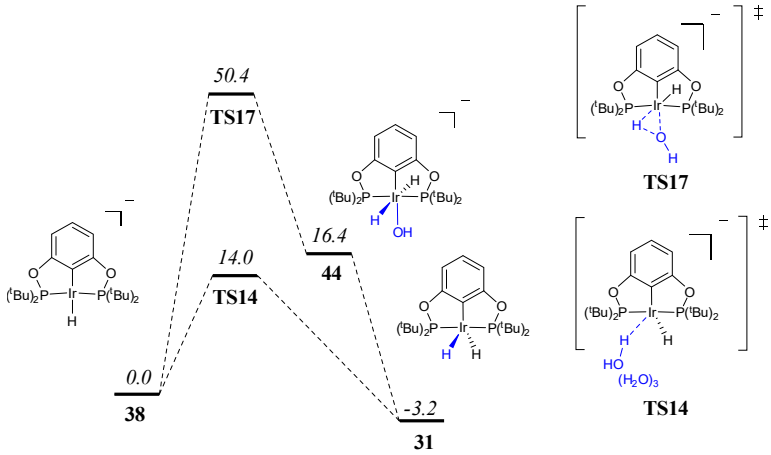

Scheme 40. Gibbs free energy profile (in kcal mol^{-1}) for complex (PCP)IrH$_2$ regeneration.

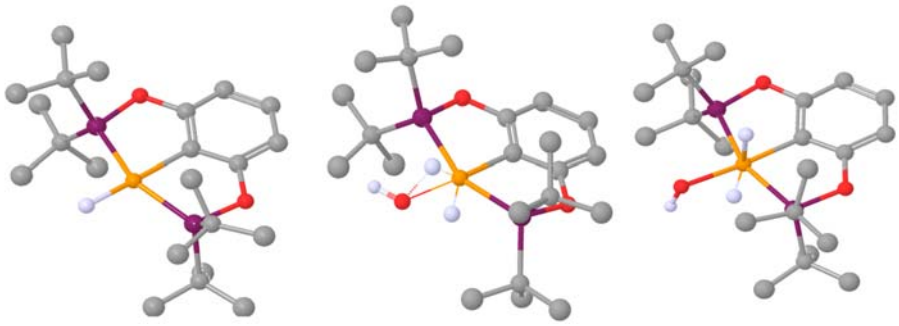

Figure 10. Geometries of the complexes **38**, **TS17** and **44**. Hydrogen atoms, which are irrelevant for the reaction, have been removed for clarity.

In contrast to the intramolecular pathway, the intermolecular pathway needs much less reorganization. In **TS14** the hydride ligand only slightly deviates from its initial equatorial position and the C–Ir–H angle decreases from 178.7° in complex **38** to 171.2° in **TS14** (**Figure 11**). The bond with the other hydride is already formed and the Ir–H distance is 1.642 Å, which is only by 0.051–0.053 Å longer than in the complex **31**. The most significant geometry rearrangement is the change in bend angles, although in the penta-coordinated complexes bend angles are very flexible. As a result, the oxidative addition of water through the intermolecular pathway has a lower barrier of 14.0 kcal mol^{-1}, while **TS14** is also assigned to late transition state since its geometry is close to the geometry of product **31**.

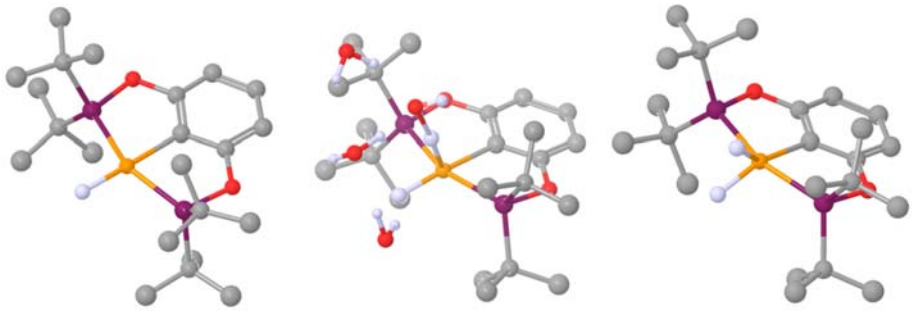

38 **TS14** **31**

Figure 11. Geometries of the complexes **38**, **TS14** and **31**. Hydrogen atoms, which are irrelevant for the reaction, have been removed for clarity.

The same trend can be observed during the [(PCP)IrH]$^-$ anion regeneration. Here the oxidative addition of water through the intramolecular pathway is not as unfavourable as for complex **38**, since complex **42** is less crowded and less geometric rearrangements are needed. This is in agreement with the earlier observation[160] that oxidative addition is more favourable for metals with lower coordination numbers. The protonation of complex **42** through the intramolecular pathway occurs with a barrier of 21.1 kcal mol^{-1} or with a barrier of 12.8 kcal mol^{-1} if it goes through the intermolecular pathway (**Scheme 41**).

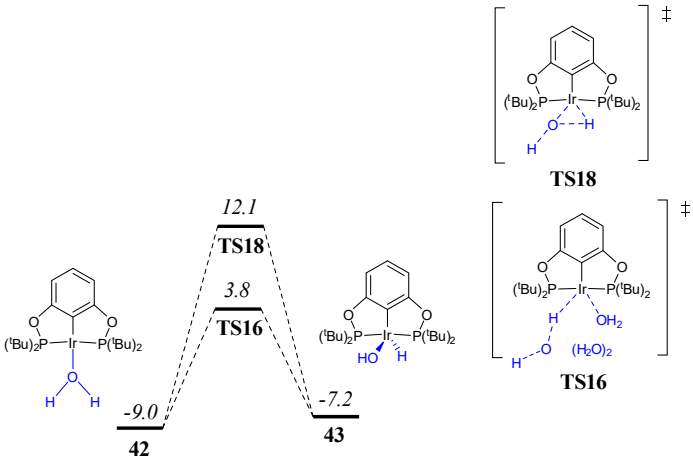

Scheme 41. Gibbs free energy profile (in kcal mol^{-1}) for complex [(PNP)IrH]$^-$ regeneration.

If the catalytic complex regeneration occurs through the intermolecular pathways, the barriers for proton transfer are almost the same (14.0 kcal mol^{-1} for complex **31** and 12.8 kcal mol^{-1} for complex **38**), but if the water molecule is split intramolecularly, the difference in energy is significant (50.4 and 21.1 kcal mol^{-1}, respectively). Both geometries (**TS17** and **TS18**) are closer to products than to reactants (**Figure 10** and **12**), but for **TS18** less rearrangements are needed and it is by 29.3 kcal mol^{-1} lower in energy than **TS17**. In **TS18** the Ir–O bond is by 0.19 Å

shorter than in complex **42** and by 0.19 Å longer than in complex **43**. The newly formed Ir–H bond in **TS18** is by 0.07 Å longer than in **43**. Angles are more distorted, but as discussed previously (**Sections 4.2.1.** and **4.3.1.**), in penta-coordinated complexes the angles are very flexible.

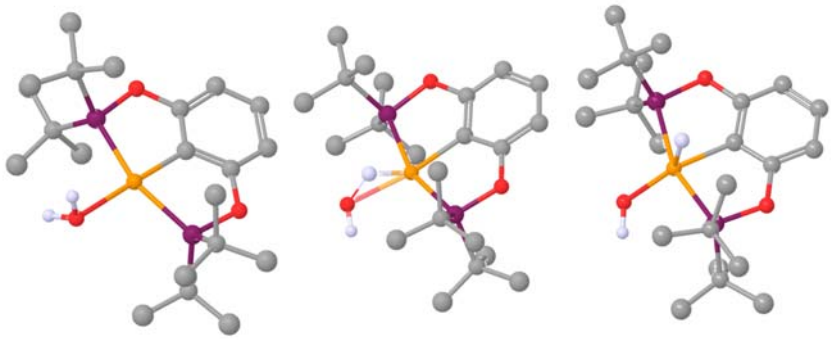

42 **TS18** **43**

Figure 12. Geometries of the complexes **42**, **TS18** and **43**. Hydrogen atoms, which are irrelevant for the reaction, have been removed for clarity.

4.4.4. Summary

Reaction mechanism for CO_2 hydrogenation by (PCP)IrH_2 complex, proposed based on the experimental data, was modelled and a cycle catalysed by the $[(PCP)IrH]^-$ anion formed *in situ* was proposed. Several pathways for regeneration of catalytic complexes were studied and analysed. Additionally, coordination number change was explained using the 18-electron rule.

CONCLUSIONS

In this work, the complexation of 3-methylcyclopentane-1,2-dione with $Ti(OiPr)_4$, the formation of titanium TADDOLate complexes in Kulinkovich reaction, and the CO_2 reduction catalysed by (PNP)Ir and (PCP)Ir complexes were studied using computational chemistry. All results agree well with experimental data (NMR and voltammograms). The predominant generation of hexa-coordinate $Ti(OiPr)_2(Sub\text{-}\kappa^2O,O)_2$ complex was explained. Participation of five-coordinated titanium TADDOLate complexes in the Kulinkovich reaction was confirmed. Based on the already proposed reaction mechanisms reaction pathways were modelled for CO_2 reduction by iridium pincer complexes, as well as alternative reaction pathways that agree or at least do not contradict with NMR data. The possible reasons of coordination number change in $Ti(OiPr)_x(Sub\text{-}\kappa^2O,O)_y$ and (PCP)Ir complexes were discussed. Based on the results of DFT calculations, the following conclusions have been made:

For $Ti(OiPr)_x(Sub\text{-}\kappa^2O,O)_y$ complexes:

- due to the chelate effect the Sub ligand will coordinate in bidentate mode, if the coordination number of the metal cation is less than six;
- the most energetically favourable geometry is achieved when a π-accepting ligand is situated in *trans*-position to the π-donating ligand;
- the energetically most costly variant is associated with a location of a π-donor ligand opposite to another π-donor and a π-acceptor *trans* to another π-acceptor.

For complexes $Ti(TADDOL)(X)_x(OiPr)_y$:

- the bulky TADDOL ligand is situated in axial-equatorial position and the smallest monodentate ligands tend to occupy the other two equatorial positions;
- the replacement of monodentate ligands does not cause significant change in the geometry of TADDOL;

For (PNP)Ir complexes:

- ligands with either σ- or π-donating properties raise the partial charge of *trans* hydrids and a π-accepting CN^- ligand gives the opposite effect;
- the formation of a hydrogen bond between one of the CO_2 oxygens and a hydrogen of *cis* ligand facilitates CO_2 insertion by decreasing the barrier by about 2.0 kcal mol^{-1};
- the replacement of *cis* H^- by OH^- in the (PNP)Ir complex changes the barrier of catalyst regeneration from 25.9 to 36.3 kcal mol^{-1} in the analogous transition states;
- the hydrogen molecule splitting through an electrophilic substitution is favourable by 10.2 kcal mol^{-1} compared to a chelate-assisted cleavage.

For (PCP)Ir complexes:

- the intermolecular pathway for the regeneration of (PCP)Ir complexes by water splitting is more favourable than the intramolecular pathway;
- the oxidative addition of water to the (PCP)Ir complex is more favoured when iridium has lower coordination numbers.

REFERENCES

(1) Fechete, I.; Wang, Y.; Védrine, J. C. *Catal. Today* **2012**, *189* (1), 2–27.

(2) Carey, F. A.; Sundberg, R. J. *Advanced organic chemistry Part B: Reactions and synthesis*, 5th ed.; Springer, 2008.

(3) Cramer, C. J. *Essentials of Computational Chemistry: Theories and Models*, 2nd ed.; Wiley-VCH John Willey & Sons, Ltd: Chichester, 2004.

(4) Koch, W.; Holthausen, M. C. *A Chemist's Guide to Density Functional Theory*, 2nd ed.; Wiley-VCH, Ed.; Weinheim, 2001.

(5) Head-Gordon, M.; Rico, R. J.; Oumi, M.; Lee, T. *Chem. Phys. Lett.* **1994**, *219* (1–2), 21–29.

(6) Maurice, D.; Head-Gordon, M. *Mol. Physics.* **1999**, *96* (10), 1533–1541.

(7) Møller, C.; Plesset, M. S. *Phys. Rev.* **1934**, *46* (7), 618–622.

(8) Krishnan, R.; Pople, J. A. *Int. J. Quantum Chem.* **1978**, *14* (1), 91–100.

(9) Purvis, G. D. I.; Bartlett, R. J. *J. Phys. Chem.* **1982**, *76* (4), 1910–1919.

(10) Hohenberg, P.; Kohn, W. *Phys. Rev. B* **1964**, *136* (3), 864–871.

(11) Kohn, W.; Sham, L. J. *Phys. Rev. A* **1965**, *140* (4), 1133–1138.

(12) Perdew, J. P.; Burke, K.; Ernzerhof, M. *Phys. Rev. Lett.* **1996**, *77* (18), 3865–3868.

(13) Becke, A. D. *Phys. Rev. A* **1988**, *38* (6), 3098–3100.

(14) Perdew, J. P. *Phys. Rev. B* **1986**, *33* (12), 8822–8824.

(15) Cohen, A. J.; Mori-Sanchez, P.; Yang, W.; *Chem. Rev.* **2012**, *112* (1), 289–320.

(16) Tao, J.; Perdew, J. P.; Staroverov, V. N.; Scuseria, G. E. *Phys. Rev. Lett.* **2003**, *91* (14), 146401–146404.

(17) Lee, C.; Yang, W.; Parr, R. G. *Phys. Rev. B* **1988**, *37* (2), 785–789.

(18) Becke, A. D. *J. Chem. Phys.* **1993**, *98* (7), 5648–5652.

(19) Zhao, Y.; Truhlar, D. G. *Theor. Chem. Acc.* **2008**, *120* (1), 215–241.

(20) Karton, A.; Tarnopolsky, A.; Schatz, G. C.; Martin, J. M. L. *J. Phys. Chem. A* **2008**, *112* (50), 12868–12886.

(21) Zhang, Y.; Xu, X.; Goddard, W. A. *Proc. Natl. Acad. Sci. U. S. A.* **2009**, *106* (13), 4963–4968.

(22) Grimme, S. *J. Comput. Chem.* **2006**, *27* (15), 1787–1799.

(23) Karton, A.; Gruzman, D.; Martin, J. M. L. *J. Phys. Chem. A* **2009**, *113* (29), 8434–8447.

(24) Marom, N.; Tkatchenko, A.; Scheffler, M.; Kronik, L. *J. Chem. Theory Comput.* **2010**, *6* (1), 81–90.

(25) Grimme, S.; Antony, J.; Ehrlich, S.; Krieg, H. *J. Chem. Phys.* **2010**, *132* (15), 154104-1–19.

(26) Labanowski, J. K. *Simplified Introduction to AB Initio Basis Sets. Terms and*

Notation http://www.ccl.net/cca/documents/basis-sets/basis.html (accessed Mar 1, 2016).

(27) Hay, P. J.; Wadt, W. R. *J. Chem.Phys.* **1985**, *82* (1), 270–283.

(28) Bader, R. F. W. *Atoms in Molecules: A Quantum Theory*; Oxford University Press: Oxford, 1990.

(29) Bader, R. F. W. *Theory of Atoms in Molecules* http://www.chemistry.mcmaster.ca/aim/aim_1.html (accessed Mar 11, 2017).

(30) Matta, C. F.; Boyd, R. J. In *The Quantum Theory of Atoms in Molecules: From Solid State to DNA and Drug Design*; Matta, C. F., Boyd, R. J., Eds.; Wiley-VCH: Weinheim, 2007; pp 1–34.

(31) Tomasi, J.; Mennucci, B.; Cammi, R. *Chem. Rev.* **2005**, *105* (8), 2999–3093.

(32) Cramer, C. J.; Truhlar, D. G. In *Solvent Effects and Chemical Reactivity*; Tapia, O., Bertran, J., Eds.; Kluwer Academic Publishers: New York, 2002; pp 1–80.

(33) Tannor, D. J.; Marten, B.; Murphy, R.; Friesner, R. A.; Sitkoff, D.; Nicholls, A.; Ringnalda, M.; Goddard, W. A.; Honig, B. *J. Am. Chem. Soc.* **1994**, *116* (8), 11875–11882.

(34) Cortis, C. M.; Langlois, J.-M.; Beachy, M. D.; Friesner, R. A. *J. Chem. Phys.* **1996**, *105* (13), 5472–5484.

(35) Skyner, R. E.; McDonagh, J. L.; Groom, C. R.; Van, M. T.; Mitchell, J. B. O. *Phys. Chem. Chem. Phys.* **2015**, *17* (9), 6174–6191.

(36) Mennucci, B. *Wiley Interdiscip. Rev. Comput. Mol. Sci.* **2012**, *2* (3), 386–404.

(37) Marten, B.; Kim, K.; Cortis, C.; Friesner, R. A.; Murphy, R. B.; Ringnalda, M. N.; Sitkoff, D.; Honig, B. *J. Phys. Chem.* **1996**, *100* (95), 11775–11788.

(38) Jaguar version 7.5; Schrödinger, LLC: Portland, OR, 2007.

(39) Klamt, A. *J. Phys. Chem.* **1995**, *99* (7), 2224–2235.

(40) Ahlrichs, R.; Bär, M.; Häser, M.; Horn, H.; Kölmel, C. *Chem. Phys. Lett.* **1989**, *162* (3), 165–169.

(41) TURBOMOLE V5.10, (2008) a development of University of Karlsruhe, 1989–2007, TURBOMOLE GmbH, since 2007. Available at http://wwwturbomolecom.

(42) TURBOMOLE V6.5 (2013), a development of University of Karlsruhe and Forschungszentrum Karlsruhe GmbH, 1989-2007, TURBOMOLE GmbH, since 2007; available from http://www.turbomole.com.

(43) Cramer, C. J.; Truhlar, D. G. In *Reviews in Computational Chemistry*; Lipkowitz, K. B., Boyd, D. B., Eds.; VCH Publishers: New York, 1995; pp 1–55.

(44) Engel, T. Reid, P. *Physical Chemistry*; Benjamin-Cummings: San Francisco, 2006.

(45) *Transition State of Biochemical Processes*; Gandour, R. D., Schowen, R. L., Eds.; Plenum Press: New York, 1978.

(46) Meek, S. J.; Pitman, C. L.; Miller, A. J. M. *J. Chem. Educ.* **2016**, *93* (2), 275–286.

(47) Aledo, J. C.; Lobo, C.; Esteban, A. *BAMBED* **2003**, *31* (4), 234–236.

(48) Jensen, F. *Introduction to Computational Chemistry*; Wiley-VCH John Willey &

Sons: Chichester, 1998.

(49) Atkins, P.; Overton, T.; Rourke, J.; Weller, M.; Armstrong, F. *Shriver and Atkins Inorganic Chemistry*, 4th ed.; Oxford University Press: Oxford, 2006.

(50) Tachibana, A.; Fukui, K. *Theor. Chim. Acta* **1978**, *49* (4), 321–347.

(51) Tachibana, A.; Fukui, K. *Theor. Chim. Acta* **1980**, *57* (1), 81–94.

(52) Fukui, K. *Acc. Chem. Res.* **1981**, *14* (12), 363–368.

(53) *Web of science* http://apps.webofknowledge.com/WOS_GeneralSearch_input.do?product=WOS&search_mode=GeneralSearch&SID=Z2CshPufNG5BKIZQKdi&preferencesSaved= (accessed Oct 10, 2016).

(54) Crabtree, R. H. *Chem. Rev.* **2015**, *115* (1), 127–150.

(55) Hegedus, L.; Lipshurtz, B.; Nozaki, H.; Reetz, M.; Rittmeyer, P.; Smith, K.; Totter, F.; Yamamoto, H. *Organometallics in synthesis: a manual*; Schlosser, M., Ed.; John Wiley & Sons: Chichester, 1994.

(56) Qian, Y.; Huang, J.; Bala, M. D.; Lian, B.; Zhang, H.; Zhang, H. *Chem. Rev.* **2003**, *103* (7), 2633–2690.

(57) Kulinkovich, O. G.; Sviridov, S. V.; Vasilevskii, D. A.; Pritytskaya, T. S. *Ж. Орг. Хим.* **1989**, *25* (10), 2244–2245.

(58) Leeuwen, P. W. N. M. *Homogeneous Catalysis: Understanding the Art*; Kluwer Academic Pulishers: Netherlands, 2004.

(59) Chong, E.; Qayyum, S.; Schafer, L. L.; Kempe, R. *Organometallics* **2013**, *32* (6), 1858–1865.

(60) Prochnow, I.; Kubiak, R.; Frey, O. N.; Beckhaus, R.; Doye, S. *ChemCatChem* **2009**, *1* (1), 162–172.

(61) Lühning, L. H.; Brahms, C.; Nimoth, J. P.; Schmidtmann, M.; Doye, S. *Z. Anorg. Allg. Chem.* **2015**, *641* (12–13), 2071–2082.

(62) Naktode, K.; Das, S.; Bhattacharjee, J.; Nayek, H. P.; Panda, T. K. *Inorg. Chem.* **2016**, *55* (3), 1142−1153.

(63) Lee, N. E.; Buchwald, S. L. *J. Am. Chem. Soc.* **1994**, *116* (13), 5985–5986.

(64) Willoughby, C. A.; Buchwald, S. L. *J. Am. Chem. Soc* **1994**, *116* (26), 11703–11714.

(65) Bexrud, J. A.; Eisenberger, P.; Leitch, D. C.; Payne, P. R.; Schafer, L. L. *J. Am. Chem. Soc.* **2009**, *131* (6), 2116–2118.

(66) Katsuki, T.; Sharpless, K. B. *J. Am. Chem. Soc.* **1980**, *102* (18), 5974–5976.

(67) Morgans, D. J.; Sharpless, K. B. *J. Am. Chem. Soc.* **1981**, *103* (2), 462–464.

(68) Sharpless, K. B.; Woodard, S. S.; Finn, M. G. *Pure Appl. Chem.* **1983**, *55* (11), 1823–1836.

(69) Ian, D.; Williams, S. F.; Pedersen, K.; Sharpless, B.; Lippard, S. J. *J. Am. Chem. Soc.* **1984**, *106* (21), 643–6431.

(70) Corey, E. J. *J. Org. Chem.* **1990**, *55* (6), 1693–1694.

(71) Potvin, P. G.; Bianchet, S. *J. Org. Chem.* **1992**, *57* (24), 6629–6635.

(72) Gao, Y.; Hanson, R. M.; Klunder, J. M.; Ko, S. Y.; Masamune, H.; Sharpless, K. B. *J. Am. Chem. Soc.* **1987**, *109* (19), 5765–5780.

(73) Woodard, S. S.; Finn, M. G.; Sharpless, K. B. *J. Am. Chem. Soc.* **1991**, *113* (1), 106–113.

(74) Jørgensen, K. A.; Wheeler, R. A.; Hoffmann, R. *J. Am. Chem. Soc.* **1987**, *109* (11), 3240–3246.

(75) Wu, Y.-D.; Lai, D. K. W. *J. Am. Chem. Soc.* **1995**, *60* (3), 673–680.

(76) Wu, Y.-D.; Lai, D. K. W. *J. Am. Chem. Soc* **1995**, *117* (45), 11327–11336.

(77) Martin, V. S.; Woodard, S.; Katsuki, T.; Yamada, Y.; Ikeda, M.; Sharpless, K. B. *J. Am. Chem. Soc.* **1981**, *103*, 6237–6240.

(78) Bach, R. D.; Wolber, G. J.; Coddens, B. A. *J. Am. Chem. Soc.* **1984**, *106* (20), 6098–6099.

(79) Cui, M.; Adam, W.; Shen, J. H.; Luo, X. M.; Tan, X. J.; Chen, K. X.; Ji, R. Y.; Jiang, H. L. *J. Org. Chem.* **2002**, *67* (5), 1427–1435.

(80) Kulinkovich, O. G.; Shevchuk, T. A.; Isakov, V. E.; Prokhorevich, K. N. *Russ. J. Org. Chem.* **2006**, *42* (5), 679–684.

(81) Kananovich, D. G.; Kulinkovich, O. G. **2008**, *64*, 1536–1547.

(82) de Meijere, A.; Kozhushkov, S. I.; Savchenko, A. I. *J. Organomet. Chem.* **2004**, *689* (12), 2033–2055.

(83) Kulinkovich, O. G. *Russ. Chem. Bull.* **2004**, *53* (5), 1065–1086.

(84) Bekish, A. V.; Kulinkovich, O. G. *Tetrahedron Lett.* **2005**, *46* (41), 6975–6978.

(85) Kulinkovich, O. G.; Sviridov, S. V.; Vasilevski, D. A. *Synthesis (Stuttg).* **1991**, *3*, 234.

(86) Epstein, O. L.; Savchenko, A. I.; Kulinkovich, O. G. *Russ. Chem. Bull.* **2000**, *49* (2), 378–380.

(87) Wu, Y. –D.; Yu, Z.-X. *J. Am. Chem. Soc.* **2001**, *123* (24), 5777–5786.

(88) Kulinkovich, O. G.; Kananovich, D. G. *Eur. J. Org. Chem.* **2007**, *2007* (13), 2121–2132.

(89) Kulinkovich, O. G.; Isakov, V.; Kananovich, D. G. *Chem. Rec.* **2008**, *8* (5), 269–278.

(90) Corey, E. J.; Rao, S. A.; Noe, M. C. *J. Am. Chem. Soc.* **1994**, *116* (20), 9345–9346.

(91) Racouchot, S.; Sylvestre, I.; Ollivier, J.; Kozyrkov, Y.; Pukin, A.; Kulinkovich, O. G.; Salaün, J. *Eur. J. Org. Chem.* **2002**, *2002* (13), 2160–2176.

(92) Konik, Y. A.; Kananovich, D. G.; Kulinkovich, O. G. *Tetrahedron* **2013**, *69* (32), 6673–6678.

(93) Kulinkovich, O. G.; Kananovich, D. G.; Lopp, M.; Snieckus, V. *Adv. Synth. Catal.* **2014**, *356* (17), 3615–3626.

(94) Jollie, D. *Platinum 2008*; Johnson Matthey: Royston, 2008.

(95) Sunley, G. J.; Watson, D. J. *Catal. Today* **2000**, *58* (4), 293–307.

(96) Nixon, T. D.; Whittlesey, M. K.; Williams, J. M. J. *Dalton Trans.* **2009**, No. 5, 753–762.

(97) Nugent, T. C.; El-Shazly, M. *Adv. Synth. Catal.* **2010**, *352* (5), 753–819.

(98) Suzuki, T. *Chem. Rev.* **2011**, *111* (3), 1825–1845.

(99) Dobereiner, G. E.; Crabtree, R. H. *Chem. Rev.* **2010**, *110* (2), 681–703.

(100) Guillena, G.; Ramón, D. J.; Yus, M. *Angew. Chemie - Int. Ed.* **2007**, *46* (14), 2358–2364.

(101) Choi, J.; MacArthur, A. H. R.; Brookhart, M.; Goldman, A. S. *Chem. Rev.* **2011**, *111* (3), 1761–1779.

(102) Hopmann, K. H.; Bayer, A. *Organometallics* **2011**, *30* (9), 2483–2497.

(103) Campos, J.; Hintermair, U.; Brewster, T. P.; Takase, M. K.; Crabtree, R. H. *ACS Catal.* **2014**, *4* (3), 973–985.

(104) Church, T. L.; Andersson, P. G. *Coord. Chem. Rev.* **2008**, *252* (5–7), 513–531.

(105) Appel, A. M.; Bercaw, J. E.; Bocarsly, A. B.; Dobbek, H.; Dubois, D. L.; Dupuis, M.; Ferry, J. G.; Fujita, E.; Hille, R.; Kenis, P. J. A.; Kerfeld, C. A.; Morris, R. H.; Peden, C. H. F.; Portis, A. R.; Ragsdale, S. W.; Rauchfuss, T. B.; Reek, J. N. H.; Seefeldt, L. C.; Thauer, R. K.; Waldrop, G. L. *Chem. Rev.* **2013**, *113* (8), 6621–6658.

(106) Olah, G. A.; Prakash, G. K. S.; Goeppert, A. *J. Am. Chem. Soc.* **2011**, *133* (33), 12881–12898.

(107) Mikkelsen, M.; Jørgensen, M.; Krebs, F. C. *Energy Environ. Sci.* **2010**, *3*, 43–81.

(108) Wang, W.; Wang, S. P.; Ma, X. B.; Gong, J. L. *Chem. Soc. Rev.* **2011**, *40* (7), 3703–3727.

(109) Jhong, H. R. M.; Ma, S.; Kenis, P. J. *Curr. Opin. Chem. Eng.* **2013**, *2* (2), 191–199.

(110) *NIST Chemistry WebBook* http://webbook.nist.gov/ (accessed Apr 5, 2015).

(111) Benson, E. E.; Kubiak, C. P.; Sathrum, A. J.; Smieja, J. M. *Chem. Soc. Rev.* **2009**, *38* (1), 89–99.

(112) Tanaka, R.; Yamashita, M.; Nozaki, K. *J. Am. Chem. Soc.* **2009**, *131* (40), 14168–14169.

(113) Ahlquist, M. S. G. *J. Mol. Catal. A* **2010**, *324* (1–2), 3–8.

(114) Yang, X. *ACS Catal.* **2011**, *1* (8), 849–854.

(115) Li, J.; Yoshizawa, K. *Bull. Chem. Soc. Jpn.* **2011**, *84* (10), 1039– 1048.

(116) Tanaka, R.; Yamashita, M.; Chung, L. W.; Morokuma, K.; Nozaki, K. *Organometallics* **2011**, *30* (24), 6742−6750.

(117) Kang, P.; Cheng, C.; Chen, Z.; Schauer, C. K.; Meyer, T. J.; Brookhart, M. *J. Am. Chem. Soc.* **2012**, *134* (12), 5500–5503.

(118) Kang, P.; Meyer, T. J.; Brookhart, M. *Chem. Sci.* **2013**, *4* (9), 3497–3502.

(119) Kang, P.; Zhang, S.; Meyer, T. J.; Brookhart, M. *Angew. Chemie - Int. Ed.* **2014**, *53* (33), 8709–8713.

(120) Cao, L.; Sun, C.; Sun, N.; Meng, L.; Chen, D. *Dalt. Trans.* **2013**, *42* (16), 5755–

5763.

(121) Schultz, N. E.; Zhao, Y.; Truhlar, D. G. *J. Phys. Chem. A* **2005**, *109* (49), 11127–11143.

(122) Csonka, G. I.; Perdew, J. P.; Ruzsinszky, A. *J. Chem. Theory Comput.* **2010**, *6* (12), 3688–3703.

(123) Goerigk, L.; Grimme, S. *Phys. Chem. Chem. Phys.* **2011**, *13* (14), 6670–6688.

(124) Furche, F.; Perdew, J. P. *J. Chem. Phys.* **2006**, *124* (4), 044103–1–27.

(125) Sierka, M.; Hogekamp, A.; Ahlrichs, R. *J. Chem. Phys.* **2003**, *118* (20), 9136–9148.

(126) Eichkorn, K.; Treutler, O.; Öhm, H.; Häser, M.; Ahlrichs, R. *Chem. Phys. Lett.* **1995**, *242* (6), 283–290.

(127) Eichkorn, K.; Weigend, F.; Treutler, O.; Ahlrichs, R. *Theor. Chem. Acc.* **1997**, *97* (1), 119–124.

(128) *Turbomole v5.1 manual* http://www.turbomole-gmbh.com/manuals/version_5_10/DOK_HTML/node54.html (accessed Sep 21, 2016).

(129) Furche, F.; Ahlrichs, R.; Hättig, C.; Klopper, W.; Sierka, M.; Weigend, F. *Wiley Interdiscip. Rev. Comput. Mol. Sci.* **2014**, *4* (2), 91–100.

(130) Schäfer, A.; Horn, H.; Ahlrichs, R. *J. Chem. Phys.* **1992**, *97* (4), 2571–2577.

(131) Petersson, G. A.; Bennett, A.; Tensfeldt, T. G.; Al-Laham, M. A.; Shirley, W. A.; Mantzaris, J. *J. Chem. Phys.* **1988**, *89* (4), 2193–218.

(132) Krishnan, R.; Binkley, J. S.; Seeger, R.; Pople, J. A. *J. Chem. Phys.* **1980**, *72* (1), 650–654.

(133) The LACV3P basis set is a triple-zeta contraction of the LACVP basis set developed and tested at Schrödinger, Inc.

(134) Frisch, M. J.; Pople, J. A.; Binkley, J. S. *J. Chem. Phys.* **1984**, *80* (7), 3265–3269.

(135) Martin, J. M. L.; Sundermann, A. *J. Chem. Phys.* **2001**, *114* (8), 3408–3420.

(136) Reed, A. E.; Weinstock, R. B.; Weinhold, F. *J. Chem. Phys.* **1985**, *83* (2), 735–746.

(137) Andzelm, J.; Kölmel, C.; Klamt, A. *J. Chem. Phys.* **1995**, *103* (21), 9312–9320.

(138) Lide, D. R. *CRC Handbook of Chemistry and Physics*, 88th ed.; CRC Press, 2008.

(139) Gutowski, K. E.; Dixon, D. A. *J. Phys. Chem. A* **2006**, *110* (28), 8840–8856.

(140) Kelly, C. P.; Cramer, C. J.; Truhlar, D. G. *J. Chem. Theory Comput.* **2005**, *1* (6), 1133–1152.

(141) Todd, A.; Keith, T. K. *AIMAll* (Version 11.10.16); Gristmill Software: Overland Park, KS, 2012. Available at: http://aim.tkgristmill.com.

(142) Reile, I.; Paju, A.; Müürisepp, A. M.; Pehk, T.; Lopp, M. *Tetrahedron* **2011**, *67* (33), 5942–5948.

(143) Osadchuk, I.; Pehk, T.; Paju, A.; Lopp, M.; Öeren, M.; Tamm, T. *Int. J. Quantum Chem.* **2014**, *114* (15), 1012–1018.

(144) Mäe, G. *1,2-tsüklopentaandioonide titaani kompleksid: bakalaureusetöö*; Tallinn, 2004.

(145) Huheey, J. E.; Keiter, E. A.; Keiter, R. L. *Inorganic Chemistry*, 4th ed.; Harpercollins College, 1993.

(146) Nakagawa, Y.; Muramatsu, Y.; Harada, T. *European J. Org. Chem.* **2010**, *2010* (34), 6535–6538.

(147) Fernández-Mateos, E.; MacIá, B.; Ramón, D. J.; Yus, M. *European J. Org. Chem.* **2011**, *2011* (34), 6851–6855.

(148) Zong, H.; Huang, H.; Song, L. *Tetrahedron Asymmetry* **2016**, *27* (20–21), 1069–1074.

(149) Davis, T. J.; Balsells, J.; Carroll, P. J.; Walsh, P. J. *Tetrahedron* **2001**, *3* (5), 699–702.

(150) Balsells, J.; Davis, T. J.; Carroll, P.; Walsh, P. J. *J. Am. Chem. Soc.* **2002**, *124* (35), 10336–10348.

(151) Waltz, K. M.; Carroll, P. J.; Walsh, P. J. *Organometallics* **2004**, *23* (1), 127–134.

(152) Gillespie, P.; Ramirez, F.; Ugi, I.; Marquarding, D. *Angew. Chem. Int. Ed. Engl.* **1973**, *12* (2), 91–119.

(153) Wu, K. H.; Kuo, Y. Y.; Chen, C. A.; Huang, Y. L.; Gau, H. M. *Adv. Synth. Catal.* **2013**, *355* (5), 1001–1008.

(154) Li, Q.; Gau, H. M. *Chirality* **2011**, *23* (10), 929–939.

(155) Osadchuk, I.; Tamm, T.; Ahlquist, M. S. G. *Organometallics* **2015**, *34* (20), 4932–4940.

(156) Wang, Y.; Ahlquist, M. S. G. *Dalton Trans.* **2013**, *42* (21), 7816–7822.

(157) Wang, Y.; Wang, M.; Sun, L.; Ahlquist, M. S. G. *Chem. Commun.* **2012**, *48* (37), 4450.

(158) Ess, D. H.; Bischof, S. M.; Oxgaard, J.; Periana, R. A.; Goddard III, W. A. *Organometallics* **2008**, *27* (24), 6440–6445.

(159) McCormick, M. C.; Keijzer, K.; Polavarapu, A.; Schultz, F. A.; Baik, M. H. *J. Am. Chem. Soc.* **2014**, *136* (25), 8992–9000.

(160) Ozerov, O. V. *Chem. Soc. Rev.* **2009**, *38* (1), 83–88.

Publication I

Osadchuk, I.; Pehk, T.; Paju, A.; Lopp, M.; Öeren, M.; Tamm, T.; Isomers and conformers of complexes of $Ti(O\textit{i}Pr)_4$ with cyclopentane-1,2-dione: NMR study and DFT calculations, *International Journal of Quantum Chemistry*, **2014**, *114*, 1012-1018.

International Journal of QUANTUM CHEMISTRY

Isomers and Conformers of Complexes of Ti(O*i*Pr)$_4$ with Cyclopentane-1,2-Dione: NMR Study and DFT Calculations

Irina Osadchuk,[a] Tõnis Pehk,[b] Anne Paju,[a] Margus Lopp,[a] Mario Öeren,[a] and Toomas Tamm*[a]

^{1}H and ^{13}C NMR spectra of Ti(O*i*Pr)$_4$ complexes with 3-methyl-1,2-cyclopentanedione in deuterochloroform solution reveal formation of different compounds, depending on the molar ratio of diketone and Ti-isopropoxide. The obtained results were compared with the DFT calculations of these complexes. Both NMR study and theoretical calculations show that the most stable complex is formed with two dione and one single isopropoxide molecules. Detailed conformational analysis was required to find the relative energies of the isomers and conformers of the systems. A possibility of presence of multiple isomeric complexes, some of which come in enantiomeric pairs, was revealed. Possible abundances of the isomers were estimated on the basis of Boltzmann distribution. © 2014 Wiley Periodicals, Inc.

DOI: 10.1002/qua.24619

Introduction

Chiral titanium complexes have been found to be efficient catalysts for asymmetric chemical transformations. From these, asymmetric epoxidation of allylic alcohols[1,2] and sulfoxidation[3,4] are of the most widely used. Additionally, a number of different other Ti-catalyzed asymmetric transformations is introduced in synthetic organic chemistry (e.g., Refs. [5–10]). We have found that Ti(O*i*Pr)$_4$/tartaric ester complex serves as an asymmetric inducer for the asymmetric Baeyer–Villiger oxidation of cyclobutanones,[11] α-hydroxylation of β-hydroxyketones,[12] and a cascade oxidation of 1,2-diketones to γ-lactone carboxylic acids.[13,14]

The structure of titanium/substrate/ligand complexes is a key factor determining the activity and selectivity of the catalytic processes. There have been several experimental and computational investigations dealing with the structure of titanium/ligand complexes[15–20] and titanium/substrate/ligand clusters.[21–27] Much less attention is paid to titanium/substrate complexes.[28,29]

The complexes of 1,2-cyclopentanedione **1** (Scheme 1) with $VOCl_3$ have been studied.[30] The findings indicate that a large variability exists among the structures, depending on the components of the complex. Ligand position and orientation plays also a significant role in energy distribution and complex stability.[31–33]

We have investigated the mechanism of a Ti-based asymmetric oxidation cascade reaction of 3-alkyl-1,2-cyclopentanedione.[34] To establish the possible structure of 3-alkyl-1,2-cyclopentanedione titanium complexes that form together with the asymmetric ligand a catalytic intermediate cluster, we investigated the structure of complexes between 3-methyl-1,2-cyclopentanedione **1** and Ti(O*i*Pr)$_4$ **2** using the ^{1}H and ^{13}C NMR spectra of the solutions at different component ratios. However, the chemical and spectral data were not sufficient to establish the structure of the complexes. Therefore, possible structures of the complexes were modeled using DFT methodology and structures of possible isomers and conformers of the systems with various degrees of substitution were established. Relative energies of the structures were used to explain the equilibria observed in the NMR experiments.

The systematic conformational analysis of penta- and hexa-coordinated complexes involved creation of a list of all possible relative positions and orientations of the ligands involved. Systematic studies of complexes with bidentate asymmetric ligands are rare in the literature. We used a classification system analogous to the one used in [31]. We believe that the systematic enumeration of possible relative orientations of the mix of axially symmetric and nonaxially symmetric ligands, as presented in this study, has a value of its own in further studies of systems of analogous compositions.

Experimental: NMR Studies at Different Ratios of Ti(O*i*Pr)$_4$ and 3-Methyl-1,2-Cyclopentanedione

We prepared mixtures of 3-methyl-1,2-cyclopentanedione **1**, 2-methoxy-3-methylcyclopent-2-en-1-one, and 3-methylcyclo pent-2-en-1-one with Ti-tetraisopropoxide **2** at component ratios from 1:1 to 4:1. From the ^{1}H and ^{13}C NMR spectra of these compounds in deuterochloroform solution, we found

[a] *I. Osadchuk, A. Paju, M. Lopp, M. Öeren, T. Tamm*
Department of Chemistry, Tallinn University of Technology, Ehitajate tee 5, Tallinn 19086, Estonia
E-mail: toomas.tamm@ttu.ee
[b] *T. Pehk*
National Institute of Chemical Physics and Biophysics, Laboratory of Chemical Physics, Akadeemia tee 23, Tallinn 12618, Estonia
Contract grant sponsor: Estonian Science Foundation; contract grant number: 8255 and 8880.
Contract grant sponsor: Estonian Ministry of Education and Research; contract grant number: 0140060s12 and IUT 19-32.
Contract grant sponsor: EU European Regional Development Fund; contract grant number: 3.2.0101.08-0017.

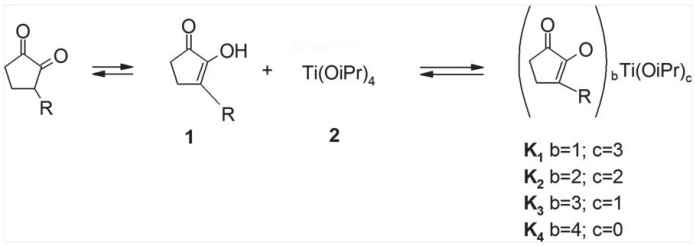

Scheme 1. Possible formal complexes of diketone **1** and Ti(*i*Pr)$_4$ **2**.

that only 3-methyl-1,2-cyclopentanedione in enolic form (presented in Scheme 1) yields complexes with titanium tetraisopropoxide. In this work, the possible enolates are denoted $\mathbf{K_1}$–$\mathbf{K_4}$ according to the number of 3-methyl-1,2-cyclopentanedienyl ligands in the complex.

The compounds **1** and **2** were mixed at different molar ratios from 1:1 to 4:1 in $CDCl_3$ solution at −20°C under argon atmosphere. NMR spectra of the reaction products reveal the formation of different Ti-enolates as well as the existence of the free initial components and isopropanol (formed in the reaction). These multicomponent multisite exchange broadened-lined spectra (clearly distinguishable) were analyzed by observing individual signals from different complexes due to relatively slow exchange rates between the complexes. Details of the analysis and a sample spectrum are available in the electronic Supplementary Information.

Enol **1**, when mixed with titanium alcoholate **2**, may form at least four different titanium enolates $\mathbf{K_1}$–$\mathbf{K_4}$ (Scheme 1). However, only three of them — $\mathbf{K_2}$ to $\mathbf{K_4}$ — were observed. In the 1:1 mixture of the components only a single new compound (determined as enolate $\mathbf{K_2}$) was detected, together with isopropanol and unreacted titanium tetraisopropoxide. In the spectrum of 2:1 mixture of the components, (ketone **1** to **2**) the same product $\mathbf{K_2}$ was observed (enolate $\mathbf{K_2}$; Scheme 2).

Formation of the same complex $\mathbf{K_2}$ was also observed at the 3:1 ratio of **1** and **2**. Additionally, in the 3:1 mixture the formation of a new complex $\mathbf{K_3}$ in considerable amount, with three molecules of ketone **1**, was observed. The presence of a complex $\mathbf{K_4}$ in the mixture was also detected. It is noteworthy that in this case considerable amount of free uncomplexed ketone remained in the solution. Increasing the ratio of **1** to **2** further to 4:1 results in additional increase of uncomplexed ketone. Summary of changes in relative amounts of different complexes and free ketone are given in Table 1. These data were obtained from the integration of NMR spectra.

Comparison of ^{13}C NMR spectra of initial free substrate **1** and its complexes $\mathbf{K_2}$ to $\mathbf{K_4}$ with Ti(O*i*Pr)$_4$ clearly point to the formation of Ti—O bond via the hydroxyl group (see details in the electronic Supplementary Information).

The experimental NMR results reveal that the relative abundances of the complexes of **1** with **2** come in the sequence $\mathbf{K_2} > \mathbf{K_3} > \mathbf{K_4} > \mathbf{K_1}$. The $\mathbf{K_2}$ is formed first, and it is the single complex observed at low **1** to **2** ratios. Upon increasing ratios to 3:1 and 4:1, two new complexes $\mathbf{K_3}$ and $\mathbf{K_4}$ appear in the NMR spectra. The lines of $\mathbf{K_1}$ are not observed in NMR spectra at all. It was impossible to obtain quantitative data about the relative stability of these complexes from the measured mixtures, because in these multicomponent mixtures free **1** is present in significant amounts, as is also free isopropanol, which forms in the course of the reaction. Its presence results in remarkable broadening of signals in NMR spectra of measured samples. To get more information about the relative stability of complexes $\mathbf{K_1}$–$\mathbf{K_4}$ and to verify conclusions made on the basis of the NMR spectra, a computational study was undertaken.

Computations: DFT Modeling of the Complex Structures

Calculations of the structure of the complexes were carried out using DFT approach according to standard computational chemistry methodology. Initially, relative location and orientations of the ligands were set up by following simple chemical

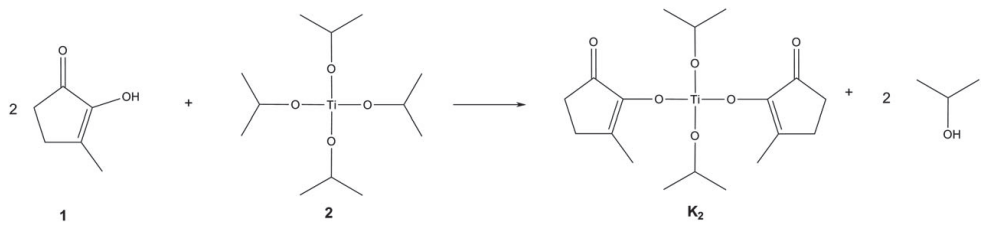

Scheme 2. Formation of complex $\mathbf{K_2}$.

Table 1. Distribution of diketone **1** molecules between different solute molecules in the deuterochloroform at different diketone **1** and Ti(O*i*Pr)$_4$ **2** ratios.

No	Ratio 1:2	Free ketone	Ti(O*i*Pr)$_4$	K_2	K_3	K_4
1	1:1	–	0.5	0.5	–	–
2	2:1	–	–	2	–	–
3	3:1	0.80	–	0.75	1.15	0.30
4	4:1[a]	2.40	–	0.15	1.15	0.30

[a] some insoluble precipitate also formed.

intuition. However, the relative energies of the complexes did not correlate with the experimental findings reported above. Therefore, a careful and systematic search for lowest energy isomers and conformers of the complexes was required to reach an understanding of the experimental findings.

The original optimizations and conformational searches were performed with the BP86 functional and the SV(P) basis set. The selected lowest-energy geometries were refined with the def2-TZVP basis set.[35] Solvent effects ($CDCl_3$ solvent, $\varepsilon = 4.81$ at 293 K[36]) were accounted for with the COSMO continuum model. Geometries of the structures were fully optimized, and minima were verified with vibrational analysis. Gas-phase zero-point vibrational energies were added to the solvent-optimized electronic energies.[37] Turbomole version 5.10[38] software was used. Final geometries and original energies in Hartree are available in the electronic Supplementary Information.

Titanium tetraisopropoxide

Conformational analysis of this molecule was performed by changing the eight torsional angles corresponding to the rotation around Ti—O and O—C bonds. In the lowest energy conformers, the hydrogen atom at the tertiary carbon is directed toward the oxygen atom of a neighboring isopropoxy group. The lowest energy conformer (Fig. 1) has S_4 symmetry, and each hydrogen at the tertiary carbons is pointed at an oxygen of another O—*i*Pr group in such arrangement that no oxygen has more than one hydrogen pointing at it. Excluding possible rotations and reflections of the whole molecule, such arrangement is unique.

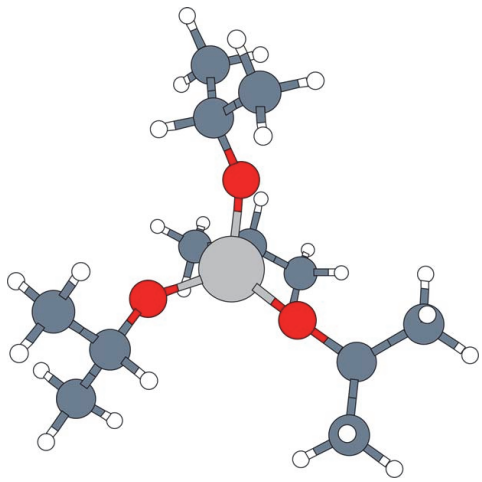

Figure 1. The lowest-energy conformer of titanium tetraisopropoxide. [Color figure can be viewed in the online issue, which is available at wileyonlinelibrary.com.]

Complex K_1

In the conformational analysis, rotation about five torsional angles (three defining the position of each O—*i*Pr groups and two defining the position of the cyclopentanedione [C(2)—O(3)—Ti(4)—O(4) and C(1)—C(2)—O(3)—Ti(4)] were considered (Fig. 2). The bend angles C(2)—O(3)—Ti(4) in the starting geometries were set to 110 and 170 degrees to test for presence or absence of a Ti—O bond.

In this text, we shall use the terms "conformer" and "isomer" interchangeably, because the barriers for interconversion between the structures are unknown. The NMR data did not reveal presence of distinct isomers, so we are inclined to favor rapid interconversion and, consequently, do not distinguish between isomers at room temperature.

In all conformers, the orientation of the five-membered cycle is coplanar with the titanium atom as well as one of the

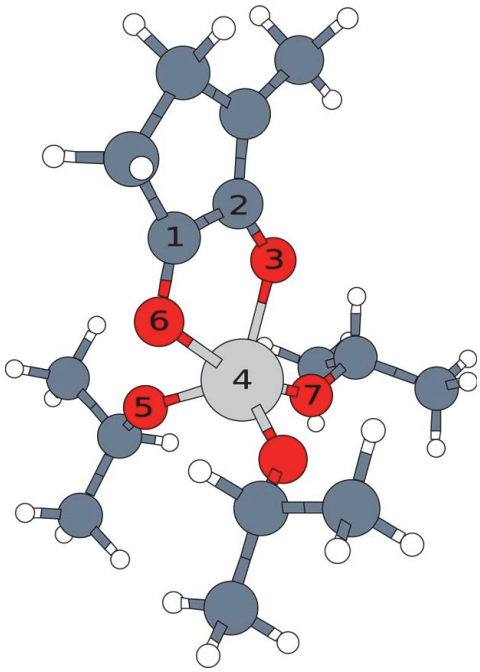

Figure 2. The lowest-energy conformer of the complex K_1. [Color figure can be viewed in the online issue, which is available at wileyonlinelibrary.com.]

Table 2. Conformers of the complex $\mathbf{K_1}$. [Color table can be viewed in the online issue, which is available at wileyonlinelibrary.com.]

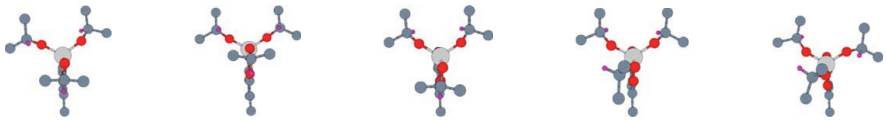

Conformer	1a, 1b	2	3	4a, 4b	5a, 5b
ΔE (kJ/mol)	0.00	0.00	0.60	1.14	2.25
%	43.5 (2×21.7)	17.4	14.9	25.3 (2×12.6)	14.9 (2×7.5)

isopropoxy oxygens (atom 7 in Fig. 2). The distance between substrate carbonyl oxygen atom and titanium atom was quite small: 2.27. . .2.63 Å in all converged calculations. This suggests that a weak chemical bond forms between Ti(4) and O(6).

The presence of a chemical bond was tested by performing an atoms-in-molecules[39] (AIM) analysis with the AIMAll[41] software. A bond critical point exists along the Ti(4)—O(6) path, but the bond delocalization index (DI, interpreted as bond order) as calculated in the AIM model is only 0.22, suggesting the presence of a weak chemical bond. For comparison, the Ti(4)—O(3) bond has a DI 0.51, the other three Ti—O bonds are 0.81–0.86, and the carbon–carbon single bonds in the system are all very close to 1.0. If we take the bond with DI = 0.22 into account, the coordination number of titanium in this compound becomes five. This coordination is reflected in the figures, by drawing a bond between the corresponding atoms.

We also checked whether further increase of coordination number would be favorable by adding a sixth ligand, an isopropanol molecule. Performed calculations showed that six-coordinated $\mathbf{K_1}$ complex is higher in energy relative to the products: the lowest-energy conformer was 14.5 kJ/mol higher in energy than isolated reactants.

Eight conformers of the complex $\mathbf{K_1}$ with five-coordinated titanium were found. In all cases the position of the five-membered cyclic ligand remains the same and conformers differ from each other only by the position of isopropoxy groups. These positions can be uniquely described in all eight conformers by the directions of the hydrogen atoms at the tertiary carbons (shown in magenta color in Table 2). The prevalences of conformers were calculated as Boltzmann distribution and are given in Table 2. Enantiomeric structures are marked with the same number, distinguished by the letter in the designation. Detailed geometries and energies of the systems are available in the electronic Supplementary Information.

Complex K_2

Conformational analysis of this complex involved rotation of both the isopropoxy ligands along the Ti—O and O—C bonds, as well as altering the relative positions of the two pentanedione ligands. The results indicate that both pentanedione ligands are bidentate (Fig. 3), like in the complex $\mathbf{K_1}$. In the majority of the optimized structures, the distance between the pentanedione carbonyl oxygen atom and titanium atom was between 2.22 and 2.37 Å. AIM bond DIs for the two Ti—O bonds of each ligand are near 0.2 and 0.5, just like in $\mathbf{K_1}$. We presume that a similar weak bond is formed as in the previous case. The titanium atom therefore has coordination number six (Fig. 3).

In a near-octahedral complex with two similar monodentate and two similar asymmetric bidentate ligands, eight ways to position the substrate cycles exist. Six of them form three enantiomeric pairs (mirror images of each other), whereas two are C_s-symmetric if rotations of the monodentate ligands are ignored. The latter differ from each other by the orientation of the methyl groups of the pentanedione. As noted above, in the absence of information about isomerization barriers, we cannot distinguish between conformers and isomers of the system. We assume a Boltzmann distribution of the systems with differing energies, corresponding to free rapid interconversion of the isomers.

We denote the asymmetric isomers by three prefixes (e.g., *cis-cis-trans*), where the first one indicates the relative positioning of the isopropoxy ligands, the second one denotes the

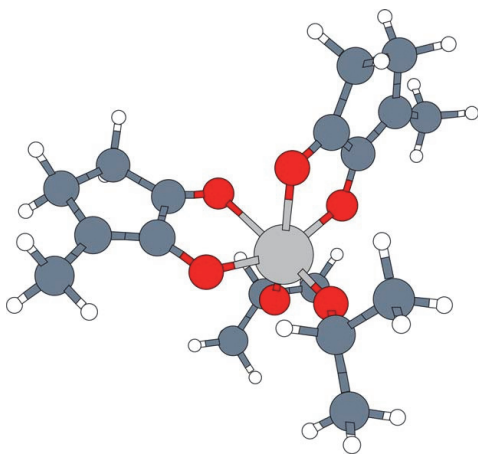

Figure 3. The lowest-energy conformer of the complex $\mathbf{K_2}$. [Color figure can be viewed in the online issue, which is available at wileyonlinelibrary.com.]

Table 3. Conformers of complex $\mathbf{K_2}$. [Color table can be viewed in the online issue, which is available at wileyonlinelibrary.com.]

	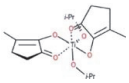	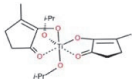	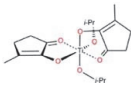	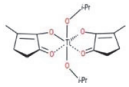	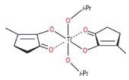
Conformer	Λ, Δ-*cis-cis-trans*	Λ, Δ-*cis-cis-cis*	Λ, Δ-*cis-trans-cis*	*trans-syn*	*trans-anti*
ΔE (kJ/mol)	0.00	5.78	25.72	28.61	54.54
%	94.0 (2×47.1)	6.0 (2×2.9)	0.0 (2×0.0)	0.0	0.0

relative position of the carbonyl oxygens (weaker/longer chemical bonds) of the pentanedione, and the third prefix determines the locations of the stronger/shorter titanium–oxygen bonds with pentanediones. The positions of the methyl substituents of the substrate are uniquely determined, being *anti* in the *cis-cis-trans* and *cis-trans-cis* complexes and *syn* in the *cis-cis-cis* case. Λ and Δ describe the chirality of enantiomeric complexes.

In the symmetric isomers, the cyclic ligands lie on the same plane, and we only need to indicate the relative positions of the isopropoxy ligands (*trans* in both cases) and the methyl substituents of the pentanediones (*syn* or *anti*). Structures and relative energies of the eight isomers are listed in Table 3.

Positions of the pentanedione ligands have significant influence on the energy of complex $\mathbf{K_2}$. Boltzmann probabilities of the last four conformers (Λ-*cis-trans-cis,* Δ-*cis-trans-cis, trans-syn, and trans-anti*) are very low, practically equal to zero, because difference in energies between those conformers and the lowest-energy conformer (*cis-cis-trans*) is more than 25 kJ/mol. The energy of the complex is also influenced by the rotation of isopropoxy ligand, although the effects have smaller magnitude than the energy differences associated with position of pentanediones. The lowest-energy minima with respect to this rotation are reported in all cases.

We conclude that the *cis-cis-trans* isomer is the prevalent one in the solution, with a small (~3%) presence of the cis-*cis-cis* isomers. Assuming rapid interconversion, the probability of the remaining isomers is close to zero.

Complex K_3

Initial geometries of the conformers of $\mathbf{K_3}$ were generated by fixing the positions of the two bidentate ligands, whereas the positions of the remaining pentanedione ligand and isopropoxy ligand were changed by altering torsional angles corresponding to rotation of the five-membered ring around Ti—O bond and Ti—O*i*Pr in the case of isopropoxy ligand. The titanium atom prefers to remain six-coordinate, not forming the seventh bond with the other oxygen of the additional cyclopentanedione ligand. The ligand remains monodentate.

Ten different ways to situate the bidentate pentanedione cycles exist in the complex $\mathbf{K_3}$. The two additional conformers, when compared to those of $\mathbf{K_2}$, arise from different relative positions of the monodentate ligands, which are now distinguishable (O*i*Pr and the substrate), unlike in $\mathbf{K_2}$, where they were chemically identical (O*i*Pr). The two variants of the *cis-cis-cis* isomer will be denoted with prime (′) and second (″) symbols (Table 4). In this table, the lowest relative energies of different spatial structures of complexes $\mathbf{K_3}$ are given.

The most preferable pentanedione position in $\mathbf{K_3}$ again appears to be *cis-cis-trans*, with smaller but relevant probability of the *cis-cis-cis′* and *cis-cis-cis″* isomers. Prevalence of the remaining isomers is close to zero.

The bond DIs for the bidentate ligands are slightly higher than in the previous cases, averaging 0.25 for the weaker bond and 0.53 for the stronger one. The singly bound pentanedione has a bond index 0.69 and the O*i*Pr ligand −0.90.

Complex K_4

Initial geometries of the conformers of $\mathbf{K_4}$ were generated by fixing the positions of two bidentate cyclic ligands and the positions of the remaining two pentanediones were changed by altering torsional angles corresponding to rotation of the five-membered ring around Ti—O bond.

Exhaustive search for all conformers of this complex would have been computationally too demanding. Therefore a subset of the full conformational space was scanned. The simplifications were based on assumed similarity of relative energies of isomers of $\mathbf{K_4}$ on one hand, and $\mathbf{K_2}$ and $\mathbf{K_3}$ on the other hand. As expected (Table 5), the *cis-cis-trans* isomer turned out to be most preferable here too. The bond DIs (bond orders) of the bidentate ligands increase further being 0.27 and 0.58, respectively. The singly bound pentanediones have stronger bonds, with a DI of 0.72. Thus, we see a systematic increase of bond

Table 4. Conformers of complex $\mathbf{K_3}$.[a] [Color table can be viewed in the online issue, which is available at wileyonlinelibrary.com.]

	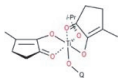	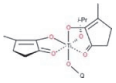	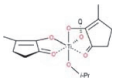
Conformer	Λ, Δ-*cis-cis-trans*	Λ, Δ-*cis-cis-cis′*	Λ, Δ-*cis-cis-cis″*
ΔE (kJ/mol)	0.00	6.44	8.37
%	93.9 (2×46.9)	4.4 (2×2.2)	1.8 (2×0.9)
	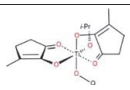	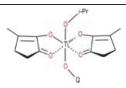	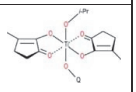
Conformer	Λ, Δ-*cis-trans-cis*	*Trans-syn*	*Trans-anti*
ΔE (kJ/mol)	26.91	31.21	57.70
%	0.0 (2×0.9)	0.0	0.0

[a] Q = pentanedione.

Table 5. Relative energies of conformers of K_4.

Conformer	Λ, Δ-*cis-cis-trans*	Λ, Δ-*cis-cis-cis*	Λ, Δ-*cis-trans-cis*	*trans-syn*	*trans-anti*
ΔE (kJ/mol)	0.00	5.36	25.42	32.14	53.40
%	92.8 (2×46.4)	7.2 (2×3.6)	0.0 (2×0.0)	0.0	0.0

order as the number of pentanedione ligands in the complexes is increased.

Discussion

The DFT results indicate that after two or more substitutions of isopropyl ligands at the titanium atom with 3-methyl-1,2-cyclopentanedione molecules, it is most probable that two cyclopentanedione ligands are bidentate and are situated in *cis-cis-trans* positions relative to each other. The probability that the bidentate pentanediones are situated in *cis-cis-cis* positions is significantly lower, whereas the existence probability of the other relative positions of bidentate pentanediones is practically zero. The Boltzmann probabilities of various isomers of all three complexes $\mathbf{K_2}$–$\mathbf{K_4}$ are summarized in Table 6.

Relative energies of complex formation of all complexes are depicted in Figure 4. The energy of the lowest-energy stereoisomer for each system is presented. Formation of the complexes $\mathbf{K_2}$ and $\mathbf{K_3}$ is more preferable than formation of the complex $\mathbf{K_1}$, with the formation of $\mathbf{K_2}$ being more favorable by 16 kJ/mol of Gibbs free energy than formation of $\mathbf{K_1}$. This is in good agreement with experimental findings. The NMR results presented above showed presence of complexes $\mathbf{K_2}$, $\mathbf{K_3}$, as well as small amounts of $\mathbf{K_4}$. No $\mathbf{K_1}$ was found in the experiment. Moreover, the formation of complex $\mathbf{K_2}$ is more favorable than formation of the complexes with a larger number of ligands. This is also in good agreement with experiment: in reactions with different molar ratios of reagents the complex $\mathbf{K_2}$ was always formed, the complexes $\mathbf{K_3}$ and $\mathbf{K_4}$ were formed only then the molar ratio of substrate and $Ti(O\mathit{i}Pr)_4$ was larger than 2:1.

The calculations did not fully explain the absence of $\mathbf{K_1}$ in the spectra. It is computed to have slightly lower Gibbs energy than $\mathbf{K_4}$, which was observed. This discrepancy could be attributed both to the experiments, where ketone **1** to alcoholate **2**

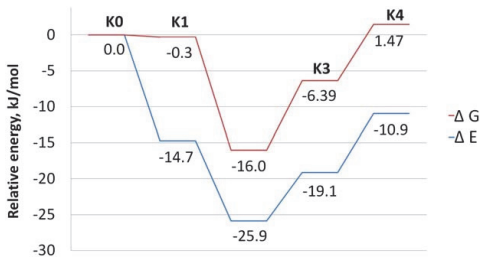

Figure 4. Relative energies of the lowest-energy isomers of the complexes $\mathbf{K_1}$–$\mathbf{K_4}$. The reactants are indicated as $\mathbf{K_0}$. [Color figure can be viewed in the online issue, which is available at wileyonlinelibrary.com.]

Table 6. Relative probabilities of the isomers of complex is $\mathbf{K_2}$–$\mathbf{K_4}$.

Conformer	Λ, Δ-*cis-cis-trans*	Λ, Δ-*cis-cis-cis*	Λ, Δ-*cis-trans-cis*	*trans-syn*	*trans-anti*
$\mathbf{K_2}$	94.0	6.0	0.0	0.0	0.0
$\mathbf{K_3}$	94.0	6.2	0.0	0.0	0.0
$\mathbf{K_4}$	92.8	7.2	0.0	0.0	0.0

ratios less than 1:1 were not investigated, as well as to calculations, where an exhaustive conformational search of $\mathbf{K_4}$ could not be performed.

Conclusions

The results of calculations support the experimental finding that formation of $\mathbf{K_2}$ is most favored. Also, coordination of both oxygen atoms to titanium that was suggested by the NMR spectrum is also supported by the calculations.

Formation of $\mathbf{K_3}$ is slightly unfavorable and it is in accordance with the experiment—complex $\mathbf{K_3}$ forms only in the case of excess of ketone **1**. Formation of complex $\mathbf{K_4}$ is even less favored. In our experiments, we found only traces of $\mathbf{K_4}$ in the solution, even when fourfold excess of ketone **2** was used. According to our calculations, complexes $\mathbf{K_2}$–$\mathbf{K_4}$ are six-coordinated, having two different types of ligands—the cyclopentanedione ligand can be coordinated in unidentate or bidentate manner depending on the composition of the complex and availability of free coordination sites at titanium.

The relative instability of triply substituted complex $\mathbf{K_3}$ can be justified by geometrical factors: in doubly substituted $\mathbf{K_2}$, Ti atom is six-coordinated with approximately octahedral geometry (Fig. 1). Addition of the third bidentate ligand replacing a unidentate one would lead to seven-coordination, or an unsaturated valence. Similar reasoning also applies to $\mathbf{K_4}$, where two of the four substrate ligands remain mono-coordinated.

A side-product of the present study is an enumeration and systematization of the possible relative orientations of the kinds of penta- and hexa-coordinated complexes where the bidentate ligands are not symmetric. The lists presented in Tables (2–5) of this work may be utilized in future studies of similar complexes.

Acknowledgments

The authors express their gratitude to Greta Neidre (Mäe) for help with chemical synthesis and measurements.

Keywords: density functional theory · NMR · conformations · isomers · complexes · titanium

How to cite this article: I. Osadchuk, T. Pehk, A. Paju, M. Lopp, M. Öeren, T. Tamm. *Int. J. Quantum Chem.* **2014**, *114*, 1012–1018. DOI: 10.1002/qua.24619

Additional Supporting Information may be found in the online version of this article.

[1] K. B. Sharpless, *J. Am. Chem. Soc.* **1980**, *102*, 5976.
[2] T. Katsuki, In *Comprehensive Asymmetric Catalysis*, Vol. *II*;, E. N. Jacobsen, A. Pfaltz, H. Yamamoto, Eds.; Springer: Berlin, **1999**; p. 621.
[3] H. B. Kagan, *Asymmetric Oxidation of Sulfides*; Wiley: Weinham, **2000**.
[4] C. Bolm, K. Muñiz, J. P. Hildebrand, In *Comprehensive Asymmetric Catalysis*, Vol. *II*; E. N. Jacobsen, A. Pfaltz, H. Yamamoto, Eds.; Springer: Berlin, **1999**; p. 697.
[5] J. T. Reeves, Z. T. Z. S. Han, G. Li, Y. Zhang, Y. Xu, D. C. Reeves, N. C. Gonella, S. Ma, H. Lee, B. Z. Lu, C. H. Senanayake, *Angew. Chem. Int. Ed.* **2012**, *51*, 1400.
[6] C. -A. Chen, K. -H. Wu, H. -M. Gau, *Angew. Chem. Int. Ed.* **2007**, *46*, 5373.
[7] A. M. Seayad, B. Ramalingam, K. Yoshinaga, T. Nagata, C. L. L. Chai, *Org. Lett.* **2009**, *12*, 264.
[8] H. Yamamoto, D. Nakashima, *SYNLETT* **2006**, 150.
[9] P. Vairaprakash, M. Periasamy, *Tetrahedron Lett.* **2008**, *49*, 1233.
[10] M. Perseghini, M. Massaccesi, Y. Liu, A. Togni, *Tetrahedron* **2006**, *62*, 7180.
[11] M. Lopp, A. Paju, T. Kanger, T. Pehk, *Tetrahedron Lett.* **1996**, *37*, 7583.
[12] M. Lopp, A. Paju, T. Kanger, T. Pehk, *Tetrahedron Lett.* **1997**, *28*, 5051.
[13] A. Paju, T. Kanger, T. Pehk, M. Lopp, *Tetrahedron Lett.* **2000**, *41*, 6883.
[14] A. Paju, K. Oja, K. Matkevičs, P. Lumi, I. Järving, T. Pehk, M. Lopp, *Hetrocycles* **2014**, *88*, 981.
[15] E. Meggers, *Eur. J. Inorg. Chem.* **2011**, *19*, 2911.
[16] Z. Flisak, K. Szczegot, *J. Mol. Catal. A: Chem.* **2003**, *206*, 429.
[17] G. Paolucci, M. Bortoluzzi, L. Sperni, *Inorg. Chem. Commun.* **2009**, *12*, 1001.
[18] G. Yang, L. Zhou, X. Han, *J. Mol. Catal. A: Chem.* **2012**, *363*, 371.
[19] F. Naso, M. A. M. Capozzi, A. Bottoni, M. Calvaresi, V. Bertolasi, F. Capitelli, C. Cardellicchio, *Chem. Eur. J.* **2009**, *15*, 13417.
[20] S. Kondo, K. Saruhashi, K. Seki, K. Matsubara, K. Miyaji, T. Kubo, K. Matsumoto, T. Katsuki, *Angew. Chem. Int. Ed.* **2008**, *47*, 10195.
[21] M. G. Finn, K. B. Sharpless, *J. Am. Chem. Soc.* **1991**, *113*, 113.
[22] P. W. N. M. van Leeuwen, D. Rivillo, M. Raynal, Z. Freixa, *J. Am. Chem. Soc.* **2011**, *133*, 18562.
[23] S. MacMillan, T. L. Tanski, J. M. Tanski, *Tetrahedron: Asymm.* **2008**, *19*, 543.
[24] P. Hegarty, R. Lau, W. B. Mortherwell, *Tetrahedron Lett.* **2003**, *44*, 1851.
[25] G. Santoni, M. Mba, M. Bonchio, W. A. Nugent, C. Zonta, G. Licini, *Chem. Eur. J.* **2010**, *16*, 645.
[26] M. Seenivasaperumal, H. -J. Federsel, K. J. Szabó, *Adv. Synth. Catal.* **2009**, *351*, 903.
[27] H. Shi, J. He, *J. Catal.* **2011**, *351*, 155.
[28] M. Hayashi, N. Nakamura, K. Yamashita, *Tetrahedron* **2004**, *60*, 6777.
[29] A. J. Hickman, L. D. Hughs, C. M. Jones, H. Li, J. E. Redford, S. J. Sobelman, J. A. Kouzelos, A. R. Johnson, *Tetrahedron: Asymm.* **2009**, *20*, 1279.
[30] R. Gryboś, A. Samotus, W. Łasocha, *Transition Met. Chem.* **2003**, *28*, 568.
[31] A. Kuhn, T. A. Tsotetsi, A. Muller, J. Conradie, *Inorg. Chim. Acta* **2009**, *362*, 3088.
[32] M. Niehues, G. Kehr, G. Erker, B. Wibbeling, R. Fröhlich, O. Blacque, H. Berke, *J. Organomet. Chem.* **2002**, *663*, 192.
[33] G. Garcķa, A. Navarro, J. M. Granadino-Roldiņ, A. Garzón, T. P. Ruiz, M. P. Fernjndez-Liencres, M. Melguizo, A. Peńas, G. Pongor, J. Eöri, J. Fernjndez-Gómez, *Chem. Phys.* **2010**, *374*, 62.
[34] I. Reile, A. Paju, A. -M. Müürisepp, T. Pehk, M. Lopp, *Teterahedron* **2011**, *67*, 5942.
[35] F. Weigend, R. Ahlrichs, *Phys. Chem. Chem. Phys.* **2005**, *7*, 3297.
[36] D. R. Lide, *CRC Handbook of Chemistry and Physics 2007–2008*, 88th ed.; CRC Press, Boca Raton, FL, **2008**.
[37] J. Ho, A. Klamt, L. Coote, *J. Phys. Chem. A* **2010**, *114*, 13442.
[38] TURBOMOLE V5.10: A Development of University of Karlsruhe and Forschungszentrum Karlsruhe GmbH 1989–2007, TURBOMOLE GmbH, since 2007, 2008, Available at: http://www.turbomole.com. Accessed January 31, 2014.
[39] R. F. W. Bader, *Atoms in Molecules: A Quantum Theory*; Oxford University Press: Oxford, **1990**.
[40] A. Todd, T. K. Keith, AIMAll (Version 11.10.16); Gristmill Software: Overland Park, KS, **2012**. Available at: http://aim.tkgristmill.com. Accessed January 31, 2014.

Received: 28 November 2013
Revised: 11 January 2014
Accepted: 17 January 2014
Published online 12 February 2014

Publication II

Osadchuk, I.; Tamm, T.; Ahlquist, M. S. G. Theoretical investigation of a parallel catalytic cycle in CO_2 hydrogenation by (PNP)IrH_3, *Organometallics*, **2015**, *34*, 4932-4940.

ORGANOMETALLICS

Article

pubs.acs.org/Organometallics

Theoretical Investigation of a Parallel Catalytic Cycle in CO_2 Hydrogenation by (PNP)IrH_3

Irina Osadchuk,[†] Toomas Tamm,[†] and Mårten S. G. Ahlquist*,[‡]

[†]Department of Chemistry, Tallinn University of Technology, Akadeemia tee 15, 12618 Tallinn, Estonia

[‡]Division of Theoretical Chemistry & Biology, School of Biotechnology, KTH Royal Institute of Technology, SE-10691 Stockholm, Sweden

Supporting Information

ABSTRACT: The (PNP)IrH_3 (2,6-bis(diisopropylphosphinomethyl)pyridine iridium trihydride) complex by Nozaki is a highly active and selective catalyst for CO_2 hydrogenation to formic acid in aqueous KOH. Previous theoretical investigations found that regeneration of the catalyst is the rate-determining step in this reaction. In the current article we present results from a computational study using density functional theory in order to consider the possibility of sequential insertion of two CO_2 molecules in two Ir−H bonds before the reaction with hydrogen. We found that insertion of a second CO_2 molecule is indeed possible; moreover, this sequential insertion allows formation of a more electrophilic iridium monohydride intermediate, and thereby the process of H_2 cleavage is facilitated. In addition, we considered the influence of ligands coplanar with the PNP ligand on the energy of CO_2 insertion into the (PNP)IrH_2X complex and found that σ- and π-donating ligands promote the reaction.

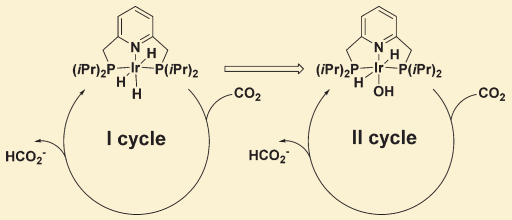

INTRODUCTION

In this report we extend our previous study[1] of the (PNP)IrH_3 complex by Nozaki[2] (Figure 1, cycle 1). Here we investigate the possibility of inserting a second CO_2 molecule before reaction with H_2 to regenerate the active hydride complex (Figure 1, cycle 2).

The use of fossil fuels during the current and previous centuries is responsible for the major part of the increased concentration of carbon dioxide in the atmosphere.[3] Recently there has been an increasing interest in using CO_2 as a feedstock due to its high abundance, low cost, low toxicity, and low critical temperature. Unfortunately, because of the thermodynamic stability and high activation energy of this linear molecule, use of CO_2 is limited to syntheses of a few products: urea and its derivatives, salicylic acids, and carbonates.[3] Recently, several attempts have been made to convert carbon dioxide into useful organic products, such as CO, methanol, and formic acid. Catalytic hydrogenation of CO_2 to formic acid is an attractive process due to its small endergonicity (eqs 1 and 2).[3i]

$$CO_2(g) + H_2(g) \rightarrow HCOOH(g)$$
$$\Delta G^\circ_{298} = +10.2 \text{ kcal mol}^{-1} \quad (1)$$

$$CO_2(g) + H_2(g) \rightarrow HCOOH(l)$$
$$\Delta G^\circ_{298} = +7.9 \text{ kcal mol}^{-1} \quad (2)$$

Given that production of hydrogen can be achieved in a sustainable way, the conversion of CO_2 and H_2 to formic acid allows for both producing a renewable fuel or raw material for many synthetic processes and sequestering of carbon dioxide from the atmosphere.[3]

Equilibrium among formic acid, CO_2, and H_2 in the presence of a catalyst has been studied since 1911.[4a,b] A more extensive discussion on the early stages of this research can be found in the book by Sabatier.[4c] Catalytic hydrogenation of CO_2 was first carried out by Inoue[4d] and has been studied by numerous groups[4] thereafter. Promising results have been obtained with molecular catalysts based on noble metals such as Ru, Rh, and Ir. For example, [(dppp)Rh(hfacac)] was suggested as an effective catalyst by Leitner and co-workers in 1995.[5a] In DMSO/NEt_3 (5/1) solvent at room temperature and a total pressure of 40 atm (CO_2/H_2 was 1/1) this catalyst had a turnover frequency (TOF) of 436 h^{-1} and turnover numbers (TON) of up to 3000.[5b] In 2001 the Lau group reported $TpRu(PPh_3)(CH_3CN)H$ as a catalyst for CO_2 hydrogenation.[6] In THF solvent in the presence of water $TpRu(PPh_3)(CH_3CN)H$ reacted with a TOF value of 63 h^{-1}. A year later Jessop and co-workers found that $RuCl(OAc)(PMe_3)_4$ catalyzed CO_2 reduction with a TOF value of 95000 h^{-1}. The reaction was performed in supercritical CO_2 with addition of NEt_3 and C_6F_5OH under high pressure (CO_2 120 atm, H_2 70 atm) and a temperature of 50 °C.[7] Excellent results have

Received: May 25, 2015
Published: September 29, 2015

DOI: 10.1021/acs.organomet.5b00448
Organometallics 2015, 34, 4932−4940

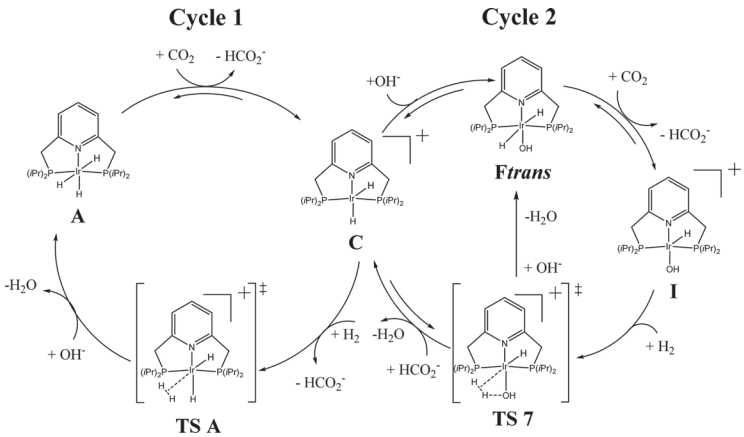

Figure 1. Proposed mechanism for CO_2 hydrogenation.

also been obtained using Ir catalysts. Himeda reported TON values up to 222000 with a half-sandwich Ir(III) complex.[8] In 2009 Nozaki found a new very efficient catalyst, an Ir(III) pincer complex.[2] In aqueous KOH, under a total pressure of 49 atm and at a temperature of 200 °C Ir(PNP)H_3 showed a TOF value of 150000 h^{-1} and a TON value of 300000. When the temperature was decreased to 120 °C, a TOF value of 73000 h^{-1} and TON value of 3500000 could be achieved. In 2012 the Milstein group reported activation of CO_2 using the Ru(PNP)H_2CO complex.[9a] In THF with an addition of DBU at 132 °C and a pressure of 40 atm (H_2/CO_2 = 3/1) a TOF value of up to 1892000 h^{-1} and a TON value of more than 266000 was achieved.[9b]

A disadvantage of all catalysts based on noble metals is their high cost. Several attempts have also been made to prepare catalysts from abundant transition metals, such as Ni,[10] Mo,[10a] Co,[11] and Fe.[12] Studies showed that $MoCl_3$ and $NiCl_2$ catalysts with dcpe had low TOF values of merely 8.4 and 15.6 h^{-1}, respectively.[10a] Catalysts based on Co and Fe were more promising. It was reported that Fe catalysts gave TON values of up to 788, TOF values of up to 156 h^{-1}, and a yield of 53%.[12a] Co catalysts also gave promising results. Co(dmpe)$_2$H[11b] in tetrahydrofuran at room temperature and 1 atm has a TOF value of 3400 h^{-1} and at a pressure of 20 atm a TOF value of 74000 h^{-1}. However, the turnover numbers and frequencies of these abundant metal catalysts are lower than those of the best noble-metal catalysts. In addition, a direct comparison is hindered by very different reaction conditions.

Numerous experimental[4,9] and theoretical[13,9] studies have been conducted to understand the reaction mechanisms. A deeper understanding of the fundamental reaction mechanisms of the catalysts for CO_2 hydrogenation is essential for finding new and more efficient catalysts.

Our previous results suggested that the regeneration of the (PNP)IrH_3 intermediate could be rate limiting. Nozaki and Morokuma's subsequent report suggested a lower barrier for this step. However, a very different treatment of the entropic components of the Gibbs free energy, a different solvation model, and a different functional make a direct comparison of the results difficult. On the basis of our finding that deprotonation of a (PNP)IrH_2(H_2) intermediate could be rate limiting, we reasoned that a more electrophilic intermediate could facilitate the rehydrogenation process. Nozaki proposed the reaction mechanism on the basis of the experimental data,[2] mainly on stoichiometric species that were readily identified by NMR spectroscopy. While these techniques cannot detect high-energy, short-lived, or low-concentration species, nothing prevents these species from being a part of the catalytic process.

■ RESULTS AND DISCUSSION

All theoretical studies agree that the catalytic reaction begins with nucleophilic attack on CO_2 by one of the axial hydride ligands in the Ir(III) pincer complex[1,14−16] (Scheme 1). We

Scheme 1. Proposed Mechanism for Insertion of CO_2 into an Ir−H Bond[a]

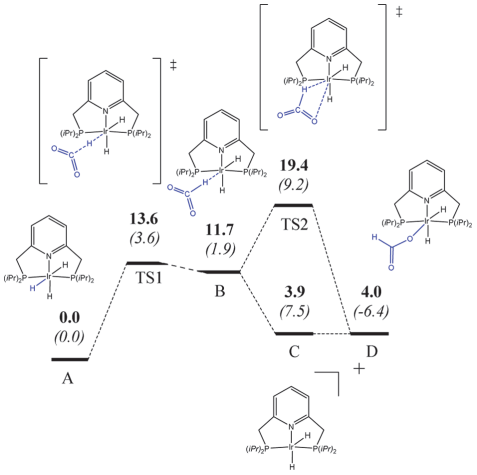

[a]Boldface numbers represent ΔG values (kcal mol^{-1}), and numbers in parentheses are ΔH values (kcal mol^{-1}).

found this addition to proceed via a free energy barrier of 13.6 kcal mol^{-1}. This is in good agreement with our previous

DOI: 10.1021/acs.organomet.5b00448
Organometallics 2015, 34, 4932−4940

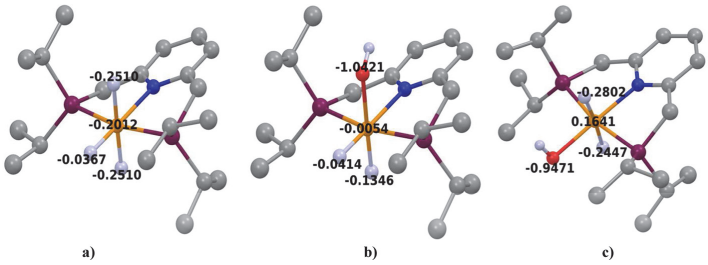

Figure 2. Geometries of complexes (a) **A**, (b) **Fcis**, and (c) **Ftrans**. Hydrogen atoms have been removed for clarity, except for those relevant to the reaction.

results ($\Delta G^{\ddagger}$ = 14.5 kcal mol^{-1}) and other reports by Yang ($\Delta H^{\ddagger}$ = 4.0 kcal mol^{-1})[15] and also Li and Yoshizawa ($\Delta E^{\ddagger}$ = 6.5 kcal mol^{-1}).[16] Morokuma's result differed more ($\Delta G^{\ddagger}$ = 4.2 kcal mol^{-1}).[14] However, this discrepancy is probably due to the neglect of translational and rotational entropies by Morokuma's group.

After CO_2 has been reduced to $HCOO^-$ and complex **C** or **D** has been formed (Scheme 1), there are several potential pathways for the catalyst regeneration (complex **A**). We previously proposed that formate ligand dissociates from complex **B** and H_2 coordinates to the vacant site on Ir(III) (Figure 1, cycle 1, **TSA**).[1] After that, the complex is deprotonated by a hydroxide anion from the solution and the trihydride catalyst (complex **A**) is regenerated. The activation free energy for catalyst regeneration is $\Delta G^{\ddagger}$ = 26.1 kcal mol^{-1}.

Morokuma and co-workers suggested two competing pathways.[14] The first goes through deprotonation of the methylene group of the PNP ligand, with simultaneous dearomatization of the pyridine ring. In this case the formate ligand is replaced by a hydroxide anion and then the hydroxyl ligand abstracts one proton from the methylene group following the dissociation of H_2O. H_2 binds to the vacant coordination site, and regeneration of the catalyst occurs by splitting the H_2 molecule and simultaneous aromatization of the pyridine ring. The second competing pathway is that proposed by us,[1] without dearomatization of the pyridine ring. In this pathway formate ligand dissociation is followed by coordination of an H_2 molecule and the catalyst is regenerated by deprotonating a coordinated H_2 by a hydroxide from the solution. Although the rate-determining steps in these reactions are different, the calculated activation barriers are very close in energy; $\Delta G^{\ddagger}$ values are 14.4 and 12.7 kcal mol^{-1} for the first and second reaction paths, respectively.

The same system was also computationally studied by Yang.[15] He concluded that the reaction path with H_2 splitting by hydroxide anion from the solution is about 20 kcal mol^{-1} lower in enthalpy ($\Delta H^{\ddagger}$ = 18.6 kcal mol^{-1}) than the pathway with dearomatization and aromatization of the pyridine ring ($\Delta H^{\ddagger}$ = 38.5 kcal mol^{-1}).

One more theoretical study on this system was performed by Li and Yoshizawa.[16] They came to the conclusion that formate ligand elimination from the Ir complex occurs by hydroxide anion substitution. They also looked at possibilities for formic acid elimination accompanied by the reduction of Ir(III) to Ir(I) or dearomatization of the pyridine ring. The activation barrier for formic acid reduction with Ir reduction ($\Delta E^{\ddagger}$) was 26.1 kcal mol^{-1}, and formic acid elimination through dearomatization had a barrier of 30.0 kcal mol^{-1}, which are much higher in energy than those going through hydroxyl ligand substitution (ΔE = 3.9 kcal mol^{-1}). Further, Li and Yoshizawa proposed the formation of H_2O accompanied by dearomatization of the pyridine ring, followed by catalyst regeneration (complex **A**) through splitting of H_2 and aromatization of the pyridine ring. The last step has an energetic barrier $\Delta E^{\ddagger}$ of 15.6 kcal mol^{-1}.

The Pidko group[9] also came to the conclusion that Ru(PNP)H_2CO complex regeneration by dearomatization of the pyridine ring is possible but is not a favorable reaction pathway ($\Delta G^{\ddagger}$ = 22.7 kcal mol^{-1}). They concluded that the major pathway for catalyst regeneration proceeds through H_2 splitting by the $HCOO^-$ anion. Under an excess of H_2 this has an activation barrier ($\Delta G^{\ddagger}$) of 12.4 kcal mol^{-1} and the activation barrier is 15.5 kcal mol^{-1} when regeneration proceeds through a formate complex.

However, all of the aforementioned authors agree that regeneration of the catalyst (PNP)IrH_3 (complex **A**) is the rate-determining step. A recent study by Mondal et al.[17] suggests that for certain metals (e.g. cobalt) hydride transfer may be rate-limiting instead. However, this study did not consider iridium and the overall setup of the catalytic system was different.

In this work we reason that, since regeneration of the catalyst is likely the rate-limiting step in the reaction, there may be the possibility of a reaction with a second CO_2 molecule. CO_2 insertion into the initial catalyst **A** is slightly exothermic, meaning that, even if the reaction is endergonic, it could very well be part of the catalytic reaction. We propose that the hydroxyl ligand in the equatorial position could be a reasonable substitute for the hydride ligand, especially considering that the reaction is taking place in aqueous KOH. The influence of a hydroxyl ligand in an axial position on CO_2 insertion was previously studied by Crabtree et al.[18] They found that a hydroxyl ligand in the axial position changes the trans hydride NBO charge from −0.012 in the initial complex to +0.050, thereby hindering CO_2 insertion into trans hydrides. Our calculations confirm this. The hydroxyl ligand alters the trans hydride NBO charge from −0.2510 in complex **A** to −0.1346 in **Fcis** (Figure 2). At the same time a hydroxyl ligand in an equatorial position changes the hydride charge to −0.2802, making the CO_2 electrophilic attack favorable.

We investigated several possibilities of formation of the **Ftrans** complex. The hydroxide anion can be associated directly by complex **C** (Scheme 2), even though the barrier for this insertion is excessively high: 50.5 kcal mol^{-1}. Another possibility is that complex **Ftrans** is formed indirectly. One possible pathway is association of H_2O to form complex **Etrans** followed

DOI: 10.1021/acs.organomet.5b00448
Organometallics 2015, 34, 4932−4940

Scheme 2. Relative Gibbs Free Energies for Complex F*trans* Formation[a]

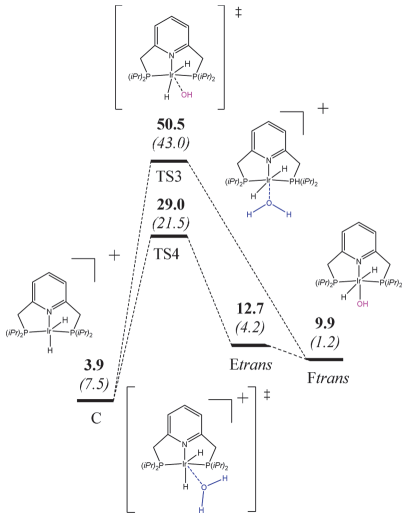

[a]Boldface numbers represent ΔG values (kcal mol^{-1}), and numbers in parentheses are ΔH values (kcal mol^{-1}).

Scheme 3. Relative Gibbs Free Energies for Complex F*trans* Formation[a]

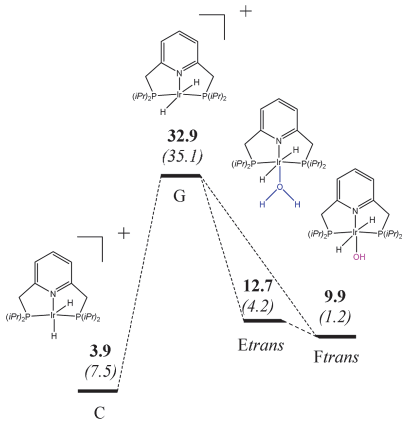

[a]Boldface numbers represent ΔG values (kcal mol^{-1}), and numbers in parentheses are ΔH values (kcal mol^{-1}).

by deprotonation (Scheme 2). The barrier for this association will be 29.0 kcal mol^{-1}. This barrier is also relatively high, but the reaction could still be possible considering the reaction conditions (aqueous KOH solution at 120 °C).

One more possibility for complex **F*trans*** formation is the conversion of complex **C** to **G** following either association of an H_2O molecule or an OH^- anion (Scheme 3). Our calculations showed that this transformation proceeds without a barrier, with ΔG = 32.9 kcal mol^{-1}.

Further investigation showed that insertion of the second CO_2 into hydroxyl complex **F*trans*** proceeds via a barrier of

Scheme 4. Relative Gibbs Free Energies for Second CO_2 Reduction[a]

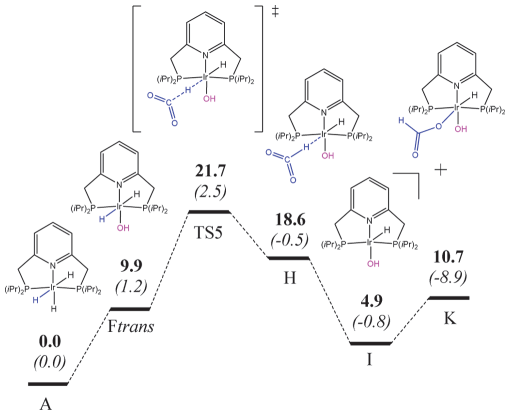

[a]Boldface numbers represent ΔG values (kcal mol^{-1}), and numbers in parentheses are ΔH values (kcal mol^{-1}).

Scheme 5. Relative Gibbs Free Energies for Complex F*trans* Regeneration[a]

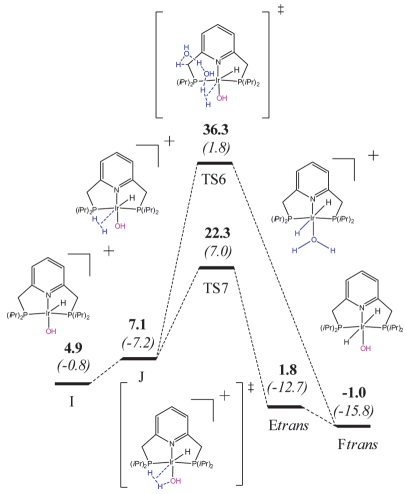

[a]Boldface numbers represent ΔG values (kcal mol^{-1}), and numbers in parentheses are ΔH values (kcal mol^{-1})

21.7 kcal mol^{-1} relative to complex **A** (Scheme 4). After the intermediate **H** is formed, it is readily transformed into complex **I** through dissociation of an $HCOO^-$ ligand or into complex **K** through dissociation and association of an $HCOO^-$ ligand.

After the second CO_2 is reduced, there are two scenarios for catalyst **F*trans*** regeneration (Schemes 5 and 6). In the first scenario a hydrogen molecule fills the vacant position in complex **I** (Scheme 5). Further on, there are again two possibilities. In the first case a hydroxide anion from the solution attacks the positively charged hydrogen atom and splits the hydrogen

DOI: 10.1021/acs.organomet.5b00448
Organometallics 2015, 34, 4932−4940

Scheme 6. Relative Gibbs Free Energies for Complex F*trans* Regeneration[a]

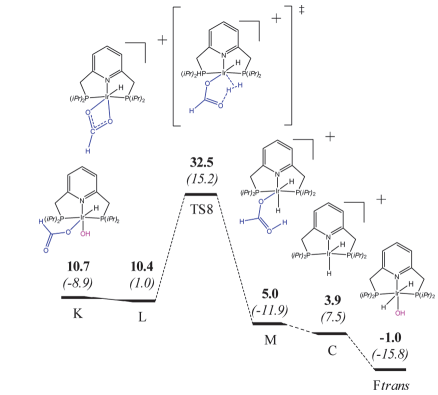

[a]Boldface numbers represent ΔG values (kcal mol^{-1}), and numbers in parentheses are ΔH values (kcal mol^{-1}).

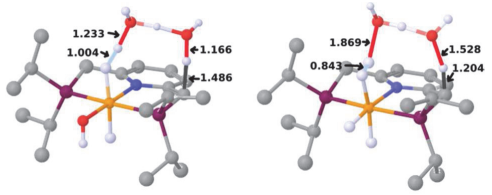

Figure 3. Geometries of complexes **TS6** and **TSA** for complex F*trans* and complex **A** regeneration. Hydrogen atoms have been removed for clarity, except for those relevant to the reaction.

molecule (**TS6**). This path of catalyst regeneration was proposed in our previous work for regeneration of complex **A** ($\Delta G^{\ddagger}$ = 21.2 kcal mol^{-1}).[1] However, in the present situation this pathway is hindered by a high barrier of 36.3 kcal mol^{-1}. We believe that the higher regeneration energy is due to a more distorted geometry (Figure 3). In **TS6** the H−H bond in the hydrogen molecule is elongated to 1.004 Å, in comparison to 0.843 Å in the analogous complex with a hydride ligand in place of the hydroxyl ligand. At the same time the distance between the hydroxyl oxygen and the methylene proton increases to 1.486 Å, in comparison to 1.204 Å in the analogous complex with a hydride.

Another possibility for regeneration of the catalytic complex F*trans* is proton transfer to the hydroxyl ligand to form the aqua complex E*trans* (Scheme 5). The barrier for the hydrogen molecule splitting is 22.3 kcal mol^{-1} (**TS7**). The water ligand can then be deprotonated by hydroxide to transform to a hydroxyl ligand and to regenerate complex F*trans*, since the hydroxide has the function of a pendant base.[19]

The third scenario for complex F*trans* regeneration is loss of the hydroxyl ligand by complex **K** to form a complex with the formate ligand coordinated in a bidentate fashion (**L**) (Scheme 6). Here the splitting of the hydrogen molecule (**TS8**) has a barrier of $\Delta G^{\ddagger}$ = 32.5 kcal mol^{-1}.

In comparison with the results described above, **TS7** appears to be favored by 10.2 kcal mol^{-1} on the free energy surface. The difference in energy between **TS7** and **TS8** can be explained by different types of transition states (Figures 4 and 5). **TS7** can be categorized as an electrophilic substitution (ES) and **TS8** as a chelate-assisted cleavage with a six-membered ring (M6). Ess et al.[20] concluded that the difference in energy originated mostly from distortion energy and charge transfer stabilization energy. Looking at the transition state geometries (Figure 4), it appears that **TS7** has a geometry very similar to that of the precursor complex **J**. The main changes are the H−Ir−O angle, which increases by 11.0° from 92.1 to 103.1°, and the O−Ir−O angle, which decreases by 14.0° from 82.8 to 68.8°, in comparison to those of complex **J**. In **TS7** there is also significant bond breaking, as the the H−H bond elongates by 0.169 Å. In contrast, the geometry of **TS8** is better described as a transition state for ligand association, where the H_2 molecule is replacing one of the coordinating oxygens at the iridium center. From the intrinsic reaction coordinate (IRC) calculations we

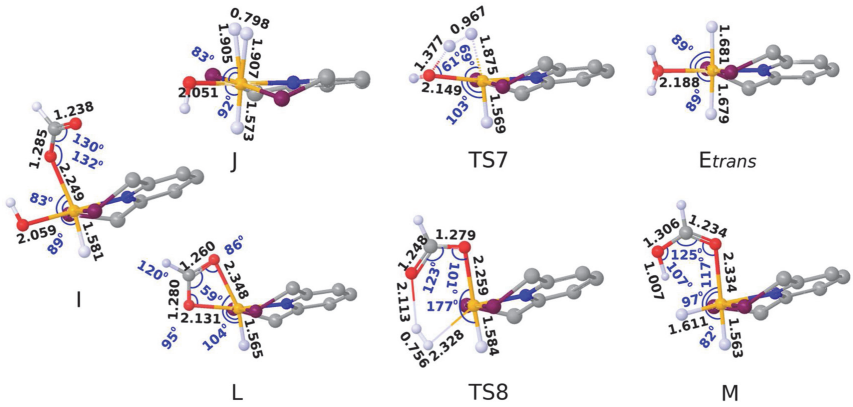

Figure 4. Geometries of complexes **I**, **J**, **L**, **TS6**, **TS7**, E*trans*, and **M**. Isopropoxide groups and hydrogen atoms have been removed for clarity, except for those hydrogens relevant to the reaction.

DOI: 10.1021/acs.organomet.5b00448
Organometallics 2015, 34, 4932−4940

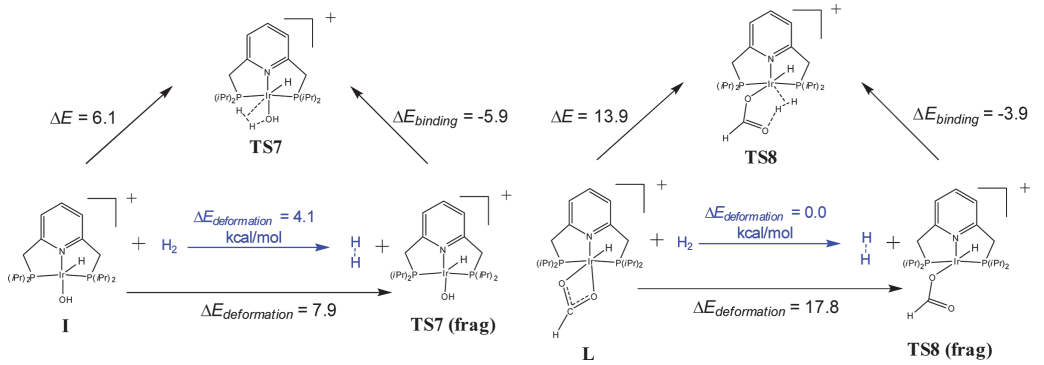

Figure 5. Activation strain energy for **TS7** and **TS8** (kcal mol^{-1}).[21]

Scheme 7. Energy Profile for CO_2 Hydrogenation at 25 °C and 1 atm

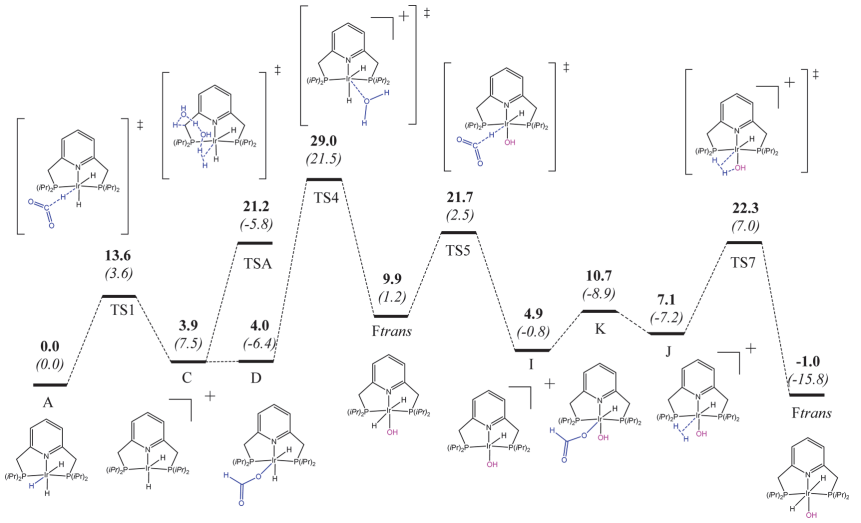

Table 1. Energy Profile for CO_2 Hydrogenation under Different Reaction Conditions

		ΔG, kcal mol^{-1}										
P, atm	*T*, °C	**TS1**	**C**	**TSA**	**D**	**TS4**	**F**	**TS5**	**I**	**K**	**J**	**TS7**
1	25	13.6	3.9	21.2	4.0	29.0	9.9	21.7	4.9	10.7	7.1	22.3
59.2	120	13.6	5.3	18.3	4.1	28.7	9.5	21.3	6.0	10.5	7.9	23.4
49.3	200	11.9	5.5	15.9	2.5	28.0	9.1	19.3	5.9	8.6	7.5	23.3

found that, once the hydrogen gets closer to the iridium center following **TS8**, the H−H bond is cleaved spontaneously. On the basis of this observation we agree with the statement that cleavage via a chelate-assisted path could be facile, as in our case the formation of the chelate is relatively difficult. Hence, the electrophilic substitution path is favored via **TS7** over the chelate-assisted path via **TS8**.

To further analyze the difference between the two transition states, we performed single-point calculations on the H_2 and iridium complex fragments of **TS7** and **TS8** (Figure 5). From these results we found that the distortion energies needed to reach **TS7** and **TS8** are 12.0 and 17.8 kcal mol^{-1}, respectively (**TS7 (frag)** and **TS8 (frag)**), and the energies of interactions are −5.9 and −3.9 kcal mol^{-1}, respectively. This shows that the distortion of the fragments to get to the transition state geometry is less for **TS7** in comparison to **TS8** and also that the interaction between the two fragments favors **TS7** over **TS8**, although to a lesser extent than the distortion.

We showed above that insertion of the second CO_2 before reaction with H_2 is possible; moreover, regeneration of the

DOI: 10.1021/acs.organomet.5b00448
Organometallics 2015, 34, 4932−4940

catalyst has a moderate barrier of 22.3 kcal mol^{-1} at 25 °C. The actual reaction is performed under high-pressure, high-temperature conditions, however. In Scheme 7 and Table 1 the key steps for the CO_2 hydrogenation under other reaction conditions are shown. The increase in temperature and pressure above the standard values appears to lower the H−H cleavage barrier for cycle 1 much more than for other steps. However, since the solvation model is parametrized for room temperature, the interpretation of this result should be made with caution.

Interestingly, we found that the equatorial hydroxyl ligand promoted the CO_2 insertion in comparison to the trihydride complex **A**, decreasing its relative free energy barrier from 13.6 to 11.6 kcal mol^{-1}. In order to better understand the influence of the ligand coplanar with the pincer ligand, we tried different donor−acceptor ligands (Scheme 8, Table 2). Complexes with

Scheme 8. CO_2 Reduction using Different Ligands

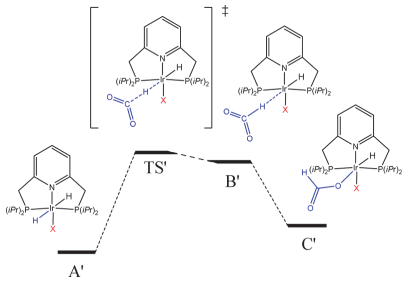

Table 2. Influence of Different Equatorial Ligands on the Energy of CO_2 Insertion

	ΔG, kcal mol^{-1}				
ligand	TS1′	B′	C′	charge	bond length, Å
CN^-	16.7	16.8	7.1	−0.232	1.677
I^-	15.3	12.4	5.3	−0.248	1.676
Cl^-	14.6	12.0	3.8	−0.250	1.679
F^-	14.6	12.3	4.2	−0.260	1.681
H^-	13.6	11.7	4.0	−0.251	1.678
CH_3^-	12.1	7.3	1.7	−0.253	1.68
OH^-	14.2[a]	10.7[a]	3.7[a]	−0.245	1.678
	11.6[b]	8.6[b]	0.8[b]	−0.280	1.687
SH^-	13.9[a]	11.5[a]	3.1[a]	−0.248	1.68
	12.2[b]	9.9[b]	3.7[b]	−0.253	1.677

[a]Without hydrogen bond formation. [b]With hydrogen bond formation.

alternative ligands are marked with a prime symbol (e.g. **A**′), and the free energies are given relative to the corresponding complex **A**′ (Tables 2 and 3).

Ligands with either σ- or π-donating properties decrease the activation energy of CO_2 insertion by increasing partial charge of the reacting hydride ligand, hence making it more nucleophilic. In contrast, the complex with a π-accepting CN^- ligand had the highest insertion barrier. There appears to be a weak linear relationship (R^2 = 0.40) between the partial charge on hydride and the barrier for the insertion of CO_2 (Chart 1). However, the present selection of ligands is too small and diverse for an in-depth statistical analysis. Visualization of the frontier molecular orbitals revealed that, while most of the ligands have a significant participation in the

Chart 1. Dependence of CO_2 Insertion Energy on NBO Charge on Hydride

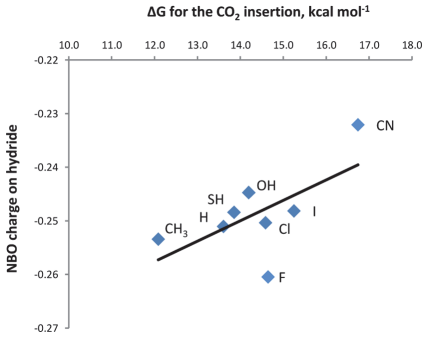

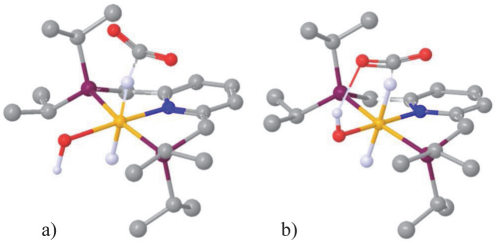

Figure 6. Possibilities for CO_2 insertion into complexes OH^- and SH^- (a) without a hydrogen bond and (b) with a hydrogen bond.

HOMO, the H^- and CH_3^- ligands give almost no contribution there.

It should also be mentioned that in the case of the OH^- and SH^- ligands additional decrease of the CO_2 insertion barrier is possible due to stabilization between the hydrogen from the aforementioned ligands and the oxygen on CO_2 (Figure 6). This stabilization decreases barriers by 2.6 and 1.7 kcal mol^{-1} for OH^- and SH^-, respectively.

Our calculations showed that the product formed from insertion into the (PNP)IrH_2CN complex is 0.1 kcal mol^{-1} higher in energy than the transition state. However, the IRC calculation showed that our structure is the appropriate transition state. We attribute the discrepancy to inaccuracy of the method. Despite this nuance, we conclude that ligands coplanar with the pincer ligand have influence on the energy barrier of CO_2 insertion. However, this influence is smaller than the influence of ligands situated in a position trans to hydride as shown by Hazari.[18] This is expected, since the trans influence is usually more pronounced than the cis effect. Nevertheless, the influence of the ligands cis to the reacting hydride is observed and could be utilized to optimize reactivity.

We also considered the energy for catalyst regeneration. All halogens needed higher energy for catalyst regeneration, and the reaction is endergonic (Table 3). In contrast, complexes with equatorial OH^- or CH_3^- ligands have low barriers for catalyst regeneration and in the case of OH^- the reaction is exergonic. For complexes with equatorial CN^- and H^- ligands we could not find transition state analogues to **TS**′ and hydrogen splitting occurs through **TS**″ (Scheme 9).

DOI: 10.1021/acs.organomet.5b00448
Organometallics 2015, 34, 4932−4940

Table 3. Influence of Different Equatorial Ligands on the Energy of Catalyst Regeneration

	ΔG, kcal mol^{-1}		
ligand	D′	TS2′/TS2″	C′
CN^-	6.3	28.0″	
I^-	0.5	41.1	33.1
Cl−	0.6	37.0	32.7
SH^-	−1.3	18.6	7.7
H^-	−4.7	21.2	
CH_3^-	−5.2	8.7	2.9
F−	0.0	22.8	18.8
OH^-	−2.7	12.3	−8.2

Scheme 9. Catalyst Regeneration

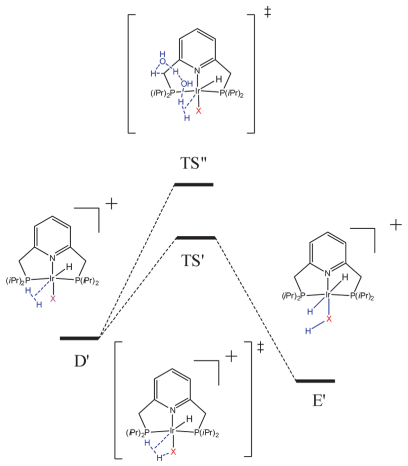

CONCLUSIONS

We investigated the possibility of subsequent insertion of two CO_2 molecules before the reaction with H_2 to regenerate the catalyst in (PNP)IrH_3 complex by Nozaki. We found that the (PNP)IrH_2OH intermediate complex with an hydroxyl ligand trans to N (***Ftrans***) can be the active species in hydrogenation of CO_2. We also found that a hydroxyl ligand in an equatorial position facilitates CO_2 insertion into the catalytic complex by increasing the nucleophilicity of the hydride ligands. When the formate complex is formed, cleavage of a H_2 molecule and regeneration of the catalyst can proceed via two paths. In the first path formate dissociates and H_2 coordinates to the vacant site and is finally deprotonated by the hydroxyl ligand with a barrier of 22.3 kcal mol^{-1}. In the second scenario the hydroxyl ligand dissociates and H_2 is deprotonated by the formate ligand with a barrier of 32.5 kcal mol^{-1}. Thereby the first pathway where H_2 is deprotonated by the hydroxyl ligand is favored by 10.3 kcal mol^{-1}, in comparison to the second path involving formate. In addition, the reaction with a second CO_2 molecule clearly enhanced the reactivity toward dihydrogen and we conclude that the cycle is likely parallel to that previously proposed. The limiting step in cycle 2 is the generation of ***Ftrans***. However, once generated, the highest barrier in cycle 2 is 17.4 kcal mol^{-1}, corresponding to the H_2 cleavage step **TS7**.

Further, we investigated the influence of other donor−acceptor ligands coplanar with the pincer ligand on the barrier of CO_2 insertion. Ligands with either σ- or π-donating properties were found to decrease the activation energy of CO_2 insertion, while π-acidic ligands increased the barrier. Additional stabilization can be achieved with OH^- and SH^- ligands by interaction between their protons and the oxygen on CO_2.

COMPUTATIONAL DETAILS

All calculations were performed using the Jaguar 7.5 program package.[22] For all atoms in all calculations except the final energy corrections the B3LYP functional,[23] LACVP** effective core potential,[24] and basis set were used. For final single-point energy corrections the M06 functional[25] and the LACV3P**++ basis set augmented with two f functions on iridium (α = 1.189 and 0.395) were used. All geometries were optimized under vacuum. To take solvent effects into account, single-point solvation energies were calculated using a Poisson−Boltzmann self-consistent reaction field (PBF) as implemented in Jaguar[26] with a dielectric constant of 80.37 and a probe radius of 1.4 Å to simulate water. For small molecules and ions (water, hydroxide, and formate) experimental solvation energies were used[27] to get more accurate energy profiles.[28] The calculations of the harmonic vibrational frequencies were performed to define the nature of all intermediates and transition states. The transition states were confirmed by intrinsic reaction coordinate (IRC) calculations. The Gibbs free energy and enthalpies were calculated by using eqs 3 and 4:

$$G = E(\text{M06/LACV3P**++(2f)}) + G_{\text{solv}} + \text{ZPE} + H_{\text{corr}}^{298} - TS_{\text{corr}}^{298} \quad (3)$$

$$H = E(\text{M06/LACV3P**++(2f)}) + G_{\text{solv}} + \text{ZPE} + H_{\text{corr}}^{298} \quad (4)$$

Here G_{solv}, H_{corr}, and S_{corr} represent the correction terms from solvation model and vibrational analysis, respectively.

Since the PBF solvation model assumes 1 M (gas) to 1 M (sol), we corrected the gas concentration to 1 atm by adding $\Delta G_{\text{conc}} = RT \ln 24.46$ to all solvated species (1.9 kcal mol^{-1} at 25 °C, 2.5 kcal mol^{-1} at 120 °C, and 3.0 kcal mol^{-1} at 200 °C).

ASSOCIATED CONTENT

Supporting Information

The Supporting Information is available free of charge on the ACS Publications website at DOI: 10.1021/acs.organomet.5b00448.

Geometries and energies of selected complexes (PDF)
Cartesian coordinates of all complexes (XYZ)

AUTHOR INFORMATION

Corresponding Author

*E-mail for M.S.G.A.: ahlqui@kth.se.

Notes

The authors declare no competing financial interest.

ACKNOWLEDGMENTS

We are grateful to Mario Öeren for helpful comments. Funding was provided by ESF DoRa T6 "Development of international cooperation networks by supporting the mobility of Estonian doctoral students". M.S.G.A. acknowledges Vetenskapsrådet for financial support and SNIC for computational resources.

REFERENCES

(1) Ahlquist, M.S G. *J. Mol. Catal. A: Chem.* **2010**, *324*, 3−8.
(2) Tanaka, R.; Yamashita, M.; Nozaki, K. *J. Am. Chem. Soc.* **2009**, *131*, 14168−14169.

DOI: 10.1021/acs.organomet.5b00448
Organometallics 2015, 34, 4932−4940

(3) (a) Wang, W.; Wang, S.; Ma, X.; Gong, J. *Chem. Soc. Rev.* **2011**, *40*, 3703−3727. (b) Benson, E. E.; Kubiak, C. P.; Sathrum, A. J.; Smieja, J. M. *Chem. Soc. Rev.* **2009**, *38*, 89−99. (c) Mikkelsen, M.; Jørgensen, M.; Krebs, F. C. *Energy Environ. Sci.* **2010**, *3*, 43−81. (d) Smieja, J. M.; Kubiak, C. P. *Inorg. Chem.* **2010**, *49*, 9283−9289. (e) Himeda, Y. *Eur. J. Inorg. Chem.* **2007**, *2007*, 3927−3941. (f) Halmann, M. M.; Steinberg, M. *Greenhouse gas carbon dioxide mitigation science and technology*; CRC Press: Boca Raton, FL, 1999. (g) Jhong, H. R.; Ma, S.; Kenis, P. *Curr. Opin. Chem. Eng.* **2013**, *2*, 191−199. (h) Appel, A. M.; Bercaw, J. E.; Bocarsly, A. B.; Dobbek, H.; DuBois, D. L.; Dupuis, M.; Ferry, J. G.; Fujita, E.; Hille, R.; Kenis, P.J. A.; Kerfeld, C. A.; Morris, R. H.; Peden, C.H. F.; Portis, A. R.; Ragsdale, S. W.; Rauchfuss, T. B.; Reek, J.N. H.; Seefeldt, L. C.; Thauer, R. K.; Waldrop, G. L. *Chem. Rev.* **2013**, *113*, 6621−6658. (i) http://webbook.nist.gov.

(4) (a) Sabatier, P.; Maihle, A. *Compt. Rend.* **1911**, *152*, 1212−1215. (b) Bredig, G.; Carter, S. R. *Ber. Dtsch. Chem. Ges.* **1914**, *47*, 541−545. (c) Sabatier, P. *Catalysis in Organic Chemistry*; van Nostrand: New York, 1922. (d) Inoue, Y.; Izumida, H.; Sasaki, Y.; Hashimto, H. *Chem. Lett.* **1976**, 863−864. (e) Jószai, I.; Jóo, F. *J. Mol. Catal. A: Chem.* **2004**, *224*, 87−91. (f) Kolesnichenko, N. V.; Kremleva, E. V.; Teleshov, A. T.; Ezhova, N. N.; Ganin, D. A.; Te, V.; Slivinskii, E. V. *Pet. Chem.* **2006**, *46*, 22−24. (g) Zhao, G.; Jóo, F. *Catal. Commun.* **2011**, *14*, 74−76. (h) Tsai, J.; Nicholas, K. M. *J. Am. Chem. Soc.* **1992**, *114*, 5117−5124. (i) Elek, J.; Nádasdi, L.; Papp, G.; Laurenczy, G.; Joó, F. *Appl. Catal., A* **2003**, *255*, 59−67. (j) Gao, Y.; Kuncheria, J. K.; Jenkins, H. A.; Puddephatt, R. J.; Yap, G. P. A. *J. Chem. Soc.. Dalton Trans.* **2000**, 3212−3217. (k) Kovács, G.; Schubert, G.; Joó, F.; Pápai, I. *Catal. Today* **2006**, *115*, 53−60. (l) Man, M. L.; Zhou, Z.; Ng, S. M.; Lau, C. P. *Dalton Trans.* **2003**, 3727−3735. (m) Ogo, S.; Kabe, R.; Hayashi, H.; Harada, R.; Fukuzimi, S. *Dalton Trans..* **2006**, 4657−4663. (n) Federsel, C.; Jackstell, R.; Boddien, A.; Laurenczy, G.; Beller, M. *ChemSusChem* **2010**, *3*, 1048−1050. (o) Moret, S.; Dyson, P. J.; Laurenczy, G. *Nat. Commun.* **2014**, *5*, 4017.

(5) (a) Fornika, R.; Görls, H.; Seemann, B.; Leitner, W. *J. Chem. Soc., Chem. Commun.* **1995**, 1479−1481. (b) Hutschka, F.; Dedieu, A.; Eichberger, M.; Fornika, R.; Leitner, W. *J. Am. Chem. Soc.* **1997**, *119*, 4432−4443.

(6) Yin, C.; Xu, Z.; Yang, S.; Ng, S. M.; Wong, K. Y.; Lin, Z.; Lau, C. P. *Organometallics* **2001**, *20*, 1216−1222.

(7) Munshi, P.; Main, A. D.; Linehan, J. C.; Tai, C.; Jessop, P. G. *J. Am. Chem. Soc.* **2002**, *124*, 7963−7971.

(8) Himeda, Y.; Onozawa-Komatsuzaki, O.; Sugihara, H.; Kasuga, K. *Organometallics* **2007**, *26*, 702−712.

(9) (a) Vogt, M.; Gargir, M.; Iron, M. A.; Diskin-Posner, Y.; Ben-David, Y.; Milstein, D. *Chem. - Eur. J.* **2012**, *18*, 9194−9197. (b) Filonenko, G. A.; Hensen, E. J. M.; Pidko, E. A. *Catal. Sci. Technol.* **2014**, *4*, 3474−3485. (c) Filonenko, G. A.; Conley, M. P.; Coperet, C.; Lutz, M.; Hensen, E. J. M.; Pidko, E. A. *ACS Catal.* **2013**, *3*, 2522−2526. (d) Filonenko, G. A.; van Putten, R.; Schulpen, E. N.; Hensen, E. J. M.; Pidko, E. A. *ChemCatChem* **2014**, *6*, 1526−1530.

(10) (a) Tai, C.; Chang, T.; Roller, B.; Jessop, P. G. *Inorg. Chem.* **2003**, *42*, 7340−7341. (b) Laird, M. F.; Pink, M.; Tsvetkov, N. P.; Fan, H.; Gaulton, K. G. *Dalton Trans* **2009**, 1283−1285.

(11) (a) Federsel, C.; Zeibart, C.; Jackstell, R.; Baumann, W.; Beller, M. *Chem. - Eur. J.* **2012**, *18*, 72−75. (b) Jeletic, M. S.; Mock, M. T.; Appel, A. M.; Linehan, J. C. *J. Am. Chem. Soc.* **2013**, *135*, 11533−11536.

(12) (a) Federsel, C.; Boddien, A.; Jackstell, R.; Jennerjahn, R.; Dyson, P. J.; Scopelliti, R.; Laurenczy, G.; Beller, M. *Angew. Chem., Int. Ed.* **2010**, *49*, 9777−9780. (b) Langer, R.; Diskin-Posner, Y.; Leitus, G.; Shimon, L. J. W.; Ben-David, Y.; Milstein, D. *Angew. Chem., Int. Ed.* **2011**, *50*, 9948−9952. (c) Ziebart, C.; Federsel, C.; Anbarasan, P.; Jackstell, R.; Baumann, W.; Spannenberg, A.; Beller, M. *J. Am. Chem. Soc.* **2012**, *134*, 20701−20704. (d) Boddien, A.; Mellmann, D.; Gartner, F.; Jackstell, R.; Junge, H.; Dyson, P. J.; Laurenczy, G.; Ludwig, R.; Beller, M. *Science* **2011**, *333*, 1733−1736. (e) Boddien, A.; Loges, B.; Gärtner, F.; Torborg, C.; Fumino, K.; Junge, H.; Ludwig, R.; Beller, M. *J. Am. Chem. Soc.* **2010**, *132*, 8924−8934.

(13) (a) Kovács, G.; Schubert, G.; Joó, F.; Pápai, I. *Catal. Today* **2006**, *115*, 53−60. (b) Urakawa, A.; Iannuzzi, M.; Hutter, J.; Baiker, A. *Chem. - Eur. J.* **2007**, *13*, 6828−6840. (c) Ohnishi, Y.; Matsunaga, T.; Nakao, Y.; Sato, H.; Sakaki, S. *J. Am. Chem. Soc.* **2005**, *127*, 4021−4032. (d) Ohnishi, Y.; Nakao, Y.; Sato, H.; Sakaki, S. *Organometallics* **2006**, *25*, 3352−3363. (e) Kozuh, S.; Azerraf, C. *ChemCatChem* **2011**, *3*, 1348−1353. (f) Ostapowicz, T. G.; Hölscher, M.; Leitner, W. *Chem. - Eur. J.* **2011**, *17*, 10329−10338. (g) Hou, C.; Jiang, J.; Zhang, S.; Wang, G.; Zhang, Z.; Ke, Z.; Zhao, C. *ACS Catal.* **2014**, *4*, 2990−2997.

(14) Tanaka, R.; Yamashita, M.; Chung, L. W.; Morokuma, K.; Nozaki, K. *Organometallics* **2011**, *30*, 6742−6750.

(15) Yang, X. *ACS Catal.* **2011**, *1*, 849−854.

(16) Li, J.; Yoshizawa, K. *Bull. Chem. Soc. Jpn.* **2011**, *84*, 1039−1048.

(17) Mondal, B.; Neese, F.; Ye, S. *Inorg. Chem.* **2015**, *54*, 7192−7198.

(18) Schmeier, T. J.; Dobereiner, G. E.; Crabtree, R. H.; Hazari, N. *J. Am. Chem. Soc.* **2011**, *133*, 9274−9277.

(19) (a) Wang, Y.; Wang, M.; Sun, L.; Ahlquist, M. S. G. *Chem. Commun.* **2012**, *48*, 4450−4452. (b) Wang, Y.; Ahlquist, M. S. G. *Dalton Trans.* **2013**, *42*, 7816−7822.

(20) Ess, D. H.; Bischof, S. M.; Oxgaard, J.; Periana, R. A.; Goddard, W. A., III *Organometallics* **2008**, *27*, 6440−6445.

(21) van Zeist, W.-J.; Bickelhaupt, F. M. *Org. Biomol. Chem.* **2010**, *8*, 3118−3127.

(22) *Jaguar 7.5*; Schrödinger LLC, Portland, OR.

(23) (a) Becke, A. D. *J. Chem. Phys.* **1993**, *98*, 5648−5652. (b) Lee, C.; Yang, W.; Parr, R. G. *Phys. Rev. B: Condens. Matter Mater. Phys.* **1998**, *37*, 785−789.

(24) (a) Wadt, W. R.; Hay, P. J. *J. Chem. Phys.* **1985**, *82*, 284−298. (b) Hay, P. J.; Wadt, W. R. *J. Chem. Phys.* **1985**, *82*, 270−283.

(25) Zhao, Y.; Truhlar, D. G. *Theor. Chem. Acc.* **2008**, *120*, 215−241.

(26) (a) Tannor, D. J.; Marten, B.; Murphy, R.; Friesner, R. A.; Sitkoff, D.; Nicholls, A.; Rignalda, M.; Goddard, W. A., III; Honig, B. J. *J. Am. Chem. Soc.* **1994**, *116*, 11875−11882. (b) Marten, B.; Kim, K.; Cortis, C.; Friesner, R. A.; Murphy, R. B.; Rignalda, M. N.; Sitkoff, D.; Honig, B. *J. Phys. Chem.* **1996**, *100*, 11775−11788.

(27) Kelly, C. P.; Cramer, C. J.; Truhlar, D. G. *J. Phys. Chem. B* **2006**, *110*, 16066−16081.

(28) Keith, J. A.; Nielsen, R. J.; Oxgaard, J.; Goddard, W. A., III *J. Am. Chem. Soc.* **2007**, *129*, 12342−12343.

DOI: 10.1021/acs.organomet.5b00448
Organometallics 2015, 34, 4932−4940

Publication III

Osadchuk, I.; Tamm, T.; Ahlquist, M. S. G. Reduced state of iridium PCP pincer complexes in electrochemical CO_2 hydrogenation, *ACS Catalysis*, **2016**, *6*, 3834–3839.

ACS Catalysis

Letter

pubs.acs.org/acscatalysis

Reduced State of Iridium PCP Pincer Complexes in Electrochemical CO_2 Hydrogenation

Irina Osadchuk,[†] Toomas Tamm,[†] and Mårten S. G. Ahlquist*

Division of Theoretical Chemistry & Biology, School of Biotechnology, KTH Royal Institute of Technology, 10691 Stockholm, Sweden

Supporting Information

ABSTRACT: We present a computational study on the mechanism for electrochemical reduction of CO_2 using a PCP pincer iridium(III) dihydride complex. Our results point toward a mechanism that involves an *in situ*-generated iridium(I) hydride as the active species for the CO_2 to formate reduction. The iridium(III) path can operate in parallel but is associated with higher activation free energies in the reaction between the metal hydride and CO_2, compared to the reaction at the *in situ*-generated iridium(I) species.

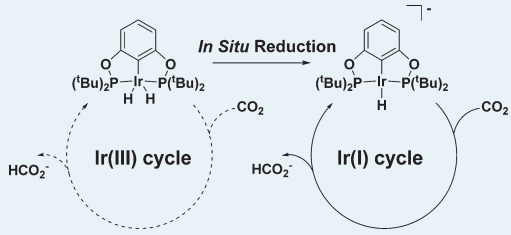

KEYWORDS: *iridium, electrochemical reduction, hydrogenation, CO_2 reduction, carbon dioxide, formate, DFT, reaction mechanism*

There are several strategies for using CO_2 as a feedstock for industrial chemical synthesis such as urea, salicylic acid, aromatic polycarbonates, organic carbonates, and especially for liquid fuels.[1,2] CO_2 as a feedstock has the advantages of being renewable, abundant, inexpensive, and nontoxic carbon source, but its usage in industrial chemistry is very limited, because of the large input of energy required to transform CO_2 into other chemicals.[2,3] In order to decrease the energy needed for conversion of CO_2, different methods, such as chemical transformation,[4−7] photochemical reduction,[8−10] biological conversion,[11,12] and chemical and electrochemical reduction,[13−24] have been used. Electrochemical reduction of CO_2 to liquid fuel is appealing, especially in the case when renewable energy sources such as hydro, geothermal or wind energy are used.[3] CO_2 could be electrochemically reduced to different products (e.g. CO, formic acid, methanol or methane; see eqs 1−5).[18]

$$CO_2 + 2H^+ + 2e^+ \rightarrow HCOOH \quad (E^\circ = -0.61\ V) \tag{1}$$

$$CO_2 + 2H^+ + 2e^+ \rightarrow CO + H_2O \quad (E^\circ = -0.52\ V) \tag{2}$$

$$CO_2 + 4H^+ + 4e^+ \rightarrow HCHO + H_2O \quad (E^\circ = -0.48\ V) \tag{3}$$

$$CO_2 + 6H^+ + 6e^+ \rightarrow CH_3OH + H_2O \quad (E^\circ = -0.38\ V) \tag{4}$$

$$CO_2 + 8H^+ + 8e^+ \rightarrow CH_4 + 2H_2O \quad (E^\circ = -0.61\ V) \tag{5}$$

Direct electrochemical reduction of CO_2 requires −1.90 V.[18] In order to minimize the potential, as well to increase the selectivity and efficiency, different electrodes have been tried (such as Cu,[20−24] Fe,[24,25] Co,[9,24] Ni,[24] Sn,[26,27] Au,[28,29] Ag,[29] Pt[30]), the influence of electrode structure[17,25−27,31] and pH dependence[10,29] on the CO_2 reduction have been investigated, and different catalysts have been explored. In 1992, *cis*-$[Os(byp)_2(CO)H]^+$ was reported to operate at −1.4 V at a Pt electrode with high selectivity,[32] with CO yields up to 80%. In 1997, Caix et al. found that reduction to formate up to 50% could be reached with $[(\eta^5\text{-}Me_5C_5)Rh(bpy)Cl]^+$ in CH_3CN/H_2O at −1.7 V.[33] $Et_4N[Fe_4N(CO)_{12}]$ reduced CO_2 to formate in acetonitrile at a potential of −1.23 vs SCE.[34] In 2011, Meyer and co-workers suggested $[Ru(tpy)(Mebim\text{-}py)(Solvent)]^{2+}$ as a selective catalyst for CO_2 reduction to CO.[35] This catalyst reduced CO_2 to CO in $^n Bu_4NPF_6/CH_3CN$ at potentials between −1.25 V and −1.55 V. Formate was formed as a byproduct to <20%. In 2012, Brookhart's group reported $(PCP)IrH_2$ as a catalyst for selective reduction of CO_2 to formate.[36] In $^n Bu_4NPF_6/CH_3CN$ with 5% water and 0.1 M $^n Bu_4NPF_6$ $(PCP)IrH_2$ had selectivity up to 85% and TON of 40 at a potential of −1.4 V at a glassy carbon electrode (GCE). This group also proposed the water-soluble analogue of $(PCP)IrH_2$ complex[37] and immobilized it on carbon nanotube electrodes.[38] The immobilized catalyst showed high selectivity of up to 96% and very high TON of 203000 in water at potentials between −1.1 V and −1.4 V NHE. Ahn et al. recently reported a $(PN^HP)IrH_3$ catalyst for CO_2 reduction to formate with a Faradaic activity of >99% at −1.5 V vs Fc/Fc^+.[39]

As part of our effort to understand the nature and reactivity of iridium complexes, we present a computational study on a catalytic system in water developed by Brookhart and co-workers.[37] In their report, they suggested a mechanism containing three main steps (see Figure 1):

(1) coordination of an acetonitrile molecule to the (PCP)-IrH_2 pincer complex and its activation;

Received: May 2, 2016
Published: May 10, 2016

DOI: 10.1021/acscatal.6b01233
ACS Catal. 2016, 6, 3834−3839

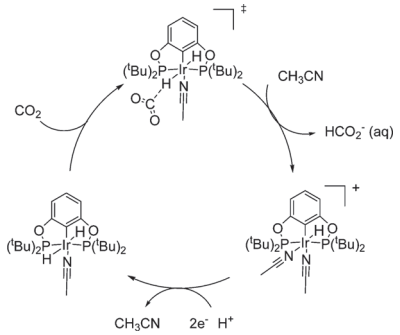

Figure 1. Proposed catalytic cycle in the original report.

(2) insertion of CO_2 followed by formate formation and release; and
(3) association of a second acetonitrile molecule and reduction to the starting catalytic complex.[36]

While this mechanism is possible, other mechanisms have not been excluded. Here, we will show mechanisms involving iridium in both the trivalent oxidation state (Ir(III)) and monovalent oxidation state (Ir(I)); our results favor the Ir(I) state as the main catalytic state.

■ Ir^{III} DIHYDRIDE MECHANISM

The mechanism proposed in the original experimental report starts with the association of a CH_3CN molecule to the trigonal bipyramidal Ir^{III} pincer complex forming the octahedral hexacoordinated complex **B** with the two hydrides in *trans* position to each other (see Scheme 1). We calculate this

Scheme 1. Gibbs Free Energy Profile (in kcal mol^{-1}) for Proposed Reduction of CO_2 to Formate by Ir^{III} Complex with Incorporated Acetonitrile Molecule

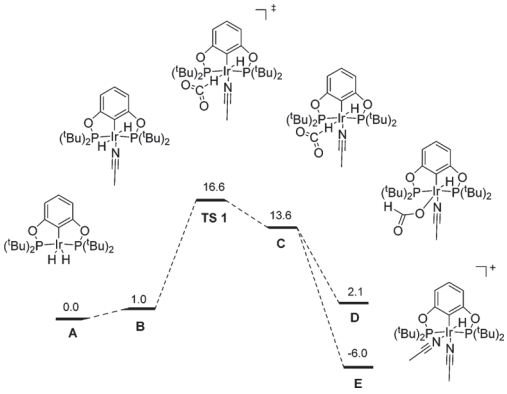

association to be slightly endergonic, by 1.0 kcal mol^{-1}. Then, one of the *trans* hydrides can react with the electrophilic carbon in CO_2, resulting in the formation of intermediate **C** via transition state **TS1** with a barrier of 16.6 kcal mol^{-1}. We also tested the reactivity of the cis isomer of **B** and found that the transition state for insertion was slightly higher than **TS1**. Intermediate **C** has a slightly lower Gibbs free energy than **TS1**, at 13.6 kcal mol^{-1}, compared to the starting complex **A**. Furthermore, we expect formate complex **C** rearrangement to complexes **D** and **E**, as both were observed experimentally. Based on our previous studies on (PNP)Ir complexes, we assume the conversion from **C** to **D** and **E** to proceed via dissociation of the weak agostic Ir···HCO_2^- bond, followed by either reassociation of formate or association of an acetonitrile molecule.[4b,c]

Alternatively, complex **A** could react directly with CO_2 without association of CH_3CN prior to the reaction (Scheme 2). This reaction path has a higher free energy of activation

Scheme 2. Gibbs Free Energy Profile (in kcal mol^{-1}) for Reduction of CO_2 to Formate Directly by Ir^{III} Complex A without Any Solvent Incorporation

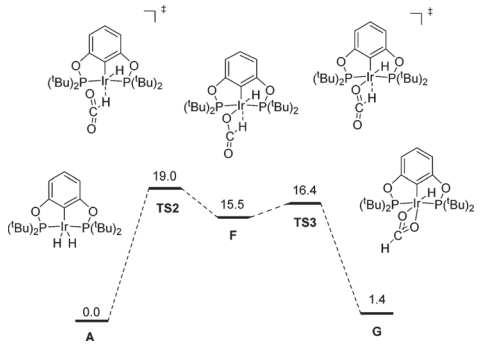

with the highest point at at 19.0 kcal mol^{-1} (**TS2**). After CO_2 insertion and rearrangement complex **G** is formed in a reaction that is endergonic by 1.4 kcal mol^{-1}. We assessed the possibility for formation of differently coordinated complexes, following the formation of **G**; all of these possibilities are described in the Supporting Information (Scheme S1). The rate of this reaction was measured experimentally at −65 °C.[36] The activation free energy was determined to 15.3 kcal mol^{-1} and the reaction free energy was determined to be −5.9 kcal mol^{-1}. Assuming that the enthalpy (H) and entropy (S) are constant, we can calculate the activation free energy, determining it to be 15.7 kcal mol^{-1} and the reaction free energy to be −2.1 kcal mol^{-1}, in good agreement with the experimental data. In the presence of acetonitrile, we expect **G** to convert to **E**, based on the energetics.

The results above show that the Ir^{III} complex **A** can also react with CO_2, although reaction with Ir^{III} complex **B** is more favorable. However, to complete the cycle, the dihydride catalyst must be regenerated. We assume that the reduction of low-energy complex **E** to the iridium(I) complex **H** is a more likely mechanism, based on the experimental observations by Brookhart.[36] **H** was not directly observed, but a two-electron reduction followed by the formation of the dihydride from reaction with water indicates its formation. The calculated two-electron potential of −0.82 V does not agree with the experimental onset potential at −1.1 V. However, the irreversible peak for reduction of **E** found in the experimental paper could indicate non-Nernstian behavior.[40] The observed onset is then more likely to be occurring at the Ir^{III}/Ir^{II} potential. We calculate this reduction potential to be −1.15 V, which is in much better agreement with the experimental

DOI: 10.1021/acscatal.6b01233
ACS Catal. 2016, 6, 3834−3839

results. The Ir^{II}/Ir^{I} reduction potential is calculated to be −0.5 V.

If Ir^{III} is the catalytically active species completion of the catalytic cycle, the catalyst must be protonated to form an iridium(III) dihydride complex. One possibility is that the process proceeds via oxidative addition of a water molecule to the Ir^{I} intermediate **H**. We calculate this process to have an excessively high barrier of 50.4 kcal mol^{-1} (see Scheme 3). We

Scheme 3. Gibbs Free-Energy Profile (in kcal mol^{-1}) for the Oxidative Addition of a Water Molecule

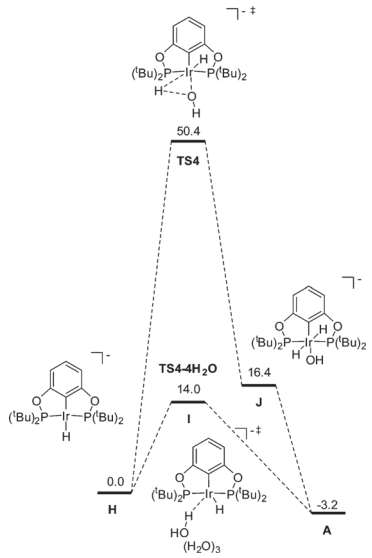

are linking this high barrier with significant rearrangement of the complex needed for adopting the transition-state geometry. From the stable square planar geometry in complex **H**, Ir rearranges to an almost octahedral geometry, where the hydride is bent almost entirely over to the axial position (Figure 2).

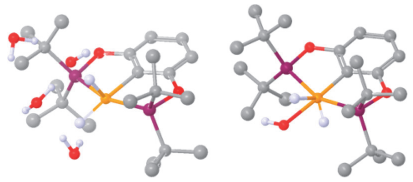

Figure 2. Geometry of **TS4−4H$_2$O** (left) and **TS4** (right). Hydrogen atoms have been removed for the sake of clarity, except the ones in proximity of the Ir center.

Such significant distortion of the geometry would have to be matched by a very strong interaction between the iridium center and the reacting water molecule. Since the barrier is calculated at 50.4 kcal mol^{-1} the iridium water interaction can clearly not compensate for the large distortion.

In the experiment, the formation of the dihydride is observed after **E** is reduced; therefore, a mechanism must exist. We optimized a complex of **H** with four explicit water molecules. Under vacuum, we could not locate any proton transfer transition state to form **A** and hydroxide. However, when we performed a scan of the H−O distance of one of the water molecules and calculated the energy at the M06/LACV3P**++ level and corrected the energy with the PBF solvation energy, a maximum was found at an H−O distance of 1.6 Å. The structure showed one imaginary vibration, corresponding to the formation of **A** and hydroxide; therefore, we used this structure as an approximate transition state. The free-energy barrier for the formation of **A** from **E** was calculated to be 14.0 kcal mol^{-1}, which should be rapid at room temperature. In this transition state geometry, the rearrangement needed at the Ir complex is very small.

To summarize, the Ir^{III} mechanism rate-limiting step is found to be the formation of the C−H bond at via **TS1**. The C−H bond formation is facilitated by the association of acetonitrile and higher concentrations of this co-solvent could facilitate the reaction. The reduction of the Ir^{III} monohydride appears at the Ir^{III}/Ir^{II} peak. Once Ir^{I} is formed the protonation to form **A** is facile.

■ Ir^{I} HYDRIDE MECHANISM

There is an alternative reaction at the iridium(I) hydride intermediate **H**. A reaction analogous to the insertion of CO_2 into the Ir−H bond at **A** could occur at **H**, forming an Ir^{I}−O_2CH intermediate (Scheme 4). In the absence of CO_2, **H** is

Scheme 4. Gibbs Free-Energy Profile (in kcal mol^{-1}) for CO_2 Reaction by Ir^{I} Complex H

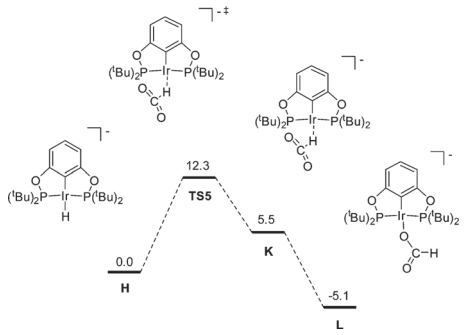

transformed to the Ir^{III} dihydride; however, in the presence of CO_2, there should be competition between carboxylation and protonation. The activation free energy is calculated to be 12.3 kcal mol^{-1}, indicating that this reaction should actually be more facile than the corresponding reaction at Ir^{III}; that is in agreement with previous theoretical studies of Bernskoetter et al.,[41] who also found the insertion of CO_2 in the Ir^{I} complex to be more energetically favorable. The CO_2 insertion in the Ir^{I} complex is an exergonic process with a ΔG value of −5.1 kcal mol^{-1}. This reaction free energy is almost optimal, because it adds a driving force to the reaction without falling into a free-energy minima where the catalyst pool. Evidently, in the presence of CO_2 the iridium(I) hydride can react with very similar activation energies to give either **A** or **L**. If **L** forms, it still must be converted to an Ir^{III} hydride that can be reduced back to the proposed active Ir^{I} hydride. We have located a plausible mechanism that is initiated by ligand exchange of the formate to water to form an Ir^{I}−OH_2 complex **N** (see Scheme

DOI: 10.1021/acscatal.6b01233
ACS Catal. 2016, 6, 3834−3839

5). Ligand exchange can be concerted or through intermediate **M**. Formation of the Ir^{I} hydride is again found to be most

Scheme 5. Gibbs Free-Energy Profile (in kcal mol^{-1}) for Oxidative Addition of Water[a]

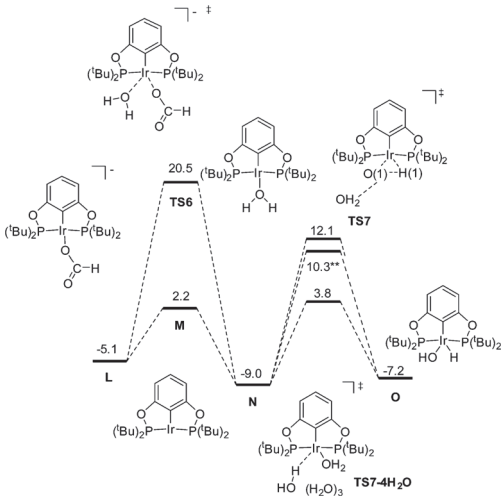

[a]In the formation of O from N, both oxidative addition (**TS7**) and proton transfer via a water chain was considered (**TS7·4H$_2$O**), where the proton transfer mechanism was clearly favored. The free energies are relative to **H** in Scheme 4. The double asterisk symbol (**) indicates a water molecule without hydrogen bonding.

favored via proton transfer from water to the iridium center, with a barrier of 12.8 kcal mol^{-1}. At **N** oxidative addition of water is not as disfavored as for **H**, but proton transfer is still the most-favored mechanism. It has been seen previously that oxidative addition to metals is favored by lower coordination numbers at the metal.[42] A plausible explanation is that there is much less geometric rearrangement of the catalyst when the coordination is lower. Looking at **TS7** (Figure 3), we see that

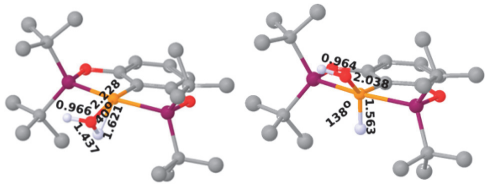

Figure 3. Geometry of (left) **TS7** and (right) **O**. Hydrogen atoms have been removed for clarity except the ones in proximity of the iridium center.

the geometry is already close to the trigonal bipyramidal geometry. The newly formed bonds Ir−O(1) and Ir−H(1) are not fully formed where the Ir−O(1) bond is 0.19 Å and Ir−H(1) 0.07 Å longer, compared to complex **O**.

Once complex **O** is formed, we must regenerate **H** via a two-electron reduction. Our calculated potential for the reduction of **O** is identical to that of **E** at −1.17 V via the Ir^{II} intermediate. If we summarize the Ir^{I} mechanism, we found that the highest free-energy barrier was the regeneration of the Ir^{I} species H of 12.8 kcal mol^{-1}, with a very similar barrier for the C−H bond formation of 12.3 kcal mol^{-1}. From these results, it appears that the reaction of CO_2 is more likely to proceed at Ir^{I} than Ir^{III}, which had the highest barrier (16.6 kcal mol^{-1}).

■ CONCLUSIONS

We have studied the reactivity of CO_2 toward PCP-iridium hydride complexes in the trivalent (III) and monovalent (I) oxidation states. The previously proposed mechanism was found to be possible, and it was found to have an activation free energy of 16.6 kcal mol^{-1} at its rate-limiting step, the C−H bond formation at the Ir^{III} dihydride. After formation of the formate, the complex is reduced to the Ir^{I} hydride species **H**. The regeneration of the dihydride takes place via proton transfer from water to the metal center. However, at H the complex could also react with CO_2 to give an iridium(I) formate complex with a barrier of merely 12.3 kcal mol^{-1}, compared to barriers of 16.6 and 19.0 kcal mol^{-1} for the corresponding reaction at the iridium(III) complex **B** and **A**, respectively. Regeneration of the active iridium(I) hydride involves proton transfer at a tetracoordinated iridium(I) complex **N**. Also here, the proton transfer was found to be more facile, compared to oxidative addition. According to the results presented herein, the protonation of the Ir(I) species is the rate-limiting step, with an activation free energy of 12.8 kcal mol^{-1}, and the potential required for regeneration of the Ir^{I}−H complex **H** from complex **O** is −1.17 V. The proposed catalytic cycle is outlined in Figure 4.

■ COMPUTATIONAL DETAILS

All calculations were performed with the Jaguar 7.5 software package.[43] We have used the complex without the quarternary

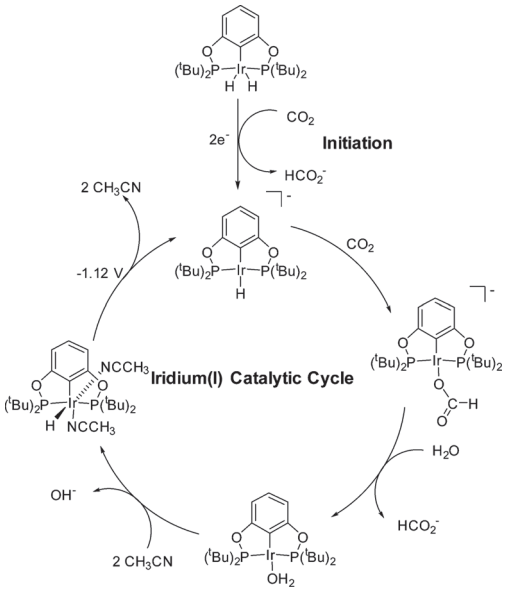

Figure 4. Proposed catalytic cycle with Ir(I) generated *in situ* from CO_2 and a two-electron reduction.

DOI: 10.1021/acscatal.6b01233
ACS Catal. 2016, 6, 3834−3839

amine, which was introduced to increase the solubility. Since the group is far from the reacting center, we assume that its effect on the intrinsic mechanism is limited. For geometry optimization the B3LYP functional[44,45] was used in combination with the LACVP**[46,47] core potential and basis set. For final single-point energy correction, we used the M06 functional[48] with the larger LACV3P**++ basis set, which we have augmented with two f-functions on iridium.[49,50] All calculations were made under vacuum, and single-point solvation energies were performed to estimate the Gibbs free energies of solvation, using the Poisson−Boltzmann self-consistent reaction field as implemented in Jaguar (PBF).[51,52] To simulate water, we used the standard parameters with the dielectric constant at 78.0 and the probe radius to 1.4 Å. Solvation free energies for small ions and molecules are taken from the literature.[53] The calculations of the harmonic vibrational frequencies were performed to define the nature of all intermediates and transition states. To confirm the transition state as connecting to the reactant and products IRC calculation were performed. The Gibbs free energy and enthalpies were calculated by using eq 6.

$$G = E(\mathrm{M06/LACV3P{**}{+}{+}2f}) + G_{\mathrm{solv}} + \mathrm{ZPE} + \Delta H_{298} - TS_{298} \quad (6)$$

A correction of 1.9 kcal mol^{-1} to the free energy was used to correct change of standard state from 1 atm to 1 M in solution phase. Gas-phase molecules were assumed to be at 1 atm. The reduction potential was calculated, relative to the absolute NHE at 4.28 V.[54] For validation of the gas-phase optimized geometries, we performed full solvent optimizations on the key transition states and their precursors. No significant changes in geometries or energies were observed and examples of solvation optimized structures are included in the Supporting Information.

■ ASSOCIATED CONTENT

Supporting Information

The Supporting Information is available free of charge on the ACS Publications website at DOI: 10.1021/acscatal.6b01233.

Molecular structure (XYZ)

Cartesian coordinates and energies of the presented complexes are available as Supporting Information (PDF)

■ AUTHOR INFORMATION

Corresponding Author

*E-mail: ahlqui@kth.se.

Present Address

†Department of Chemistry, Tallinn University of Technology, Akadeemia tee 15, 12618 Tallinn, Estonia.

Funding

ESF DoRa T6, "Development of international cooperation networks by supporting the mobility of Estonian doctoral students". Computational resources were provided by SNIC at the National Supercomputer Center in Linköping Sweden. Vetenskapsrådet is acknowledged for financial support.

Notes

The authors declare no competing financial interest.

■ REFERENCES

(1) Benson, E.; Kubiak, C.; Sathrum, A.; Smieja, J. *Chem. Soc. Rev.* **2009**, *38*, 89−99.

(2) Wang, W.; Wang, S.; Ma, X.; Gong, J. *Chem. Soc. Rev.* **2011**, *40*, 3703−3727.

(3) Mikkelsen, M.; Jørgensen, M.; Krebs, F. *Energy Environ. Sci.* **2010**, *3*, 43−81.

(4) (a) Tanaka, R.; Yamashita, M.; Nozaki, K. *J. Am. Chem. Soc.* **2009**, *131*, 14168−14169. (b) Ahlquist, M. S. G. *J. Mol. Catal. A: Chem.* **2010**, *324*, 3−8. (c) Osadchuk, I.; Tamm, T.; Ahlquist, M. S. G. *Organometallics* **2015**, *34*, 4932−4940.

(5) Langer, R.; Diskin-Posner, Y.; Leitus, G.; Shimon, L.; Ben-David, Y.; Milstein, D. *Angew. Chem., Int. Ed.* **2011**, *50*, 9948−9952.

(6) Federsel, C.; Boddien, A.; Jackstell, R.; Jennerjahn, R.; Dyson, P.; Scopelliti, R.; Laurenczy, G.; Beller, M. *Angew. Chem., Int. Ed.* **2010**, *49*, 9777−9780.

(7) Appel, A. M.; Bercaw, J. E.; Bocarsly, A. B.; Dobbek, H.; DuBois, D. L.; Dupuis, M.; Ferry, J. G.; Fujita, E.; Hille, R.; Kenis, P.J. A.; Kerfeld, C. A.; Morris, R. H.; Peden, C.H. F.; Portis, A. R.; Ragsdale, S. W.; Rauchfuss, T. B.; Reek, J.N. H.; Seefeldt, L. C.; Thauer, R. K.; Waldrop, G. L. *Chem. Rev.* **2013**, *113*, 6621−6658.

(8) Schneider, J.; Jia, H.; Muckerman, J.; Fujita, E. *Chem. Soc. Rev.* **2012**, *41*, 2036−2051.

(9) Behar, D.; Dhanasekaran, T.; Neta, P.; Hosten, C. M.; Ejeh, D.; Hambright, P.; Fujita, E. J. *J. Phys. Chem. A* **1998**, *102*, 2870−2877.

(10) Doherty, M. D.; Grills, D. C.; Muckerman, J. T.; Polyansky, D. E.; Fujita, E. *Coord. Chem. Rev.* **2010**, *254*, 2472−2482.

(11) Reda, T.; Plugge, C. M.; Abram, N. J.; Hirst, J. *Proc. Natl. Acad. Sci. U. S. A.* **2008**, *105*, 10654−10658.

(12) Varley, J. B.; Hansen, H. A.; Ammitzbøll, N. L.; Grabow, L. C.; Peterson, A. A.; Rossmeisl, J.; Nørskov, J. K. *ACS Catal.* **2013**, *3*, 2640−2643.

(13) DuBois, D. L.; Miedaner, A.; Haltiwanger, R. C. J. *J. Am. Chem. Soc.* **1991**, *113*, 8753−8764.

(14) Arana, C.; Yan, S.; Keshavarz, K. M.; Potts, K. T.; Abruha, H. D. *Inorg. Chem.* **1992**, *31*, 3680−3682.

(15) Hammouche, M.; Lexa, D.; Momenteau, M.; Savéant, J.-M. J. *J. Am. Chem. Soc.* **1991**, *113*, 8455−8466.

(16) Finn, C.; Schnittger, S.; Yellowlees, L. J.; Love, J. B. *Chem. Commun.* **2012**, *48*, 1392−1399.

(17) Jhong, H. R.; Ma, S.; Kenis, P. *Curr. Opin. Chem. Eng.* **2013**, *2*, 191−199.

(18) Whipple, D. T.; Kenis, P. J. A. *J. Phys. Chem. Lett.* **2010**, *1*, 3451−3458.

(19) Halmann, M. M.; Steinberg, M. *Greenhouse Gas Carbon Dioxide Mitigation Science and Technology*; CRC Press LLC: Boca Raton, FL, 1999.

(20) Kortlever, R.; Tan, K. H.; Kwon, Y.; Koper, M. T. M. *J. Solid State Electrochem.* **2013**, *17*, 1843−1849.

(21) Schouten, K. J. P.; Kwon, Y.; van der Ham, C. J. M.; Qin, Z.; Koper, M. T. M. *Chem. Sci.* **2011**, *2*, 1902−1909.

(22) Chen, Z.; Kang, P.; Zhang, M. T.; Stoner, B. R.; Meyer, T. J. *Energy Environ. Sci.* **2013**, *6*, 813−817.

(23) Peterson, A. A.; Abild-Pedersen, F.; Studt, F.; Rossmeisl, J.; Nørskov, J. K. *Energy Environ. Sci.* **2010**, *3*, 1311−1315.

(24) Liu, C.; Cundari, T. R.; Wilson, A. K. *J. Phys. Chem. C* **2012**, *116*, 5681−5688.

(25) Bernstein, N. J.; Akhade, S. A.; Janik, M. J. *Phys. Chem. Chem. Phys.* **2014**, *16*, 13708−13717.

(26) Zhang, S.; Kang, P.; Meyer, T.J. J. *J. Am. Chem. Soc.* **2014**, *136*, 1734−1737.

(27) Chen, Y.; Kanan, M.W. J. *J. Am. Chem. Soc.* **2012**, *134*, 1986−1989.

(28) Chen, Y.; Li, C. W.; Kanan, M. W. *J. Am. Chem. Soc.* **2012**, *134*, 19969−19972.

(29) Sreekanth, N.; Phani, K. L. *Chem. Commun.* **2014**, *50*, 11143−11146.

(30) Ertem, M. Z.; Konezny, S. J.; Araujo, C. M.; Batista, V. S. *J. Phys. Chem. Lett.* **2013**, *4*, 745−748.

(31) Lim, D.-H.; Jo, J. H.; Shin, D. Y.; Wilcox, J.; Ham, H. C.; Nam, S. W. *Nanoscale* **2014**, *6*, 5087−5092.

DOI: 10.1021/acscatal.6b01233
ACS Catal. 2016, 6, 3834−3839

(32) Bruce, M.; Megehee, E.; Sullivan, P.; Thorp, H.; O'Toole, T.; Downard, A.; Pugh, R.; Meyer, T. *Inorg. Chem.* **1992**, *31*, 4864−4873.
(33) Caix, C.; Chardon-Noblat, S.; Deronzier, A. *J. Electroanal. Chem.* **1997**, *434*, 163−167.
(34) Rail, M. D.; Berben, L. A. J. *J. Am. Chem. Soc.* **2011**, *133*, 18577−18579.
(35) Chen, Z.; Chen, C.; Weinberg, D.; Kang, P.; Concepcion, J.; Harrison, D.; Brookhart, M.; Meyer, T. *Chem. Commun.* **2011**, *47*, 12607−12609.
(36) Kang, P.; Cheng, C.; Chen, Z.; Schauer, C.; Meyer, T.; Brookhart, M. *J. Am. Chem. Soc.* **2012**, *134*, 5500−5503.
(37) (a) Kang, P.; Meyer, T.; Brookhart, M. *Chem. Sci.* **2013**, *4*, 3497−3502. (b) Polukeev, A. V.; Marcos, R.; Ahlquist, M. S. G.; Wendt, O. F. *Chem. Sci.* **2015**, *6*, 2060−2067. (c) Jonasson, K. J.; Polukeev, A. V.; Marcos, R.; Ahlquist, M. S. G.; Wendt, O. F. *Angew. Chem., Int. Ed.* **2015**, *54*, 9372−9375. (d) Polukeev, A. V.; Marcos, R.; Ahlquist, M. S. G.; Wendt, O. F. *Chem.—Eur. J.* **2016**, *22*, 4078−4086.
(38) Kang, P.; Zhang, S.; Meyer, T.; Brookhart, M. *Angew. Chem., Int. Ed.* **2014**, *53*, 8509−8713.
(39) Ahn, S. T.; Bielinski, E. A.; Lane, E. M.; Chen, Y.; Bernskoetter, W. H.; Hazari, N.; Palmore, G. T. R. *Chem. Commun.* **2015**, *51*, 5947−5950.
(40) McCormick, M. C.; Keijzer, K.; Polavarapu, A.; Schultz, F. A.; Baik, M. H. *J. Am. Chem. Soc.* **2014**, *136*, 8992−9000.
(41) Bernskoetter, W. H.; Hazari, N. *Eur. J. Inorg. Chem.* **2013**, *2013*, 4032−4041.
(42) Ozerov, O. V. *Chem. Soc. Rev.* **2009**, *38*, 83−88.
(43) *Jaguar 7.5*; Schrödinger LLC: Portland, OR, 2007.
(44) Becke, A. D. *J. Chem. Phys.* **1993**, *98*, 5648−5652.
(45) Lee, C.; Yang, W.; Parr, R. G. *Phys. Rev. B: Condens. Matter Mater. Phys.* **1988**, *37*, 785−789.
(46) Wadt, W. R.; Hay, P. J. *J. Chem. Phys.* **1985**, *82*, 284−298.
(47) Hay, P. J.; Wadt, W. R. *J. Chem. Phys.* **1985**, *82*, 270−283.
(48) Zhao, Y.; Truhlar, D. G. *Theor. Chem. Acc.* **2008**, *120*, 215−241.
(49) Martin, J. M. L. *Chem. Phys. Lett.* **1999**, *310*, 271−276.
(50) Martin, J. M. L.; Sundermann, A. J. *J. Chem. Phys.* **2001**, *114*, 3408−3420.
(51) Tannor, D. J.; Marten, B.; Murphy, R.; Friesner, R. A.; Sitkoff, D.; Nicholls, A.; Ringnalda, M.; Goddard, W. A., III; Honig, B. J. *J. Am. Chem. Soc.* **1994**, *116*, 11875−11882.
(52) Marten, B.; Kim, K.; Cortis, C.; Friesner, R. A.; Murphy, R. B.; Ringnalda, M. N.; Sitkoff, D.; Honig, B. *J. Phys. Chem.* **1996**, *100*, 11775−11788.
(53) Kelly, C. P.; Cramer, C. J.; Truhlar, D. G. *J. Phys. Chem. B* **2006**, *110*, 16066−16081.
(54) Isse, A. A.; Gennaro, A. *J. Phys. Chem. B* **2010**, *114*, 7894−7899.

DOI: 10.1021/acscatal.6b01233
ACS Catal. 2016, 6, 3834−3839

ABSTRACT

Catalysts, including catalytic complexes based on transition metals, are widely used in industry. Design of catalysts is a challenging task, since the numerous mutual influences of parts of the catalytic system should be taken into account. Only in-depth understanding of the mechanisms of catalytic reactions and knowledge of metal-ligand and ligand-ligand co-influence enables creation of effective long-lived catalysts.

The main aim of the present work was to investigate titanium and iridium complexes and the reactions catalysed by them, to analyse mutual influence of different parts of catalyst, as well as the reaction complexes, using density functional theory.

The preferential formation of hexa-coordinate $Ti(OiPr)_2(Sub\text{-}\kappa^2O,O)_2$ complex during complexation of 3-methylcyclopentane-1,2-dione with $Ti(O\mathit{i}Pr)_4$, accompanied by increase of coordination number from four to six was considered and explained in terms of *trans* and chelate effects, steric factors and the 18-electron rule. For all complexes, the Boltzmann distribution was calculated and probability > 90% for *cis-cis-trans* isomers was explained by donor-acceptor interactions of O*i*Pr and 3-methylcyclopentane-1,2-dione ligands.

Conformer search for different isomers of titanium TADDOLate complexes, which are catalytic species in the Kulinkovich reaction, was performed. It was found that bidentate TADDOL ligand is located in the axial-equatorial position in contrast to previously-assumed equatorial-equatorial position. Interrelation of ligand volume and its position was discussed in detail and influence of monodentate ligands on the geometry of TADDOL ligand was considered.

Reaction mechanism for CO_2 reduction catalysed by $(PNP)IrH_3$ complex, proposed based on the experimental data, was studied and a possible new reaction pathway catalysed by $(PNP)IrH_2OH$ complex formed *in situ* was proposed. The proposed pathway does not contradict with experiment. In order to explain preference of one pathway over another, transition state geometries were analysed. Within the framework of mutual influence of ligands, *cis*-effect and charge transfer were studied. It was found that π-donating ligands in *cis* position to hydrides, as well as possibility of hydrogen bond formation, facilitate the reaction.

For electrochemical CO_2 reduction catalysed by $(PCP)IrH_2(NCCH_3)$ complex, reaction pathway suggested based on the experimental data was modelled and a new reaction mechanism catalysed by the $(PCP)IrH^-$ anion formed *in situ*, which is also consistent with experiment, was proposed. In order to explain preference of one pathway over another, transition state geometries were analysed. Finally a change in the coordination number induced by altering of oxidation state was considered and explained using the 18-electron rule.

KOKKUVÕTE

Katalüsaatoreid, sealhulgas üleminekumetallikompleksidel põhinevaid, kasutatakse tööstuses laialdaselt. Katalüsaatorite disainimine on raske ülesanne, sest on vaja arvesse võtta arvukalt erinevaid vastastikmõjusid. Tõhusa ja pikaealise katalüsaatori loomisel on oluliseks eelduseks reaktsioonimehhanismist arusaamine ning metall-ligand ja ligand-ligand vastastikmõjude tundmine.

Käesoleva doktoritöö põhieesmärk oli titaani ja iriidiumi kompleksühendite ja nende poolt katalüüsitavate reaktsioonide uurimine ning katalüsaatorite ja reaktsioonikomplekside koostisosade vastastikmõju analüüs kasutades tihedus-funktsionaalide teooriat.

Uuriti 3-metüül-1,2-tsüklopentaan-diooni titaantetraisopropoksiidiga komplek-seerumisel eelistatult $Ti(OiPr)_2(Sub\text{-}\kappa^2O,O)_2$ kompleksi moodustumist, mille käigus koordinatsiooniarv tõuseb neljalt kuuele. Vaadeldud muutusi analüüsiti *trans*- ja kelaatefektide, steeriliste faktorite ja 18-elektroni reegli seisukohtadest. Kõikide komplekside jaoks arvutati konformeeride Boltzmanni jaotus. *Cis-cis-trans* konformeeri tõenäosus oli > 90%, mida seletati O*i*Pr ja 3-metüül-1,2-tsüklopentaan-dioon-ligandide doonor-aktseptor-interaktsiooni alusel.

TiTADDOLaat-komplekside jaoks, mis on katalüsaatorid enantioselektiivses Kulinkovichi reaktsioonis, teostati konformatsioonide ning isomeeride otsing ja leiti, et bidentaatsed TADDOL ligandid asuvad aksiaalses-ekvatoriaalses asendis, mis lükkab ümber varasemad oletused nende komplekside struktuuri kohta. Detailselt analüüsiti ligandide asendi ja suuruse vastastikmõju, samuti monodentaatsete ligandide mõju TADDOL ligandi geomeetriale.

Töös uuriti ka $(PNP)IrH_3$ kompleksi poolt katalüüsitud CO_2 taandamisreaktsiooni mehhanismi. Kirjanduses katseandmete põhjal koostatu kõrvale pakuti välja uus võimalik reaktsioonitee *in situ* moodustuva $(PNP)IrH_2OH$ kompleksi vahendusel, mis ei ole vastuolus eksperimendiga. Selgitamaks ühe reaktsioonitee eelistust teise ees teostati vastavate siirdeolekute analüüs. Ligandide vastastikmõju uurimise raames vaadeldi *cis*-efekti ja laenguülekannet. Selgus, et hüdriidioonide suhtes *cis*-asendis asetsevad π-donoorsete omadustega ligandid ja vesiniksidemete tekkimise võimalus hõlbustavad reaktsiooni.

$(PCP)IrH_2(NCCH_3)$ kompleksi poolt katalüüsitava elektrokeemilise CO_2 taandamise jaoks modelleeriti eksperimendiandmete baasil välja pakutud reaktsioonimehhanismi ning pakuti välja uudne, samuti katseandmetega sobiv, reaktsioonimehhanism, milles osaleb *in situ* moodustunud $(PCP)IrH^-$ anioon. Seletamaks ühe reaktsioonitee eelistust teise ees teostati siirdeolekute analüüs. Lähemalt uuriti ka oksüdatsiooniastme muutusest tingitud koordinatsiooniarvu muutumist uuritavates kompleksides, mille selgitamiseks tugineti 18-elektroni reeglile.

ACKNOWLEDGEMENTS

This work was conducted at the Department of Chemistry and Biotechnology of Tallinn University of Technology and the School of Biotechnology of Royal Institute of Technology. The work was financially supported by Estonian Science Foundation [grants 8255 and 8698], the Ministry of Education and Research [grants SF0140060s12, SF0142725s06], Estonian Research Council [grant IUT19-32, PUT-1683], the ESF DoRa and Graduate Schools ”Functional Materials and Technologies” and “Biomedicine and Biotechnology”.

Computations were performed on the HPC cluster at Tallinn (part of the ETAIS infrastructure) and SNIC in Sweden.

First of all, I would like to thank my supervisor Associate Professor Toomas Tamm, who introduced me to computational chemistry, and who was supporting and directing me all this time. I am grateful to my second supervisor Associate Professor Mårten Ahlquist, who brought me into topic of carbon dioxide reduction. Thank you for fruitful collaboration and provided opportunities. Special thanks to Margus Lopp, for believing in me.

I am grateful to Dr. Andrus Metsala for reviewing the thesis and Dr. Thomas Sandberg of Åbo Akademi (Finland) for reading the manuscript and providing many useful remarks. I would like to acknowledge Dr. Mario Öeren, Andre Roden, Dr. Dzmitry G. Kananovich, Dr. Marina Kudrjashova, Dr. Victor Borovkov and Dr. Jelena Hruljova for their helpful comments and discussions, for support and patience. I am grateful to my colleagues from the former chairs of inorganic, organic, green and analytical chemistry. I would also like to acknowledge bachelor student Kristina Juhhimenko for help with calculations of TADDOLate complexes.

Last but not least, I would like to thank my family for understanding and my friends for patience and unsolicited interest in chemistry, especially Natalja Jekimova and Natalia Gabaydulina for being by my side.

Curriculum vitae

1. Personal Data

Name	Irina Osadchuk
Birth date and place	29.12.1983, Narva, Estonia

2. Contact information

E-mail	irina.osadchuk@starline.ee

3. Education

2002	Elementary and secondary school in Narva, Estonia
2005	TUT, Chemical and Environmental Technology, B.Sc.
2007	TUT, Chemical and Environmental Technology, M.Sc.
2010	Tallinn Transport School, Information Technology technician.

4. Special courses

2009 December	University of Helsinki, Winter school „Chemical Bonding“
2011 February	TUT „Data analysis for chemistry“
2012 Spring	Royal Institute of Technology (KTH) „Multiscale Modelling in Chemistry and Biology“
2012 August	ÅBO Akademi University, XVII International Workshop “Quantum Systems in Chemistry and Physics”
2012 December	Royal Institute of Technology (KTH) „KCSE Winter School in Multiscale Modelling“
2012 December	University of Helsinki, Winter school „ Nuclear Motion in Molecules“
2015 – 2016	TUT “Engineering pedagogy”

5. Professional employment

2008 – 2009	Saku Brewery, laboratory assistant
2010 – 2011	TUT, researcher
2015	TUT, assistant
2011 – 2017	TUT, engineer

6. Main area of scientific work/Current research topics

Conformational analysis, modelling of reaction mechanisms, NMR calculations.

Elulookirjeldus

1. Isikuandmed

Ees- ja perekonnanimi	Irina Osadchuk
Sünniaeg ja - koht	29.12.1983, Narva, Eesti

2. Kontaktandmed

E-posti aadress	irina.osadchuk@starline.ee

3. Hariduskäik

2002	Narva Pähklimäe Gümnaasium, Eesti
2005	TTÜ, Keemia- ja keskkonnakaitse tehnoloogia, bakalaureuseõpe
2007	TTÜ, Keemia- ja keskkonnakaitse tehnoloogia, magistiõpe
2010	Tallinna Transpordikool, Infoteholoogia, tugispetsialist

4. Täiendusõpe

2009 detsember	Helsingi Ülikool, Talvekool „Chemical Bonding“
2011 veebruar	TTÜ, „Training School on Chemometrics“
2012 kevad	Kuninglik Tehnoloogiainstituut (KTH), „Multiscale Modelling in Chemistry and Biology“
2012 august	ÅBO Akademi University, XVII International Workshop “Quantum Systems in Chemistry and Physics”
2012 detsember	Kuninglik Tehnoloogiainstituut (KTH), „KCSE Winter School in Multiscale Modelling“
2012 detsember	Helsingi Ülikool, Talvekool „ Nuclear Motion in Molecules“;
2015 – 2016	TTÜ, “Engineering pedagogy“

5. Teenistuskäik

2008 – 2009	Saku Õlletehas, laborant
2010 -2011	TTÜ, Keemiainstituut, Anorgaanilise keemia õppetool, teadur
2015	TTÜ, Keemiainstituut, Anorgaanilise keemia õppetool, assistent
2013 – 2017	TTÜ, Keemiainstituut, Anorgaanilise keemia õppetool, insener

6. Teadustöö põhisuunad

Konformatsioonide otsing, reaktsioonimehhanismide modeleerimine, TMR arvutamine.

Original publications

1) I. Osadchuk, T. Pehk, A. Paju, M. Lopp, M. Öeren, T. Tamm „Isomers and conformers of complexes of $Ti(O\mathit{i}Pr)_4$ with cyclopentane-1,2-dione: NMR study and DFT calculations“ *International Journal of Quantum Chemistry*, 2014, **114**, 1012-1018.

2) I. Osadchuk, T. Tamm, M. S. G. Ahlquist „Theoretical investigation of a parallel catalytic cycle in CO_2 hydrogenation by $(PNP)IrH_3$“ *Organometallics*, 2015, **34**, 4932-4940.

3) I. Osadchuk, T. Tamm, M. S. G. Ahlquist „Reduced state of iridium PCP pincer complexes in electrochemical CO_2 hydrogenation“ *ACS Catalysis*, 2016, **6**, 3834–3839.

DISSERTATIONS DEFENDED AT
TALLINN UNIVERSITY OF TECHNOLOGY ON
NATURAL AND EXACT SCIENCES

1. **Olav Kongas**. Nonlinear Dynamics in Modeling Cardiac Arrhytmias. 1998.
2. **Kalju Vanatalu**. Optimization of Processes of Microbial Biosynthesis of Isotopically Labeled Biomolecules and Their Complexes. 1999.
3. **Ahto Buldas**. An Algebraic Approach to the Structure of Graphs. 1999.
4. **Monika Drews**. A Metabolic Study of Insect Cells in Batch and Continuous Culture: Application of Chemostat and Turbidostat to the Production of Recombinant Proteins. 1999.
5. **Eola Valdre**. Endothelial-Specific Regulation of Vessel Formation: Role of Receptor Tyrosine Kinases. 2000.
6. **Kalju Lott**. Doping and Defect Thermodynamic Equilibrium in ZnS. 2000.
7. **Reet Koljak**. Novel Fatty Acid Dioxygenases from the Corals *Plexaura homomalla* and *Gersemia fruticosa.* 2001.
8. **Anne Paju**. Asymmetric oxidation of Prochiral and Racemic Ketones by Using Sharpless Catalyst. 2001.
9. **Marko Vendelin**. Cardiac Mechanoenergetics *in silico*. 2001.
10. **Pearu Peterson**. Multi-Soliton Interactions and the Inverse Problem of Wave Crest. 2001.
11. **Anne Menert**. Microcalorimetry of Anaerobic Digestion. 2001.
12. **Toomas Tiivel**. The Role of the Mitochondrial Outer Membrane in *in vivo* Regulation of Respiration in Normal Heart and Skeletal Muscle Cell. 2002.
13. **Olle Hints**. Ordovician Scolecodonts of Estonia and Neighbouring Areas: Taxonomy, Distribution, Palaeoecology, and Application. 2002.
14. **Jaak Nõlvak**. Chitinozoan Biostratigrapy in the Ordovician of Baltoscandia. 2002.
15. **Liivi Kluge**. On Algebraic Structure of Pre-Operad. 2002.
16. **Jaanus Lass**. Biosignal Interpretation: Study of Cardiac Arrhytmias and Electromagnetic Field Effects on Human Nervous System. 2002.
17. **Janek Peterson**. Synthesis, Structural Characterization and Modification of PAMAM Dendrimers. 2002.
18. **Merike Vaher**. Room Temperature Ionic Liquids as Background Electrolyte Additives in Capillary Electrophoresis. 2002.
19. **Valdek Mikli**. Electron Microscopy and Image Analysis Study of Powdered Hardmetal Materials and Optoelectronic Thin Films. 2003.
20. **Mart Viljus**. The Microstructure and Properties of Fine-Grained Cermets. 2003.
21. **Signe Kask**. Identification and Characterization of Dairy-Related *Lactobacillus.* 2003.
22. **Tiiu-Mai Laht**. Influence of Microstructure of the Curd on Enzymatic and Microbiological Processes in Swiss-Type Cheese. 2003.
23. **Anne Kuusksalu**. 2–5A Synthetase in the Marine Sponge *Geodia cydonium*. 2003.
24. **Sergei Bereznev**. Solar Cells Based on Polycristalline Copper-Indium Chalcogenides and Conductive Polymers. 2003.
25. **Kadri Kriis**. Asymmetric Synthesis of C_2-Symmetric Bimorpholines and Their Application as Chiral Ligands in the Transfer Hydrogenation of Aromatic Ketones. 2004.

26. **Jekaterina Reut**. Polypyrrole Coatings on Conducting and Insulating Substracts. 2004.
27. **Sven Nõmm**. Realization and Identification of Discrete-Time Nonlinear Systems. 2004.
28. **Olga Kijatkina**. Deposition of Copper Indium Disulphide Films by Chemical Spray Pyrolysis. 2004.
29. **Gert Tamberg**. On Sampling Operators Defined by Rogosinski, Hann and Blackman Windows. 2004.
30. **Monika Übner**. Interaction of Humic Substances with Metal Cations. 2004.
31. **Kaarel Adamberg**. Growth Characteristics of Non-Starter Lactic Acid Bacteria from Cheese. 2004.
32. **Imre Vallikivi**. Lipase-Catalysed Reactions of Prostaglandins. 2004.
33. **Merike Peld**. Substituted Apatites as Sorbents for Heavy Metals. 2005.
34. **Vitali Syritski**. Study of Synthesis and Redox Switching of Polypyrrole and Poly(3,4-ethylenedioxythiophene) by Using *in-situ* Techniques. 2004.
35. **Lee Põllumaa**. Evaluation of Ecotoxicological Effects Related to Oil Shale Industry. 2004.
36. **Riina Aav**. Synthesis of 9,11-Secosterols Intermediates. 2005.
37. **Andres Braunbrück**. Wave Interaction in Weakly Inhomogeneous Materials. 2005.
38. **Robert Kitt**. Generalised Scale-Invariance in Financial Time Series. 2005.
39. **Juss Pavelson**. Mesoscale Physical Processes and the Related Impact on the Summer Nutrient Fields and Phytoplankton Blooms in the Western Gulf of Finland. 2005.
40. **Olari Ilison**. Solitons and Solitary Waves in Media with Higher Order Dispersive and Nonlinear Effects. 2005.
41. **Maksim Säkki**. Intermittency and Long-Range Structurization of Heart Rate. 2005.
42. **Enli Kiipli**. Modelling Seawater Chemistry of the East Baltic Basin in the Late Ordovician–Early Silurian. 2005.
43. **Igor Golovtsov**. Modification of Conductive Properties and Processability of Polyparaphenylene, Polypyrrole and polyaniline. 2005.
44. **Katrin Laos**. Interaction Between Furcellaran and the Globular Proteins (Bovine Serum Albumin β-Lactoglobulin). 2005.
45. **Arvo Mere**. Structural and Electrical Properties of Spray Deposited Copper Indium Disulphide Films for Solar Cells. 2006.
46. **Sille Ehala**. Development and Application of Various On- and Off-Line Analytical Methods for the Analysis of Bioactive Compounds. 2006.
47. **Maria Kulp**. Capillary Electrophoretic Monitoring of Biochemical Reaction Kinetics. 2006.
48. **Anu Aaspõllu.** Proteinases from *Vipera lebetina* Snake Venom Affecting Hemostasis. 2006.
49. **Lyudmila Chekulayeva**. Photosensitized Inactivation of Tumor Cells by Porphyrins and Chlorins. 2006.
50. **Merle Uudsemaa**. Quantum-Chemical Modeling of Solvated First Row Transition Metal Ions. 2006.
51. **Tagli Pitsi**. Nutrition Situation of Pre-School Children in Estonia from 1995 to 2004. 2006.
52. **Angela Ivask**. Luminescent Recombinant Sensor Bacteria for the Analysis of Bioavailable Heavy Metals. 2006.

53. **Tiina Lõugas**. Study on Physico-Chemical Properties and Some Bioactive Compounds of Sea Buckthorn (*Hippophae rhamnoides* L.). 2006.
54. **Kaja Kasemets**. Effect of Changing Environmental Conditions on the Fermentative Growth of *Saccharomyces cerevisae* S288C: Auxo-accelerostat Study. 2006.
55. **Ildar Nisamedtinov**. Application of ^{13}C and Fluorescence Labeling in Metabolic Studies of *Saccharomyces* spp. 2006.
56. **Alar Leibak**. On Additive Generalisation of Voronoï's Theory of Perfect Forms over Algebraic Number Fields. 2006.
57. **Andri Jagomägi**. Photoluminescence of Chalcopyrite Tellurides. 2006.
58. **Tõnu Martma**. Application of Carbon Isotopes to the Study of the Ordovician and Silurian of the Baltic. 2006.
59. **Marit Kauk**. Chemical Composition of $CuInSe_2$ Monograin Powders for Solar Cell Application. 2006.
60. **Julia Kois**. Electrochemical Deposition of $CuInSe_2$ Thin Films for Photovoltaic Applications. 2006.
61. **Ilona Oja Açik**. Sol-Gel Deposition of Titanium Dioxide Films. 2007.
62. **Tiia Anmann**. Integrated and Organized Cellular Bioenergetic Systems in Heart and Brain. 2007.
63. **Katrin Trummal**. Purification, Characterization and Specificity Studies of Metalloproteinases from *Vipera lebetina* Snake Venom. 2007.
64. **Gennadi Lessin**. Biochemical Definition of Coastal Zone Using Numerical Modeling and Measurement Data. 2007.
65. **Enno Pais**. Inverse problems to determine non-homogeneous degenerate memory kernels in heat flow. 2007.
66. **Maria Borissova**. Capillary Electrophoresis on Alkylimidazolium Salts. 2007.
67. **Karin Valmsen**. Prostaglandin Synthesis in the Coral *Plexaura homomalla*: Control of Prostaglandin Stereochemistry at Carbon 15 by Cyclooxygenases. 2007.
68. **Kristjan Piirimäe**. Long-Term Changes of Nutrient Fluxes in the Drainage Basin of the Gulf of Finland – Application of the PolFlow Model. 2007.
69. **Tatjana Dedova**. Chemical Spray Pyrolysis Deposition of Zinc Sulfide Thin Films and Zinc Oxide Nanostructured Layers. 2007.
70. **Katrin Tomson**. Production of Labelled Recombinant Proteins in Fed-Batch Systems in *Escherichia coli*. 2007.
71. **Cecilia Sarmiento**. Suppressors of RNA Silencing in Plants. 2008.
72. **Vilja Mardla**. Inhibition of Platelet Aggregation with Combination of Antiplatelet Agents. 2008.
73. **Maie Bachmann**. Effect of Modulated Microwave Radiation on Human Resting Electroencephalographic Signal. 2008.
74. **Dan Hüvonen**. Terahertz Spectroscopy of Low-Dimensional Spin Systems. 2008.
75. **Ly Villo**. Stereoselective Chemoenzymatic Synthesis of Deoxy Sugar Esters Involving *Candida antarctica* Lipase B. 2008.
76. **Johan Anton**. Technology of Integrated Photoelasticity for Residual Stress Measurement in Glass Articles of Axisymmetric Shape. 2008.
77. **Olga Volobujeva**. SEM Study of Selenization of Different Thin Metallic Films. 2008.
78. **Artur Jõgi**. Synthesis of 4'-Substituted 2,3'-dideoxynucleoside Analogues. 2008.
79. **Mario Kadastik**. Doubly Charged Higgs Boson Decays and Implications on Neutrino Physics. 2008.

80. **Fernando Pérez-Caballero**. Carbon Aerogels from 5-Methylresorcinol-Formaldehyde Gels. 2008.
81. **Sirje Vaask**. The Comparability, Reproducibility and Validity of Estonian Food Consumption Surveys. 2008.
82. **Anna Menaker**. Electrosynthesized Conducting Polymers, Polypyrrole and Poly(3,4-ethylenedioxythiophene), for Molecular Imprinting. 2009.
83. **Lauri Ilison**. Solitons and Solitary Waves in Hierarchical Korteweg-de Vries Type Systems. 2009.
84. **Kaia Ernits**. Study of In_2S_3 and ZnS Thin Films Deposited by Ultrasonic Spray Pyrolysis and Chemical Deposition. 2009.
85. **Veljo Sinivee**. Portable Spectrometer for Ionizing Radiation "Gammamapper". 2009.
86. **Jüri Virkepu**. On Lagrange Formalism for Lie Theory and Operadic Harmonic Oscillator in Low Dimensions. 2009.
87. **Marko Piirsoo**. Deciphering Molecular Basis of Schwann Cell Development. 2009.
88. **Kati Helmja**. Determination of Phenolic Compounds and Their Antioxidative Capability in Plant Extracts. 2010.
89. **Merike Sõmera**. Sobemoviruses: Genomic Organization, Potential for Recombination and Necessity of P1 in Systemic Infection. 2010.
90. **Kristjan Laes**. Preparation and Impedance Spectroscopy of Hybrid Structures Based on $CuIn_3Se_5$ Photoabsorber. 2010.
91. **Kristin Lippur**. Asymmetric Synthesis of 2,2'-Bimorpholine and its 5,5'-Substituted Derivatives. 2010.
92. **Merike Luman**. Dialysis Dose and Nutrition Assessment by an Optical Method. 2010.
93. **Mihhail Berezovski**. Numerical Simulation of Wave Propagation in Heterogeneous and Microstructured Materials. 2010.
94. **Tamara Aid-Pavlidis**. Structure and Regulation of BDNF Gene. 2010.
95. **Olga Bragina**. The Role of Sonic Hedgehog Pathway in Neuro- and Tumorigenesis. 2010.
96. **Merle Randrüüt**. Wave Propagation in Microstructured Solids: Solitary and Periodic Waves. 2010.
97. **Marju Laars**. Asymmetric Organocatalytic Michael and Aldol Reactions Mediated by Cyclic Amines. 2010.
98. **Maarja Grossberg**. Optical Properties of Multinary Semiconductor Compounds for Photovoltaic Applications. 2010.
99. **Alla Maloverjan**. Vertebrate Homologues of Drosophila Fused Kinase and Their Role in Sonic Hedgehog Signalling Pathway. 2010.
100. **Priit Pruunsild**. Neuronal Activity-Dependent Transcription Factors and Regulation of Human *BDNF* Gene. 2010.
101. **Tatjana Knjazeva**. New Approaches in Capillary Electrophoresis for Separation and Study of Proteins. 2011.
102. **Atanas Katerski**. Chemical Composition of Sprayed Copper Indium Disulfide Films for Nanostructured Solar Cells. 2011.
103. **Kristi Timmo.** Formation of Properties of $CuInSe_2$ and $Cu_2ZnSn(S,Se)_4$ Monograin Powders Synthesized in Molten KI. 2011.
104. **Kert Tamm**. Wave Propagation and Interaction in Mindlin-Type Microstructured Solids: Numerical Simulation. 2011.

105. **Adrian Popp**. Ordovician Proetid Trilobites in Baltoscandia and Germany. 2011.
106. **Ove Pärn**. Sea Ice Deformation Events in the Gulf of Finland and This Impact on Shipping. 2011.
107. **Germo Väli**. Numerical Experiments on Matter Transport in the Baltic Sea. 2011.
108. **Andrus Seiman**. Point-of-Care Analyser Based on Capillary Electrophoresis. 2011.
109. **Olga Katargina**. Tick-Borne Pathogens Circulating in Estonia (Tick-Borne Encephalitis Virus, *Anaplasma phagocytophilum*, *Babesia* Species): Their Prevalence and Genetic Characterization. 2011.
110. **Ingrid Sumeri**. The Study of Probiotic Bacteria in Human Gastrointestinal Tract Simulator. 2011.
111. **Kairit Zovo**. Functional Characterization of Cellular Copper Proteome. 2011.
112. **Natalja Makarytsheva**. Analysis of Organic Species in Sediments and Soil by High Performance Separation Methods. 2011.
113. **Monika Mortimer**. Evaluation of the Biological Effects of Engineered Nanoparticles on Unicellular Pro- and Eukaryotic Organisms. 2011.
114. **Kersti Tepp**. Molecular System Bioenergetics of Cardiac Cells: Quantitative Analysis of Structure-Function Relationship. 2011.
115. **Anna-Liisa Peikolainen**. Organic Aerogels Based on 5-Methylresorcinol. 2011.
116. **Leeli Amon**. Palaeoecological Reconstruction of Late-Glacial Vegetation Dynamics in Eastern Baltic Area: A View Based on Plant Macrofossil Analysis. 2011.
117. **Tanel Peets**. Dispersion Analysis of Wave Motion in Microstructured Solids. 2011.
118. **Liina Kaupmees**. Selenization of Molybdenum as Contact Material in Solar Cells. 2011.
119. **Allan Olspert**. Properties of VPg and Coat Protein of Sobemoviruses. 2011.
120. **Kadri Koppel**. Food Category Appraisal Using Sensory Methods. 2011.
121. **Jelena Gorbatšova**. Development of Methods for CE Analysis of Plant Phenolics and Vitamins. 2011.
122. **Karin Viipsi**. Impact of EDTA and Humic Substances on the Removal of Cd and Zn from Aqueous Solutions by Apatite. 2012.
123. **David Schryer**. Metabolic Flux Analysis of Compartmentalized Systems Using Dynamic Isotopologue Modeling. 2012.
124. **Ardo Illaste**. Analysis of Molecular Movements in Cardiac Myocytes. 2012.
125. **Indrek Reile**. 3-Alkylcyclopentane-1,2-Diones in Asymmetric Oxidation and Alkylation Reactions. 2012.
126. **Tatjana Tamberg**. Some Classes of Finite 2-Groups and Their Endomorphism Semigroups. 2012.
127. **Taavi Liblik**. Variability of Thermohaline Structure in the Gulf of Finland in Summer. 2012.
128. **Priidik Lagemaa**. Operational Forecasting in Estonian Marine Waters. 2012.
129. **Andrei Errapart**. Photoelastic Tomography in Linear and Non-linear Approximation. 2012.
130. **Külliki Krabbi**. Biochemical Diagnosis of Classical Galactosemia and Mucopolysaccharidoses in Estonia. 2012.
131. **Kristel Kaseleht**. Identification of Aroma Compounds in Food using SPME-GC/MS and GC-Olfactometry. 2012.

132. **Kristel Kodar**. Immunoglobulin G Glycosylation Profiling in Patients with Gastric Cancer. 2012.
133. **Kai Rosin**. Solar Radiation and Wind as Agents of the Formation of the Radiation Regime in Water Bodies. 2012.
134. **Ann Tiiman**. Interactions of Alzheimer's Amyloid-Beta Peptides with Zn(II) and Cu(II) Ions. 2012.
135. **Olga Gavrilova**. Application and Elaboration of Accounting Approaches for Sustainable Development. 2012.
136. **Olesja Bondarenko**. Development of Bacterial Biosensors and Human Stem Cell-Based *In Vitro* Assays for the Toxicological Profiling of Synthetic Nanoparticles. 2012.
137. **Katri Muska**. Study of Composition and Thermal Treatments of Quaternary Compounds for Monograin Layer Solar Cells. 2012.
138. **Ranno Nahku**. Validation of Critical Factors for the Quantitative Characterization of Bacterial Physiology in Accelerostat Cultures. 2012.
139. **Petri-Jaan Lahtvee**. Quantitative Omics-level Analysis of Growth Rate Dependent Energy Metabolism in *Lactococcus lactis*. 2012.
140. **Kerti Orumets**. Molecular Mechanisms Controlling Intracellular Glutathione Levels in Baker's Yeast *Saccharomyces cerevisiae* and its Random Mutagenized Glutathione Over-Accumulating Isolate. 2012.
141. **Loreida Timberg**. Spice-Cured Sprats Ripening, Sensory Parameters Development, and Quality Indicators. 2012.
142. **Anna Mihhalevski**. Rye Sourdough Fermentation and Bread Stability. 2012.
143. **Liisa Arike**. Quantitative Proteomics of *Escherichia coli*: From Relative to Absolute Scale. 2012.
144. **Kairi Otto**. Deposition of In_2S_3 Thin Films by Chemical Spray Pyrolysis. 2012.
145. **Mari Sepp**. Functions of the Basic Helix-Loop-Helix Transcription Factor TCF4 in Health and Disease. 2012.
146. **Anna Suhhova**. Detection of the Effect of Weak Stressors on Human Resting Electroencephalographic Signal. 2012.
147. **Aram Kazarjan**. Development and Production of Extruded Food and Feed Products Containing Probiotic Microorganisms. 2012.
148. **Rivo Uiboupin**. Application of Remote Sensing Methods for the Investigation of Spatio-Temporal Variability of Sea Surface Temperature and Chlorophyll Fields in the Gulf of Finland. 2013.
149. **Tiina Kriščiunaite**. A Study of Milk Coagulability. 2013.
150. **Tuuli Levandi**. Comparative Study of Cereal Varieties by Analytical Separation Methods and Chemometrics. 2013.
151. **Natalja Kabanova**. Development of a Microcalorimetric Method for the Study of Fermentation Processes. 2013.
152. **Himani Khanduri**. Magnetic Properties of Functional Oxides. 2013.
153. **Julia Smirnova**. Investigation of Properties and Reaction Mechanisms of Redox-Active Proteins by ESI MS. 2013.
154. **Mervi Sepp**. Estimation of Diffusion Restrictions in Cardiomyocytes Using Kinetic Measurements. 2013.
155. **Kersti Jääger**. Differentiation and Heterogeneity of Mesenchymal Stem Cells. 2013.
156. **Victor Alari**. Multi-Scale Wind Wave Modeling in the Baltic Sea. 2013.

157. **Taavi Päll**. Studies of CD44 Hyaluronan Binding Domain as Novel Angiogenesis Inhibitor. 2013.
158. **Allan Niidu**. Synthesis of Cyclopentane and Tetrahydrofuran Derivatives. 2013.
159. **Julia Geller**. Detection and Genetic Characterization of *Borrelia* Species Circulating in Tick Population in Estonia. 2013.
160. **Irina Stulova**. The Effects of Milk Composition and Treatment on the Growth of Lactic Acid Bacteria. 2013.
161. **Jana Holmar**. Optical Method for Uric Acid Removal Assessment During Dialysis. 2013.
162. **Kerti Ausmees**. Synthesis of Heterobicyclo[3.2.0]heptane Derivatives *via* Multicomponent Cascade Reaction. 2013.
163. **Minna Varikmaa**. Structural and Functional Studies of Mitochondrial Respiration Regulation in Muscle Cells. 2013.
164. **Indrek Koppel**. Transcriptional Mechanisms of BDNF Gene Regulation. 2014.
165. **Kristjan Pilt**. Optical Pulse Wave Signal Analysis for Determination of Early Arterial Ageing in Diabetic Patients. 2014.
166. **Andres Anier**. Estimation of the Complexity of the Electroencephalogram for Brain Monitoring in Intensive Care. 2014.
167. **Toivo Kallaste**. Pyroclastic Sanidine in the Lower Palaeozoic Bentonites – A Tool for Regional Geological Correlations. 2014.
168. **Erki Kärber**. Properties of ZnO-nanorod/In_2S_3/$CuInS_2$ Solar Cell and the Constituent Layers Deposited by Chemical Spray Method. 2014.
169. **Julia Lehner**. Formation of Cu_2ZnSnS_4 and $Cu_2ZnSnSe_4$ by Chalcogenisation of Electrochemically Deposited Precursor Layers. 2014.
170. **Peep Pitk**. Protein- and Lipid-rich Solid Slaughterhouse Waste Anaerobic Co-digestion: Resource Analysis and Process Optimization. 2014.
171. **Kaspar Valgepea**. Absolute Quantitative Multi-omics Characterization of Specific Growth Rate-dependent Metabolism of *Escherichia coli*. 2014.
172. **Artur Noole**. Asymmetric Organocatalytic Synthesis of 3,3'-Disubstituted Oxindoles. 2014.
173. **Robert Tsanev**. Identification and Structure-Functional Characterisation of the Gene Transcriptional Repressor Domain of Human Gli Proteins. 2014.
174. **Dmitri Kartofelev**. Nonlinear Sound Generation Mechanisms in Musical Acoustic. 2014.
175. **Sigrid Hade**. GIS Applications in the Studies of the Palaeozoic Graptolite Argillite and Landscape Change. 2014.
176. **Agne Velthut-Meikas**. Ovarian Follicle as the Environment of Oocyte Maturation: The Role of Granulosa Cells and Follicular Fluid at Pre-Ovulatory Development. 2014.
177. **Kristel Hälvin**. Determination of B-group Vitamins in Food Using an LC-MS Stable Isotope Dilution Assay. 2014.
178. **Mailis Päri**. Characterization of the Oligoadenylate Synthetase Subgroup from Phylum Porifera. 2014.
179. **Jekaterina Kazantseva**. Alternative Splicing of *TAF4*: A Dynamic Switch between Distinct Cell Functions. 2014.
180. **Jaanus Suurväli**. Regulator of G Protein Signalling 16 (RGS16): Functions in Immunity and Genomic Location in an Ancient MHC-Related Evolutionarily Conserved Synteny Group. 2014.

181. **Ene Viiard**. Diversity and Stability of Lactic Acid Bacteria During Rye Sourdough Propagation. 2014.
182. **Kristella Hansen**. Prostaglandin Synthesis in Marine Arthropods and Red Algae. 2014.
183. **Helike Lõhelaid**. Allene Oxide Synthase-lipoxygenase Pathway in Coral Stress Response. 2015.
184. **Normunds Stivrinš**. Postglacial Environmental Conditions, Vegetation Succession and Human Impact in Latvia. 2015.
185. **Mary-Liis Kütt**. Identification and Characterization of Bioactive Peptides with Antimicrobial and Immunoregulating Properties Derived from Bovine Colostrum and Milk. 2015.
186. **Kazbulat Šogenov**. Petrophysical Models of the CO_2 Plume at Prospective Storage Sites in the Baltic Basin. 2015.
187. **Taavi Raadik**. Application of Modulation Spectroscopy Methods in Photovoltaic Materials Research. 2015.
188. **Reio Põder**. Study of Oxygen Vacancy Dynamics in Sc-doped Ceria with NMR Techniques. 2015.
189. **Sven Siir**. Internal Geochemical Stratification of Bentonites (Altered Volcanic Ash Beds) and its Interpretation. 2015.
190. **Kaur Jaanson**. Novel Transgenic Models Based on Bacterial Artificial Chromosomes for Studying BDNF Gene Regulation. 2015.
191. **Niina Karro**. Analysis of ADP Compartmentation in Cardiomyocytes and Its Role in Protection Against Mitochondrial Permeability Transition Pore Opening. 2015.
192. **Piret Laht**. B-plexins Regulate the Maturation of Neurons Through Microtubule Dynamics. 2015.
193. **Sergei Žari**. Organocatalytic Asymmetric Addition to Unsaturated 1,4-Dicarbonyl Compounds. 2015.
194. **Natalja Buhhalko**. Processes Influencing the Spatio-temporal Dynamics of Nutrients and Phytoplankton in Summer in the Gulf of Finland, Baltic Sea. 2015.
195. **Natalia Maticiuc**. Mechanism of Changes in the Properties of Chemically Deposited CdS Thin Films Induced by Thermal Annealing. 2015.
196. **Mario Öeren**. Computational Study of Cyclohexylhemicucurbiturils. 2015.
197. **Mari Kalda**. Mechanoenergetics of a Single Cardiomyocyte. 2015.
198. **Ieva Grudzinska**. Diatom Stratigraphy and Relative Sea Level Changes of the Eastern Baltic Sea over the Holocene. 2015.
199. **Anna Kazantseva**. Alternative Splicing in Health and Disease. 2015.
200. **Jana Kazarjan**. Investigation of Endogenous Antioxidants and Their Synthetic Analogues by Capillary Electrophoresis. 2016.
201. **Maria Safonova**. SnS Thin Films Deposition by Chemical Solution Method and Characterization. 2016.
202. **Jekaterina Mazina**. Detection of Psycho- and Bioactive Drugs in Different Sample Matrices by Fluorescence Spectroscopy and Capillary Electrophoresis. 2016.
203. **Karin Rosenstein**. Genes Regulated by Estrogen and Progesterone in Human Endometrium. 2016.
204. **Aleksei Tretjakov**. A Macromolecular Imprinting Approach to Design Synthetic Receptors for Label-Free Biosensing Applications. 2016.
205. **Mati Danilson**. Temperature Dependent Electrical Properties of Kesterite Monograin Layer Solar Cells. 2016.

206. **Kaspar Kevvai**. Applications of ^{15}N-labeled Yeast Hydrolysates in Metabolic Studies of *Lactococcus lactis* and *Saccharomyces Cerevisiae*. 2016.
207. **Kadri Aller**. Development and Applications of Chemically Defined Media for Lactic Acid Bacteria. 2016.
208. **Gert Preegel**. Cyclopentane-1,2-dione and Cyclopent-2-en-1-one in Asymmetric Organocatalytic Reactions. 2016.
209. **Jekaterina Služenikina**. Applications of Marine Scatterometer Winds and Quality Aspects of their Assimilation into Numerical Weather Prediction Model HIRLAM. 2016.
210. **Erkki Kask**. Study of Kesterite Solar Cell Absorbers by Capacitance Spectroscopy Methods. 2016.
211. **Jürgen Arund**. Major Chromophores and Fluorophores in the Spent Dialysate as Cornerstones for Optical Monitoring of Kidney Replacement Therapy. 2016.
212. **Andrei Šamarin**. Hybrid PET/MR Imaging of Bone Metabolism and Morphology. 2016.
213. **Kairi Kasemets**. Inverse Problems for Parabolic Integro-Differential Equations with Instant and Integral Conditions. 2016.
214. **Edith Soosaar**. An Evolution of Freshwater Bulge in Laboratory Scale Experiments and Natural Conditions. 2016.
215. **Peeter Laas**. Spatiotemporal Niche-Partitioning of Bacterioplankton Community across Environmental Gradients in the Baltic Sea. 2016.
216. **Margus Voolma**. Geochemistry of Organic-Rich Metalliferous Oil Shale/Black Shale of Jordan and Estonia. 2016.
217. **Karin Ojamäe**. The Ecology and Photobiology of Mixotrophic Alveolates in the Baltic Sea. 2016.
218. **Anne Pink**. The Role of CD44 in the Control of Endothelial Cell Proliferation and Angiogenesis. 2016.
219. **Kristiina Kreek**. Metal-Doped Aerogels Based on Resorcinol Derivatives. 2016.
220. **Kaia Kukk**. Expression of Human Prostaglandin H Synthases in the Yeast Pichia pastoris. 2016.
221. **Martin Laasmaa**. Revealing Aspects of Cardiac Function from Fluorescence and Electrophysiological Recordings. 2016.
222. **Eeva-Gerda Kobrin**. Development of Point of Care Applications for Capillary Electrophoresis. 2016.
223. **Villu Kikas**. Physical Processes Controlling the Surface Layer Dynamics in the Stratified Gulf of Finland: An Application of Ferrybox Technology. 2016.
224. **Maris Skudra**. Features of Thermohaline Structure and Circulation in the Gulf of Riga. 2017.
225. **Sirje Sildever**. Influence of Physical-Chemical Factors on Community and Populations of the Baltic Sea Spring Bloom Microalgae. 2017.
226. **Nicolae Spalatu**. Development of CdTe Absorber Layer for Thin-Film Solar Cells. 2017.
227. **Kristi Luberg**. Human Tropomyosin-Related Kinase A and B: from Transcript Diversity to Novel Inhibitors. 2017.
228. **Andrus Kaldma**. Metabolic Remodeling of Human Colorectal Cancer: Alterations in Energy Fluxes. 2017.